Discovery and characterization of synthetic and natural compounds as inhibitors of shikimate kinase from *Mycobacterium tuberculosis* by LC-MS

by

Johayra J. Simithy W.

A dissertation submitted to the Graduate Faculty of
Auburn University
in partial fulfillment of the
requirements for the Degree of
Doctor of Philosophy

Auburn, Alabama
December 13, 2014

Keywords: liquid-chromatography, mass spectrometry, tuberculosis, *Mycobacterium tuberculosis*, shikimate kinase, shikimate-3-phosphate.

Approved by

Angela I. Calderón, Chair, Associate Professor of Drug Discovery and Development
C. Randall Clark, Professor of Drug Discovery and Development
Jack DeRuiter, Professor of Drug Discovery and Development
Forrest Smith, Associate Professor of Drug Discovery and Development
Douglas Goodwin, Associate Professor of Chemistry and Biochemistry

Abstract

With the increasing emergence of drug-resistant tuberculosis (TB) and the complication by HIV co-infection, *Mycobacterium tuberculosis* (*Mtb*) remains a challenging target for drug discovery. The shikimate pathway, responsible for the biosynthesis of aromatic compounds in microorganisms and higher plants but absent from mammals, has been suggested as a promising target for the development of antimicrobials and herbicides. Gene disruption studies have demonstrated that the operation of the shikimate pathway is essential for the viability of *Mtb*, and recent research focusing on the enzymes of the pathway has proposed that small molecules acting as inhibitors of these enzymes could result in a new generation of antibiotics for the treatment of tuberculosis. The work in this dissertation is focused on the applications of mass spectrometry and molecular modeling based approaches for the identification of inhibitors of *Mycobacterium tuberculosis* shikimate kinase (*Mt*SK), the fifth enzyme of the shikimate pathway.

Chapter one is an overview of tuberculosis pathogenesis and statistics, and it describes the role of the shikimate pathway in bacteria and provides structural information of shikimate kinase. A brief review on the applications of mass spectrometry in the drug discovery process is also included.

Chapter two describes the cloning, expression and purification of *Mt*SK. An enzyme-couple spectrophotometric assay was implemented to measure the kinetic parameters of *Mt*SK (K_M and k_{cat}). Values determined by this approach were consistent with the ones reported in the literature.

Chapter three describes the development of an ESI-LC-MS based assay for the kinetic characterization of *Mt*SK and for the evaluation of inhibitors. The assay is based on the direct determination of the reaction product shikimate-3-phosphate (S3P) and it was validated by evaluating a known inhibitor of shikimate kinase. Kinetic parameters of *Mt*SK determined by this method, as well as the inhibition constants and mode of inhibition of the known inhibitor were in excellent agreement with those obtained from the UV assay and those reported in the literature.

Chapter four describes the screening of a small library of synthetic antimycobacterial compounds supplied by the NIH Tuberculosis Antimicrobial Acquisition and Coordinating Facility (TAACF) using our LC-MS based functional assay and molecular docking in order to identify inhibitors of *Mt*SK. Fourteen compounds containing an oxadiazole-amide or a 2-aminobenzothiazole core scaffold showed *Mt*SK inhibitory activity at 50 μM, with the lowest IC_{50} of 1.94 μM. Induced-fit docking studies suggested that the scaffolds shared by these compounds fit well in the shikimate binding pocket of *Mt*SK.

Chapter five describes the characterization of manzamine alkaloids as inhibitors of *Mt*SK by LC-MS. Six manzamine alkaloids were characterized as mixed-type and slow tight-binding inhibitors of *Mt*SK, among them, analog 6-cyclohexamidomanzamine A showed the most potent inhibition (K_i 0.4 – 0.9 μM) of *Mt*SK. Molecular docking studies revealed that the manzamine alkaloids may bind the enzyme in two alternative binding modes, which is consistent with the mixed-type inhibition observed in the experimental studies.

Chapter six describes an approach for the characterization of the irreversible inhibition of the marine metabolite ilimaquinone on *Mt*SK. It was demonstrated that ilimaquinone is capable

of forming covalent adducts with *Mt*SK by analysis of intact protein by LC-MS. The inhibitory mechanism of IQ on *Mt*SK determined by an LC-MS based activity assay is also discussed.

Acknowledgements

I dedicate this dissertation to my family, especially to my mother Mavis Williams. Without her constant support, sacrifice and unconditional love through all these years away from home, I could not have taken on this challenge and become the person that I am today.

First and foremost, I would like to thank my research advisor, Dr. Angela Calderón, who remained supportive and optimistic through the good and bad times of my graduate research. Thank you for giving me the opportunity to be part of your group and for your guidance, patience, encouragement and constant support throughout my graduate career.

My sincere appreciation is extended to my committee members Dr. Randall Clark, Dr. Jack DeRuiter and Dr. Forrest Smith. Their lessons, discussions, ideas, and feedback have been absolutely invaluable. Thank you for always offering advice and monitoring my progress throughout graduate school.

My deepest gratitude goes to Dr. Douglas Goodwin; this work would not have been possible without his guidance. His enthusiasm in research and his knowledge are a great motivation for all his advisees, including me. Thank you for your continuous and valuable scientific inputs and encouragement to become a good researcher.

Special thanks to our collaborators, Dr. Mark Hamann from the University of Mississippi for providing the marine compounds tested on this work. Thanks to Dr. Judith Hobrath from the Southern Research Institute for her help with the molecular docking studies presented in this dissertation. I would like to thank Dr. Yonnie Wu from the Mass Spectrometry Center at Auburn

University for closely working with me and for providing valuable input in my research. I am also grateful to the National Institute of Allergy and Infectious Diseases (NIAID) for supplying the library of antitubercular compounds and AstraZeneca for supplying the standard *Mt*SK inhibitor.

I would like to extend my gratitude to previous members of Dr. Calderon's group, especially Dr. Vanisree Mulabagal and Dr. Ranjith Munigunti, for their time and patience in teaching me experimental techniques and for their support and warm welcoming attitude during my first years at Auburn University. Thanks to Nathan Reeve, Cole Sterling, Mary Smith, Emily Pipan, Lexi Burkard and Alexis Scheuermann for keeping me engaged in research and for their assistance and friendship during their time at the laboratory. I would also like to thank the current members of the group, Neil Tiwari, Amy Arnold and my fellow graduate students Ahmad Almaki, Ahmed Shaekon and Mansour Alturki for their support, humor and significant impact on my development as a scientist.

I would also like to thank previous members of Dr. Goodwin's group, especially Dr. Yu Wang for taking the time during her last semester at Auburn University to train me on various experimental techniques that have broadened my skill set. Thanks to Dr. Elizabeth Ndontsa and Gobind Gill for their help and insightful comments during our time at the laboratory. My special thanks also goes to the current graduate students Olive Njuma and Rene Fuanta for their support, companionship, and the enjoyable environment that always made me feel welcome.

I would also like to express my sincere gratitude and appreciation to all who have enriched my life, especially to Daniel Hughes for always being there when I needed you and for supporting me every step of the way. Thanks to my friends and fellow graduate students: Selamawit Ghebreamlak, Ana Maria Dmytrejchuk, Yun Wu, Abouh Coulibaly, Ben Nie and

Matthew Eggert for their unconditional friendship and for always keeping me optimistic. I could not have asked for better friends.

Finally, I would like to thank the "Secretaría Nacional de Ciencia y Tecnología" (SENACYT) in collaboration with the "Instituto para la Formación de Recursos Humanos" (IFARHU) of the Panamanian government for providing the funding for my doctoral studies.

Table of Contents

List of Figures

List of Tables

List of Abbreviations

µL	Microliter
µM	Micromolar
°C	Degree centigrade
ADP	Adenosine diphosphate
AMP	Ampicillin
ATP	Adenosine triphosphate
CAM	Chloramphenicol
DMSO	Dimethyl sulfoxide
EIC	Extracted ion chromatogram
ESI	Electrospray ionization
IPTG	Isopropyl-β-d-thiogalactopyranoside
kDa	Kilodalton
LC-MS	Liquid chromatography-mass spectrometry
LDH	Lactate dehydrogenase
MDR	Multi drug-resistant
mL	Milliliter
MS	Mass spectrometry
Mtb	*Mycobacterium tuberculosis*
*Mt*SK	*Mycobacterium tuberculosis* shikimate kinase

NAD^+	Oxidized nicotinamide adenine dinucleotide
NADH	Reduced nicotinamide adenine dinucleotide
PEP	Phosphoenol pyruvate
PK	Pyruvate kinase
PMSF	Phenylmethylsulfonyl fluoride
QTOF	Quadrupole Time-of-flight
S3P	Shikimate-3-phosphate
SK	Shikimate kinase
TB	Tuberculosis
TIC	Total ion chromatogram
XDB	Extensively drug-resistant

Chapter 1: Literature review

1.1 Introduction

Mycobacterium tuberculosis (*Mtb*), the causative agent of tuberculosis (TB), is an obligate aerobe whose sole host is humans [1]. The conventional mode of transmission of *Mtb* is through aerosol droplets containing the bacteria, released by an infected person when coughing or sneezing (Fig. 1.1) [2]. Once in the lungs, the bacillus is phagocytized as a result of the host innate immune responses that involve the recruitment of inflammatory cells to the lung. Following bacterial dissemination to the draining lymph node, dendritic cell presentation of bacterial antigens leads to T cell priming and triggers an expansion of antigen-specific T cells, which are recruited to the lung. The recruitment of T cells, B cells, activated macrophages and other leukocytes leads to the establishment of granulomas, which prevent dissemination of the mycobacteria 90-95% of the time, but do not completely eradicate the mycobacteria from the host [3]. Bacteria that remain inside the granuloma can switch to a dormant (non-replicating) state, evading host immune response for an indefinite period of time, resulting in latent infection in which no clinical symptoms are present [4]. Different factors such as immune suppression, aging, AIDS and malnutrition can cause the host immune system to deteriorate, allowing dormant bacteria to return to a replication state, which can lead to the release of *Mtb* from granulomas resulting in an active infection [5].

Worldwide, TB is the leading cause of death by a bacterial pathogen infecting approximately one-third of the world's population, mostly in highly populated third world countries in South-East Asia and Africa [6]. The World Health Organization (WHO) reported

that in 2012, 8.6 million new cases of TB were notified and that 1.3 million people died from TB [7]. Among the 8.6 million cases of incident TB, 13% were in HIV co-infected individuals, 450,000 were caused by a multi-drug resistant strain (MDR-TB) defined as resistant to both isoniazid and rifampicin, 2.9 million were women and 0.53 million were children. Among the 1.3 million people that died from TB, 320,000 individuals were HIV-positive, 170,000 died of MDR-TB, 410,000 were women and 74,000 were HIV-negative children.

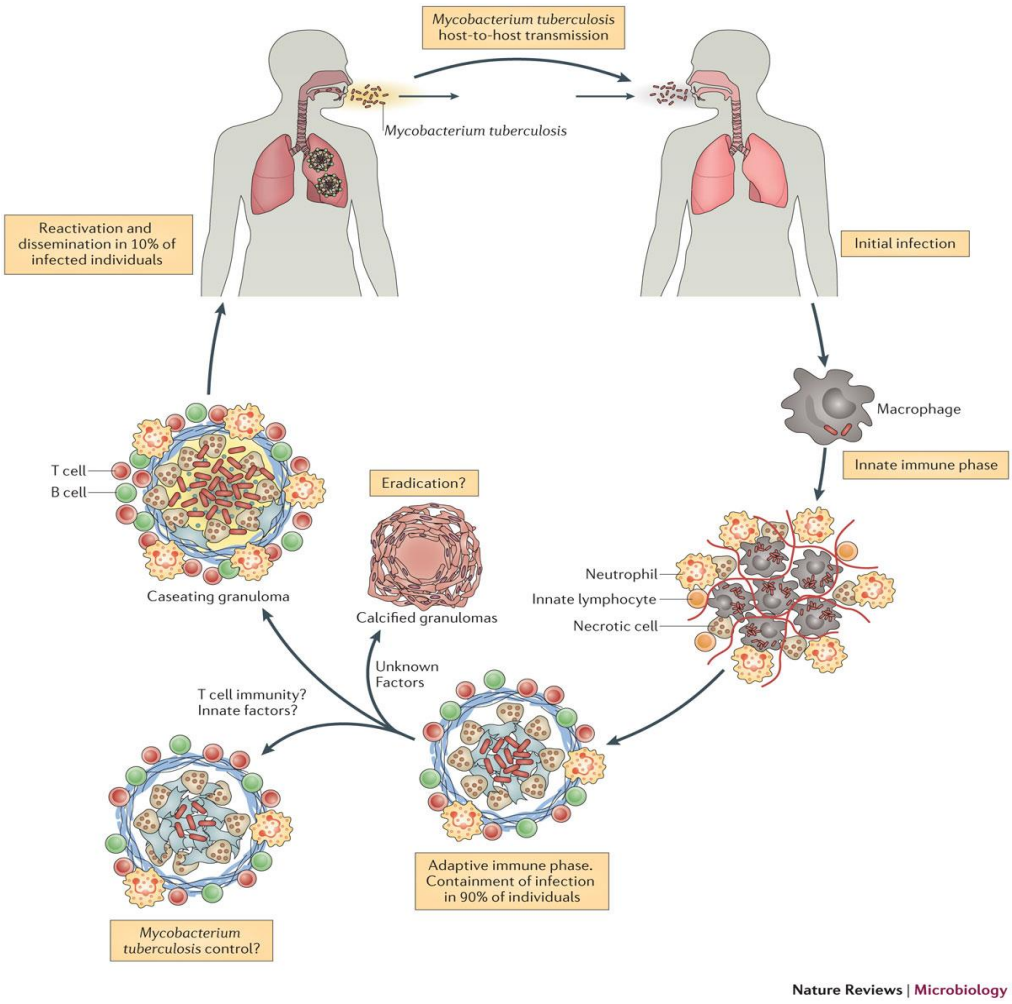

Figure 1.1. Tuberculosis pathogenesis [3].

Treatment of TB consists of four different antimicrobial agents and it usually last from 6-9 months. The most commonly used drugs are rifampin (RIF), isoniazid (INH), pyrazinamide (PZA) and ethambutol (EMB) or streptomycin (SM) [8]. When adherence with the regimen is assured, this four-drug regimen is highly effective. Unfortunately, patient compliance to this lengthy treatment is poor, and this is reflected in the rising incidence of multidrug resistant TB (MDR-TB) and extensively drug-resistant TB (XDR-TB) cases of tuberculosis throughout the world, representing a major public health concern today [9]. Even though a massive and costly control effort is achieving considerable success [10], TB association with HIV and other immunocompromising diseases in recent years has highlighted the urgent need for new and safer drug combinations and therapies.

The only FDA approved TB drug since the 1960s has been recently announced, Bedaquiline Sirturo™ for the treatment of MDR-TB [11]. Sirturo™ specifically inhibits mycobacterial ATP (adenosine 5'-triphosphate) synthase, an enzyme that is essential for the generation of energy in *Mycobacterium tuberculosis* [12]. Its associated risk of potentially lethal heart problems has emphasized the unmet and urgent need for the development of safer antitubercular drugs with novel targets and mechanisms of action to treat resistant forms of the disease.

The effectiveness of any drug is correlated to the essentiality of the biological process that it targets in the pathogen. Therefore, a vital first step in the discovery of drugs with low toxicity is the identification and elucidation of pathways exclusive to the target pathogen [13]. One pathway that offers such targets is the shikimate pathway.

1. 2 The shikimate pathway

The shikimate pathway is a metabolic route responsible for the biosynthesis of essential aromatic amino acids in higher plants and microorganisms, but not in mammals [14]. It comprises seven enzymatic steps beginning with the condensation of phosphoenol pyruvate and erythrose-4-phosphate to form chorismate (Fig. 1.2). Chorismate can be converted to the aromatic amino acids phenylalanine, tyrosine, and tryptophan through several enzymatic steps [15]. Genomic studies have demonstrated the essentiality of the pathway in bacteria, fungi, parasites, algae, parasites and higher plants. The bacterial shikimate pathway is crucial for the synthesis of many important metabolites including not only aromatic amino acids, but also folic acid and quinones, whereas mammals must obtain most aromatic compounds from their diet [16]. For example, *M. tuberculosis* growth in macrophages has been shown to require the mycobactin siderophores derived from the shikimate pathway [17]. Because this pathway is necessary for many bacteria, but is absent in mammals, the enzymes involved in the pathway provide an attractive target for the development of potentially selective and nontoxic antimicrobial agents [18].

A great deal of research focusing on the development of inhibitors of the enzymes of this pathway has been carried out in the last several years. For example, glyphosate, a selective inhibitor of the sixth enzyme of the pathway (5-enolpyruvylshikimate-3-phosphate synthase EPSPS) is the active ingredient in the wide-spectrum herbicide known as RoundUp [19]. Aside from its activity against the plant form of EPSPS, this compound has also proven to be active in vitro against the malaria parasite [20], validating the importance of the SP enzymes as targets for the design of potentially selective antimicrobial drugs [21].

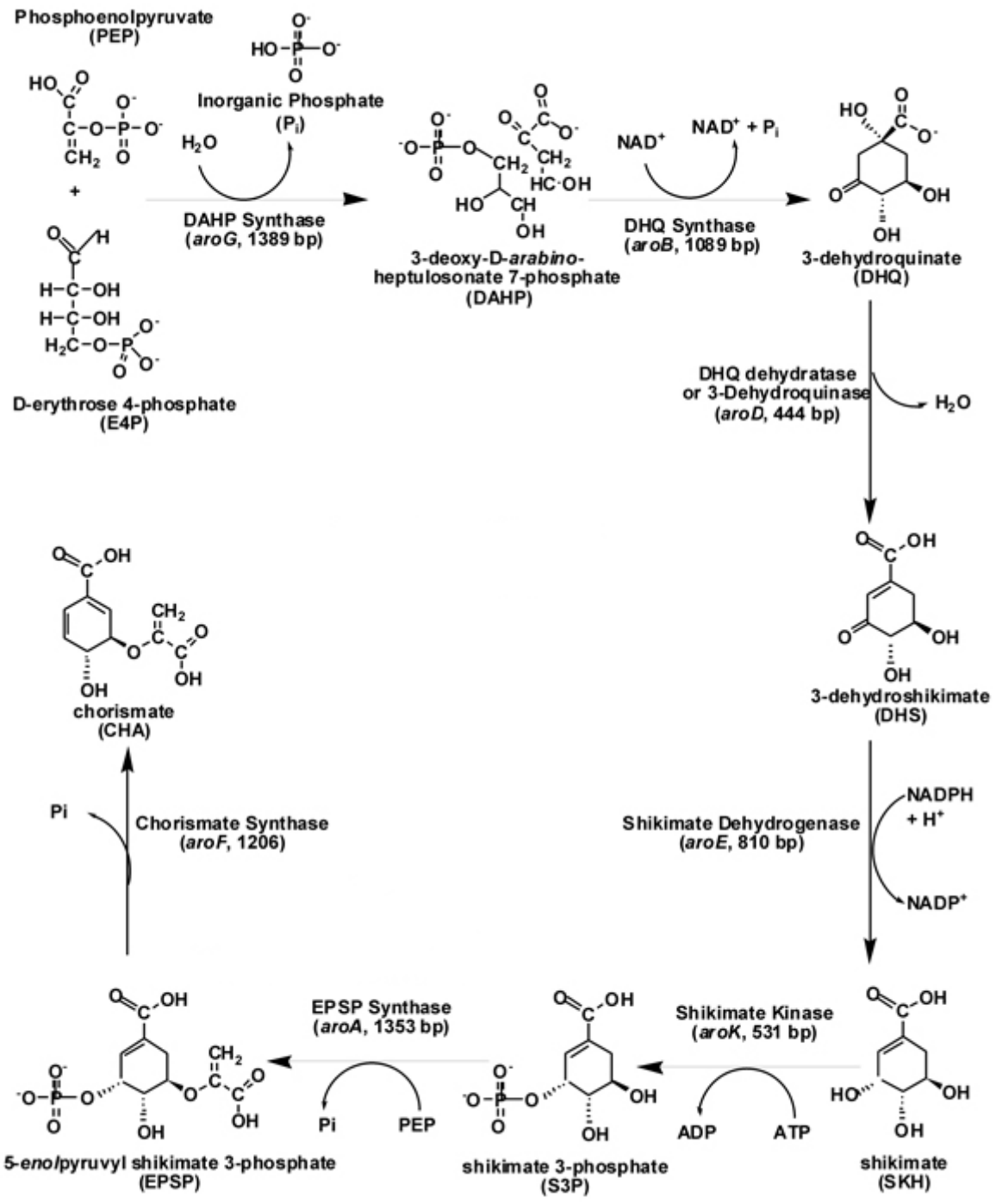

Figure 1.2. The shikimate pathway.

1.3 Shikimate kinase from *Mycobacterium tuberculosis*

Shikimate kinase (SK) (EC 2.7.1.71) is the fifth enzyme of the shikimate pathway and it catalyzes the regioespecific ATP-dependent phosphorylation of the 3-hydroxyl group of shikimate to form shikimate-3-phosphate (S3P) and adenosine diphosphate (ADP) (Fig. 1.3) [22]. The reaction mechanism is thought to proceed by deprotonation of the 3′ hydroxyl of shikimate followed by nucleophilic attack of the γ-phosphate of ATP [23]. Divalent magnesium (Mg^{2+}) is the preferred cofactor for this reaction and comparable activity can be achieved with divalent manganese [24].

Mycobacterium tuberculosis shikimate kinase (*Mt*SK) is encoded by the *aroK* gene, which is composed by 531 bp, and encodes an 18.5 kDa protein of 176 amino acids [25]. The function and structure of *Mt*SK has been thoroughly studied, and gene knockout studies have shown *Mt*SK to be vital for the growth of the bacterium [26-27]. As such, it is an attractive target for the development of a new generation of antitubercular drugs targeting the shikimate- and ATP-binding sites, which may interfere with the biosynthesis of aromatic compounds necessary for *M. tuberculosis* growth. [17].

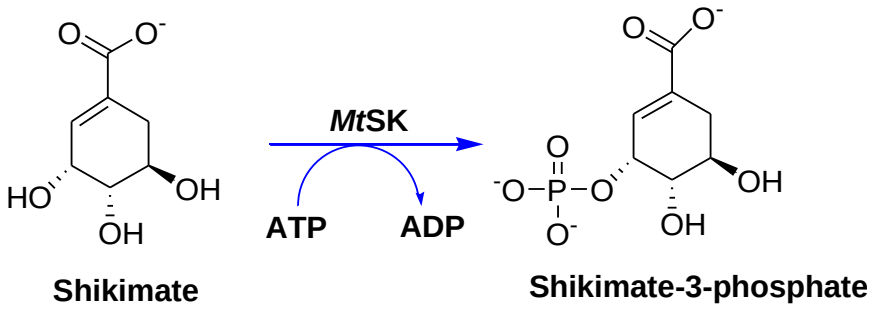

Figure 1.3. Shikimate kinase catalyzed reaction.

SK belongs to the family of nucleoside monophosphate (NMP) kinases [28] and adopts an α-β-α fold with a central five-stranded parallel β-sheet flanked by eight α-helices [23]. Several crystal structures have been determined for SK, all containing domains characteristic of NMP kinases, namely the LID, CORE, and the SB (SKM-binding) or NMP-binding (NMPB) domains [25].

For *Mt*SK, four domains have been identified (Fig. 1.4): 1) a reduced CORE (RC) domain comprising the central β-sheet and flanking α-helices [23], 2) the nucleotide-binding (NB) domain which includes the nucleotide phosphate binding loop (P-) loop (Walker-A motif, residues 9-17) [29], the adenine binding pocket (AB-loop, residues 148-155) and the segment 101-110 including α6 (residues 104-110) [30], 3) a flexible LID domain (residues 112-124) which contains catalytic and substrate binding residues and closes over the substrate binding pockets upon substrate binding [31], and 4) an extended shikimate binding (ESB) domain (residues 32-93) which includes the SB sub-domain (residues 32-61) that corresponds to the NMP-binding domain in NMP kinases [23].

Shikimate kinase undergoes large conformational changes during catalysis. These structural changes act to position the enzyme side chains appropriately around the substrates and to sequester the substrates to prevent the hydrolysis of bound ATP prior to catalysis (Fig. 1.5) [32-34]. There are two flexible regions of the structures that are responsible for movement: the nucleotide binding (NB) site and the LID domain [35]. In the absence of bound substrates, *Mt*SK adopts an open conformation characterized by a disordered LID domain oriented away from the substrate binding pocket. Upon binding of either substrate, a closed conformation characterized by closure of the LID domain over the active site is observed. ATP binding is associated with a rotation of the NB domain into the substrate binding pocket, and shikimate

binding induces a rotation of the ESB domain into the substrate binding pocket. The binding of one substrate is thought to synergistically enhance the affinity for the second substrate [23].

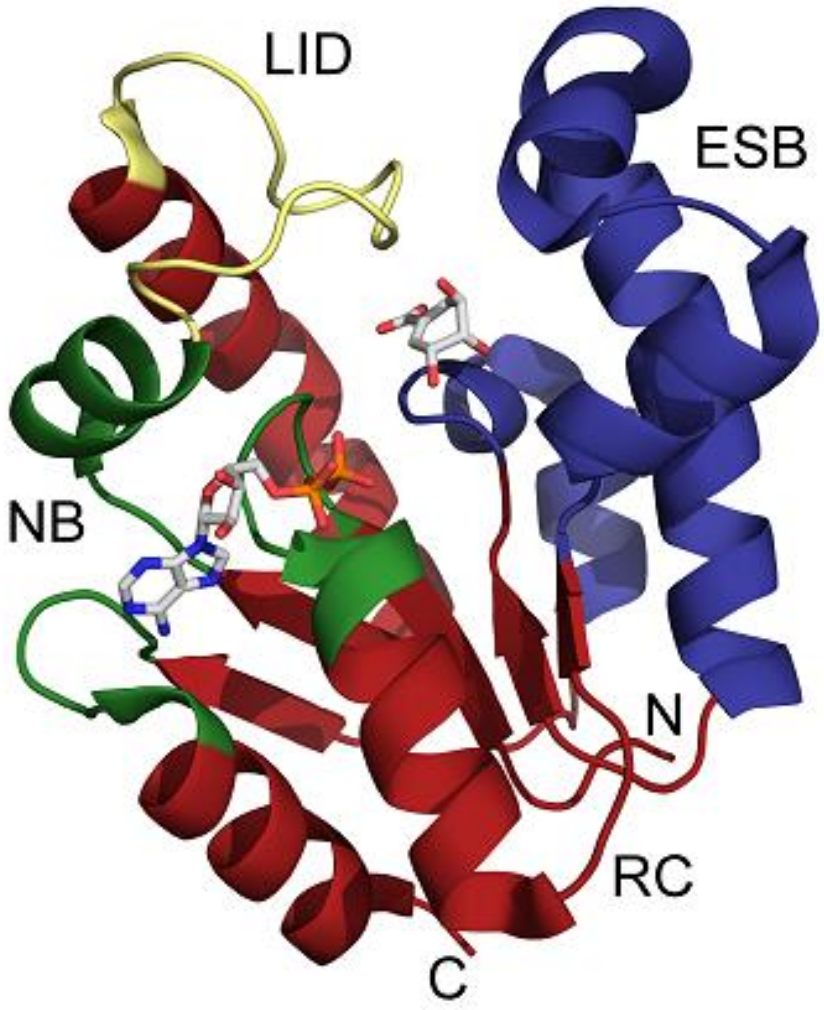

Figure 1.4. Crystal structure of shikimate kinase from *Mycobacterium tuberculosis* [PDB ID: 2IYQ]. The LID domain is shown in yellow, the reduced core (RC) domain is shown in red, the nucleotide binding (NB) domain is shown in green, and the extended shikimate binding (ESB) domain is shown in blue. Bound ADP and shikimate molecules are colored by atom (grey - C, red - O, blue - N, orange - P). The amino (N) and carboxy (C) termini of the protein are labeled.

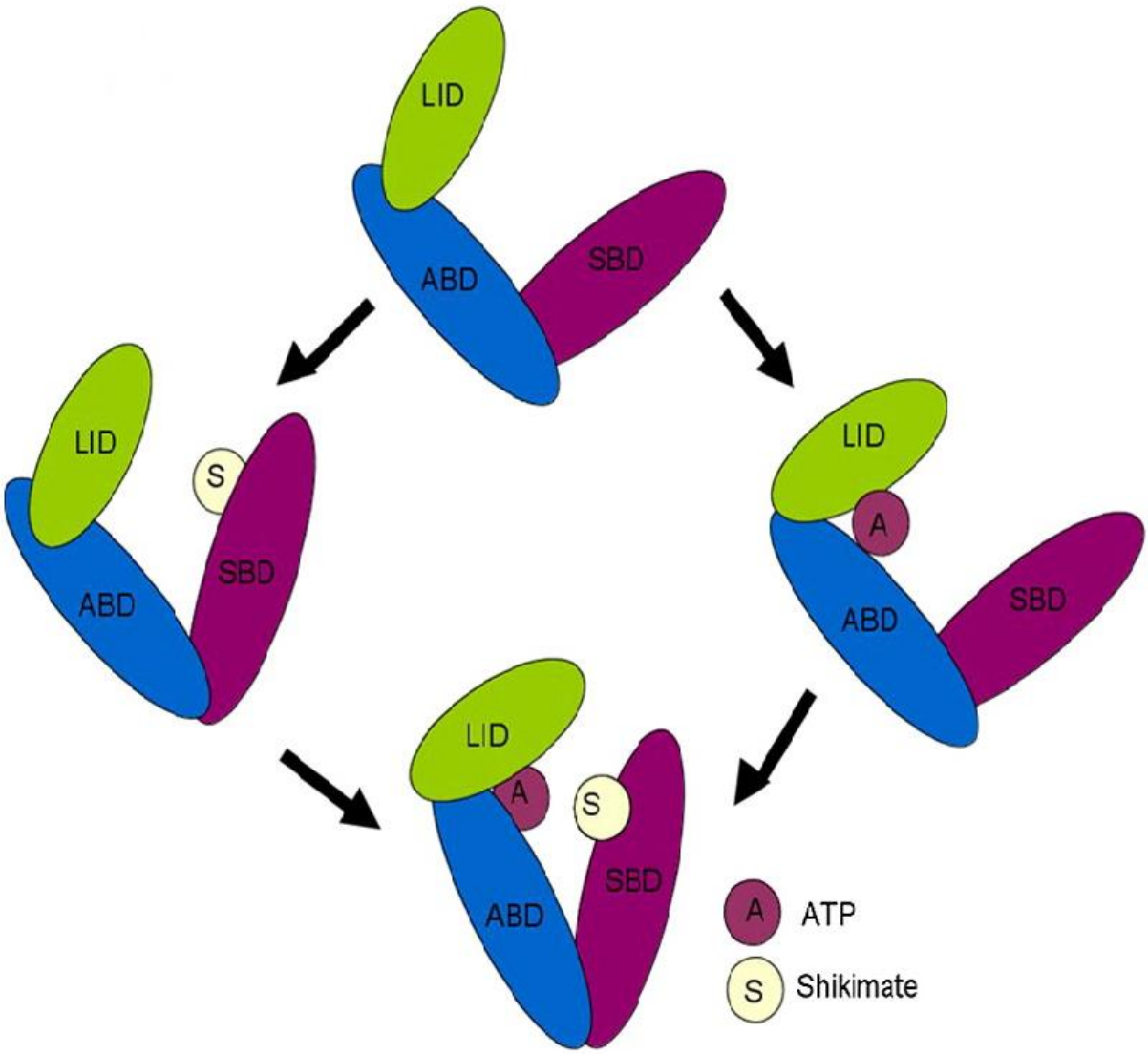

Figure 1.5. Conformational changes of shikimate kinase in response to substrate binding. The LID domain is shown in green, the extended shikimate-binding domain (ESB) is shown in purple and the nucleotide-binding domain (marked as ABD) is shown in blue. Upon binding of either shikimate or ATP to the SBD or ABD domains, respectively, movement of the LID domain over the active site is observed [36].

Several studies including crystallography, circular dichroism, fluorescence and molecular dynamic (MD) simulations have served to identify some of the key interactions in *Mt*SK essential for catalysis [37]. Shikimate is known to bind to a pocket formed by the conserved residues Asp34, Arg58, Gly80, and Arg136, where the interactions with Asp34 and Arg 136 are essential for proper positioning of shikimate [38]. Binding of ATP or ADP to *Mt*SK involves interactions with the P-loop, the AB-loop and the α6 motifs, where Arg110, Arg 117, Gly12 and Pro155 play important roles for the recognition of the adenine moiety of the nucleotides [39].

The availability of crystal structures of *Mt*SK complexed with its substrates, as well as the knowledge of the functional factors leading to *Mt*SK active site closure, have provided crucial information for the rational design of non-promiscuous inhibitors of *Mt*SK [40-41]. Given that the ATP-binding site of SK is shared by many P-loop kinases, ATP-binding-site inhibitors would most likely lack specificity [41]. However, inhibitors targeting the shikimate binding site of the enzyme would represent a unique class of drugs that could block the biosynthesis of aromatic amino acids and other compounds essential for the growth and viability of *Mycobacterium tuberculosis* [42].

1. 4 Applications of high-resolution mass spectrometry in drug discovery

In mass spectrometry (MS), mass resolution represents the capability to separate two closely spaced spectral peaks of corresponding ions with different elemental compositions, and is typically defined as the minimum mass difference, $m_2 - m_1$, between two peaks such that the valley between their sum is a specified fraction of the height of the smaller individual peak.

Mass-resolving power (R) may be defined either for a single spectral peak as $R=m/\Delta m_{50\%}$, or for two equal-magnitude peaks as $R=m_2/(m_2 - m_1)$, in which m is the molecular mass and $\Delta m_{50\%}$ is the mass spectral peak width at half maximum peak height (FWHM) (Fig. 1.6). Mass-resolving power is useful for evaluating mass analyzer performance because it is a measure of precision over a wide range of m (or m/z), whereas mass resolution determines the ability to distinguish ions of different elemental composition [43-44]. Mass accuracy (or mass error) is defined as the difference (Δm) between the measured mass (m_i) and calculated mass (m_a) from elemental composition (e.g. $C_cH_hN_nO_oS_sP_p$) of an ion or molecule, where Δm could be positive or negative and expressed in different units such as (m_i-m_a) in Da, (m_i-m_a) $\times 10^3$ in mDa and (mi-m_a) /m_a $\times 10^6$ in ppm [45].

Over the past decade, mass spectrometry has been revolutionized by access to instruments of increasingly high mass-resolving power. It has become possible to analyze small molecules and to determine their elemental compositions from accurate mass measurements. In biomolecules analysis, it has become possible to identify and characterize post-translational modifications and to map the binding surfaces of large biomolecule complexes [43].

High-resolution mass spectrometry (HRMS) has been applied to all stages of the drug discovery and development processes for many years [46]. The ability to analyze and quantify low levels of oligonucleotides, peptides, proteins and small-molecule drugs in automated, high-throughput assays has been greatly enhanced by the capabilities of HRMS [47]. With the development of new ionization techniques such as electrospray ionization (ESI) and matrix-assisted laser desorption ionization (MALDI), mass spectrometry has emerged as the main analytical tool for the identification and characterization of protein targets, structure elucidation of synthetic compounds, and early drug metabolism and pharmacokinetics studies.

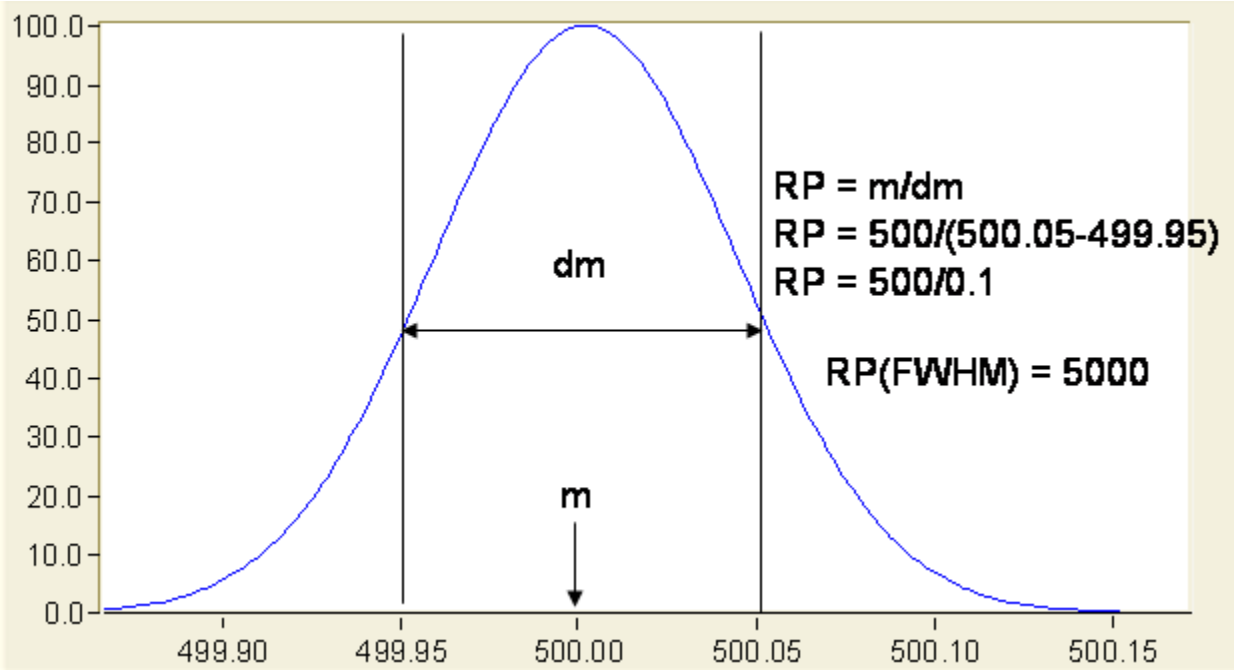

Figure 1.6. Example of mass resolving power calculated for a single peak at 50% height.

Proteins that are capable of modifying a disease state and that are amenable to interactions with small, drug-like molecules are acceptable drug targets for drug discovery processes. Target based drug discovery is an important strategy for developing new therapeutic agents. The role of mass spectrometry in this early phase comprises the identification and validation of biological targets and the development of assays to identify compounds (hits) with activity against target function.

Two MS-based strategies have been employed in recent years for the screening and evaluation of compounds: affinity-based and function-based strategies [48]. In the affinity-based approach, compounds are screened based on their binding affinities to a protein target. Affinity-based methods can detect protein-ligand binding by either direct or indirect methods. In direct

methods, a protein target is exposed to a mixture or library of compounds and then analyzed by ESI-MS [49]. For this approach, the experimental conditions must be optimized in such a way that non-covalent protein-ligand interactions are preserved throughout the ESI-MS analysis. Covalent protein–ligand complex are more easily preserved in the gas phase [50]. Interactions are detected by measuring the mass of the protein-ligand complexes directly. Indirect methods are based on the identification of binding compounds after the compounds have been separated from the target protein using a separation technique (e.g., chromatography or ultrafiltration) to isolate the protein–ligand complex from the unbound components before MS analysis (Fig. 1.7). Both direct and indirect affinity-based methods have been successfully applied to the screening of compound mixtures, including combinatorial libraries and unpurified natural product extracts in the drug discovery process [49].

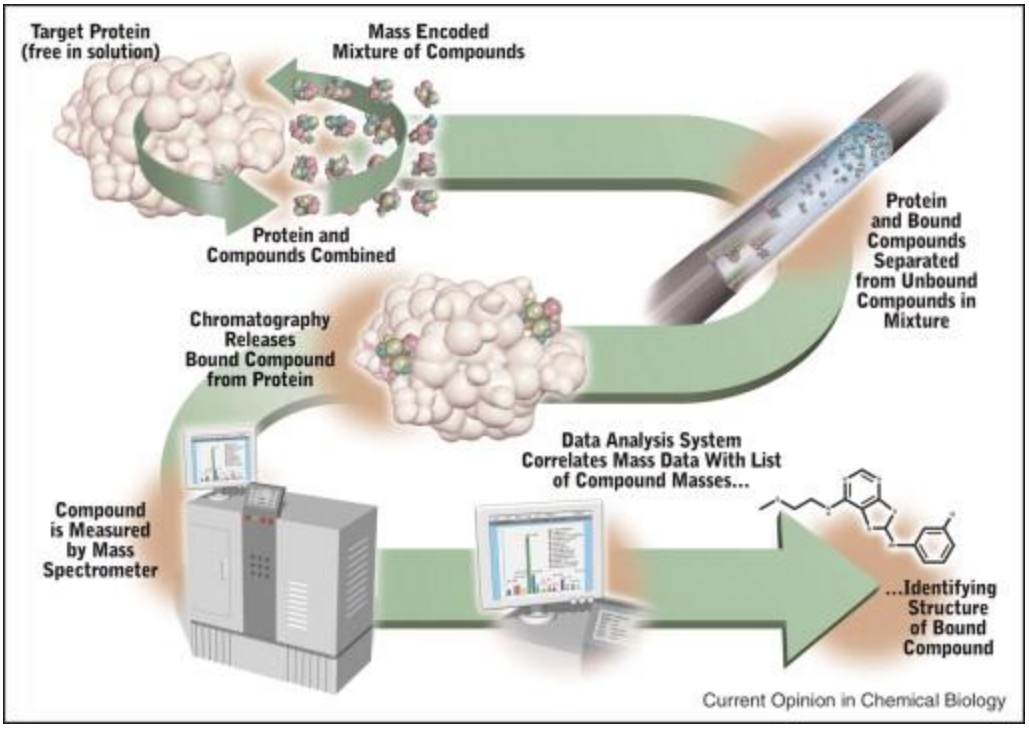

Figure 1.7. Schematic representation of the affinity-based MS strategy [49].

In the function-based approach, the effects of compounds on the function of a target (e.g., enzymatic activity) are measured. These assays often rely on quantifying either the disappearance of a substrate or the appearance of a product of an enzymatic reaction [48]. Although spectrophotometric or spectroflurometric methods are more commonly used for function-based approaches in the drug discovery workflow due to their amenability to automation and simplicity in nature, these detection methods require that the analyte to be quantified exhibits a well-resolved absorbance or fluorescence of sufficiently high signal at a desirable wavelength. Unfortunately, this is not always the case and most of the times, enzymatic coupled assays involving two or more enzymes have to be employed, complicating the hit discovery process.

Mass spectrometry has become a powerful tool in the study enzyme kinetics and the discovery of hit compounds using functional-based approaches. The main advantage of MS is that it can detect a wide range of molecules with high sensitivity and molecular selectivity eliminating the need of chromophores or secondary enzymatic reactions. MS method development is usually fast with appropriate instrumentation and false positives and false negatives are rare as the mass of an analyte or its fragments, generated by collision-induced fragmentation (CID) in a tandem mass spectrometer, is generally unique [51].

The work in this dissertation is largely focused on a function-based strategy to identify and characterize inhibitors of shikimate kinase from *Mycobacterium tuberculosis* (*Mt*SK) using electrospray ionization (ESI) and a hybrid quadruple-time-of-flight (Q-TOF) high resolution mass spectrometer. The quantitative capacity of electrospray ionization mass spectrometry (ESI-MS) makes it particularly attractive for function-based assays.

Using this approach, we have developed a functional assay that allows rapid and quantitative measurements of the enzymatic activity of *Mt*SK by monitoring the time-dependent increase or decrease in the concentration of the reaction product shikimate-3-phosphate. Natural products from marine origins and a synthetic library of compounds have been screened, and compounds that modulate the activity of *Mt*SK "hits" have been identified for further "lead optimization" and hopefully "drug candidates" in pre-clinical and clinical stages for the treatment of tuberculosis.

1.5 Project rationale

Mycobacterium tuberculosis (*Mtb*), the causative agent of tuberculosis (TB), remains a leading cause of millions of deaths every year. The emergence of resistant strains of *Mtb*, the complication with HIV co-infection and the persistent nature of TB infection requiring exceptionally long treatments, all call for the development of new antimycobacterial agents to combat TB. Recent advances in molecular tools have facilitated the identification of targets essential for *Mtb* survival and persistence, and one potential target is the shikimate pathway. This pathway is responsible for the biosynthesis of aromatic compounds in bacteria, and its essentiality has been proven in cultures of bacteria lacking the genes codifying for the enzymes of the pathway, whose growth is completely inhibited even when exogenous aromatic supplements are provided. Owing to the demonstrated essentiality and to the fact that this pathway is absent from mammalian cells, the enzymes of the shikimate pathway offer attractive targets for early stage drug discovery.

Whole-cell phenotypic screening followed by target-directed screening represent two complementary approaches to discover viable new starting point scaffolds for medicinal chemistry optimization [52]. Phenotypic whole cell screenings in tuberculosis drug discovery have proven effective for the identification of hits possessing "drug-like" characteristics, such as cell penetration, and for the early assessment of toxicity of certain scaffolds. In this work we have employed a target-based approach using mass spectrometry to identify inhibitors of shikimate kinase (*Mt*SK), the fifth enzyme of the shikimate pathway. Compounds derived from natural and synthetic sources that have shown to be active through phenotypic screenings with *Mtb* cells were evaluated against *Mt*SK. Thus, the rationale of this study is that the combination of these two approaches will lead to the identification of scaffolds with activity against *Mt*SK that have also demonstrated to be active against whole cells of *M. tuberculosis*, representing an excellent starting point for the development of safer, more marketable and cost effective drugs to treat tuberculosis.

1.6 Research objectives

The aim of this project is to functionally characterize shikimate kinase from *Mycobacterium tuberculosis* (*Mt*SK) and to identify and characterize inhibitors using mass spectrometry and docking based approaches. Only a few inhibition studies involving *Mt*SK have been performed to date, therefore, the findings reported in this research will provide insight into the rational design of inhibitors of *Mt*SK as potential drugs for the treatment of tuberculosis. The specific goals of this research are to:

1. Clone, express and purify shikimate kinase from *Mycobacterium tuberculosis*.

2. Functionally characterize *Mt*SK using conventional spectrophotometric methods.

3. Develop and validate an enzymatic assay for the kinetic evaluation of *Mt*SK and inhibition using liquid-chromatography mass spectrometry (LC-MS).

4. Screen a library of synthetic antimycobacterial compounds to identify inhibitors of *Mt*SK by LC-MS and molecular docking.

5. Identify and fully characterize manzamine alkaloids from marine sources as inhibitors of *Mt*SK using LC-MS and molecular docking approaches.

6. Identify and characterize the binding sites on the irreversible inhibition of *Mt*SK by the marine metabolite ilimaquinone.

Chapter 2: Generation and characterization of *Mycobacterium tuberculosis* shikimate kinase (*Mt*SK)

2.1 Introduction

Mycobacterium tuberculosis (*Mtb*) is a small, aerobic, non-motile bacillus and the causative agent of most cases of tuberculosis [53]. The complete genome sequence of the *Mtb* H37Rv strain was published in 1998 and genes involved in metabolic pathways have been identified by sequence homology [54]. Among the genes identified, homologues to the enzymes in the shikimate pathway designated as: *aroD* (3-dehydroquinate dehydratase), *aroB* (3-dehydroquinate synthase), *aroK* (shikimate kinase), *aroF* (chorismate synthase), *aroG* (DAHP synthase), *aroE* (shikimate dehydrogenase), and *aroA* (EPSP synthase) have been proven to be essential to the viability of *mycobacterium tuberculosis* [26]. The *aroK* gene codifying for shikimate kinase, the fifth enzyme of the shikimate pathway, is the focus of this research.

Determination of the steady-state kinetic parameters of shikimate kinase from *Mtb* has been limited compared to that from other species [31, 55]. In this chapter we describe the cloning, expression purification and the functional characterization of wild-type shikimate kinase from *Mycobacterium tuberculosis* using spectrophotometric methods. The *aroK* gene was cloned into a pET expression vector with a C-terminal six-histidine tag for purification purpose and the resulting construct was transformed into the *E. coli* strain BL21 (DE3).

2.2 Materials and methods

2.2.1 Chemicals

Imidazole, ampicillin (AMP), chloramphenicol (CAM) and phenylmethylsulfonyl fluoride (PMSF) were purchased from Sigma (St. Louis, MO). Isopropyl-β-d-thiogalactopyranoside (IPTG) was obtained from Fisher (Pittsburgh, PA). Bugbuster and benzonase nuclease were purchased from Novagen (Madison, WI). All restriction enzymes were purchased from New England Biolabs (Beverly, MA). All oligonucleotide primers were purchased from Invitrogen (Carlsbad, CA). The *E. coli* strains (BL-21-Gold [DE3] pLysS and XL-1 Blue), *Pfu* polymerase, and T4 DNA ligase were purchased from Agilent (La Jolla, CA). Nickel-nitrilotriacetic acid (Ni-NTA) resin was purchased from Qiagen (Valencia, CA). Desalting 10DG chromatography columns were purchased from Bio-Rad (Hercules, CA). The substrates adenosine-5'-triphosphate (ATP), shikimate, reduced nicotinamide adenine dinucleotide (NADH), phosphoenolpyruvate (PEP) and the enzymes pyruvate kinase (PK) and lactate dehydrogenase (LDH) used in the coupled assay were purchased from Sigma-Aldrich (St. Louis, MO). All organic solvents were HPLC or LC-MS grade and were purchased from Thermo Fisher (Hanover Park, IL). All buffers and media were prepared using water purified by a Milli-Q purification system (Millipore, Billerica, MA) or by a Barnstead EasyPure II system (18.2 MΩ/cm resistivity).

2.2.2 Construction of pET20b-*Mt*SK plasmid

The *Mt*SK gene (*aroK*) coding sequences were PCR amplified from the pProEX-*Mt*SK plasmid provided by Southern Research Institute (Birmingham, AL) and subcloned into pET-

20b(+) expression vector (Novagen, Madison, WI) using its *Nde I-Xho I* restriction sites. Two synthetic oligonucleotide primers were designed to amplify the *Mt*SK gene and to introduce an *Xho I* restriction site at its 3' end. The sequences for these primers were: (sense: 5'-Phos-ATGGCACCCAAAGCGGTTCTCGTCGGCC-3' and antisense: 5'TATCTCGAGTGTGGCCGCCTCGCTGGGGCTG-3'). For amplification of the expression vector sequence, the primers designed were (sense: 5'ACCTGCTCGAGCACCACCACC-3' and antisense: 5'-Phos-ATGTATATCTCCTTCTTAAAGTTAAACAAAATTATTTCTAGAGGG-AAACC-3').

Both PCR products were digested with *Xho I* followed by heat inactivation and ligation using T4 DNA Ligase (Quick LigationTM kit) according to manufacturer's instructions. PCR products of gene and vector carrying *Xho I* cohesive ends were ligated together and the 5' end of *Mt*SK gene was ligated with the *Nde I* site of the expression vector in a blunt-end manner. The resulting construct was used to transform *E. coli* (XL-1 Blue) by heat shock according to manufacturer's instructions. Transformants were selected on the basis of ampicillin resistance, and the plasmids from candidate colonies were isolated and verified by diagnostic restriction digest with endonucleases *Nde I and Xho 1*. A DNA sequence analysis was performed (Davis Sequencing, Davis, CA) to confirm the identity of *Mt*SK and to verify that no unintended mutations were introduced during PCR procedures. The plasmid carrying the verified *Mt*SK sequence was used to transform *E. coli* (BL-21- Gold [DE3] pLysS). Transformants were selected on the basis of ampicillin and chloramphenicol resistance.

2.2.3 *Mt*SK expression and purification

*Mt*SK expression was carried out in *E. coli* (BL-21-Gold [DE3] pLysS) using Luria-Bertani broth supplemented with ampicillin (100 µg/mL) and chloramphenicol (100 µg/mL). Cells were grown at 37ºC with constant agitation (250 rpm) to mid-log phase (OD_{600} = 0.4) and induced by IPTG (1 mM). The cells were then grown for an additional 4 hours post-induction, harvested by centrifugation at 5,000 rpm for 15 min at 4 ºC and stored at -80 ºC until purification. Expression analysis was carried out using a trichloroacetic acid (TCA) precipitation protocol as described by Varnado et al. except that 11% acrylamide SDS-PAGE gels were used [56]. A solubility test protocol was followed to determine the proper method of purification. Expression analyses revealed the presence of a protein with the anticipated molecular weight in the soluble and insoluble fractions (Fig. 2.1). Consequently, protocols were developed to purify the protein in soluble state and insoluble (i.e., inclusion body) state.

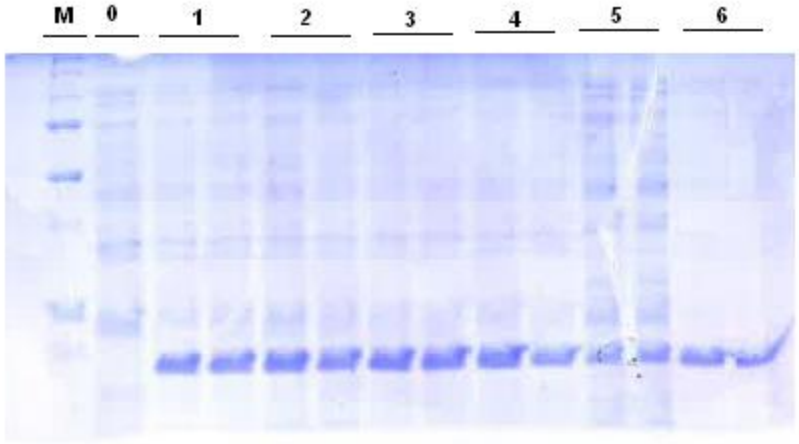

Figure 2.1. SDS-PAGE analysis of proteins precipitated by TCA protocol. Protein molecular weight marker M (λ DNA-HindIII Digest). Lanes show protein fractions of recombinant BL21(DE3)/ pET20b-*Mt*SK cells at time of induction with 1 mM IPTG (lane 0), after 1 h post-induction (lanes 1), 2 h post-induction (lanes 2), 3 h post-induction (lanes 3), and 4 h post-induction (lanes 4). Lanes 5 and 6 show the soluble and insoluble protein fractions of recombinant BL21(DE3)/pET20-*Mt*SK cells after 4 hours of induction with IPTG, respectively.

For soluble protein purification, cell pellets were resuspended in buffer A (50 mM Tris-HCl, pH 7.4; 500 mM NaCl) in the presence of PMSF (0.1 mM). The mixture was homogenized with a dounce homogenizer and lysed by sonication using a Branson Sonifier 250 (Branson Ultrasonics Corp., Danbury, CT, USA), set at output control of 3.5 and 30% duty cycle for 8 intervals of 42-s each with cooling on ice between each sonication. Following sonication, benzonase nuclease (250 U) was added, and the mixture was incubated for 2 hours at 4 ºC with gentle stirring. The cell lysate was centrifugated at 10,000 rpm for 15 min at 4 ºC, the supernatant was collected and the pellets were stored at -80 ºC for further denaturing purification. The supernatant was loaded onto a column with Ni-NTA resin by re-circulating the solution through the column at 1 mL/min overnight. After loading, the column was washed in succession with 50 mM Tris, pH 8.0, followed by buffer A supplemented with 2 mM, 20 mM, 50 mM, 100 mM, 500 mM and 1M imidazole. The eluted fractions were collected and analyzed by SDS-PAGE. The fraction containing the protein (100 mM imidazole) was concentrated by ultrafiltration with a 3 kD molecular cutoff filter (Amicon, Billerica, MA) and subjected to buffer exchange using a 10DG size exclusion column (BioRad, Hercules, CA) equilibrated with buffer A.

For denaturing purification, pellets reserved from the soluble purification procedure were resuspended in buffer B (50 mM Tris-HCl, 500 mM NaCl and 8M Urea) and homogenized at room temperature. The mixture was centrifuged at 10,000 rpm for 15 min and the supernatant was collected and mixed with Ni-NTA resin pre-equilibrated with buffer B. The protein/resin mixture was allowed to bind overnight with gently agitation at room temperature. Next day, this mixture was loaded onto an empty column, washed with 25 mL of buffer B supplemented with 20 mM imidazole and the protein was then eluted off the column with 25 mL of buffer B

supplemented with 400 mM imidazole. Urea and imidazole were removed by dialysis against buffer A for 20 hours, replacing the dialysis buffer every 4-6 hours. The concentration of *Mt*SK was measured using the Pierce BCA Protein Assay (Pierce, Rockford IL) using bovine serum albumin as a standard, according to manufacturer's instructions. Enzyme purified by denaturing conditions was employed for the results presented in this section.

2.2.4 ESI-LC-MS analysis of intact *Mt*SK

Intact *Mt*SK analysis was performed on an Agilent (Little Falls, DE) 6520 Accurate-Mass Q-TOF mass spectrometer coupled to an Agilent 1200 RRLC system. ESI was conducted using a capillary voltage of 4000 V; the nebulizing and drying gases were nitrogen supplied at 25 psig and 10 L/h, respectively, and the drying gas temperature was 350 °C. The TOF fragmentor and skimmer were set to 180 V and 65 V, respectively. Samples were injected onto a Zorbax 300SB-C18 (2.1 x 100 mm; 3.5-Micron Agilent Technologies, Inc.) column with a flow rate of 0.4 mL/min. The mobile phase consisted of water with 0.1% (v/v) formic acid (A) and acetonitrile with 0.1% (v/v) formic acid (B) with a gradient elution as follows: 30% B at 0 min, 80% B at 3 min, and 30% B at 5 min. Each run was followed by a 1 min post-run with 30% B. The total run-time analysis was 6 min and the column temperature was 27 °C. Spectra were acquired in the positive (ES+) ion mode, and full scan mass spectra (*m/z* 300–3200) were collected at a rate of 1 spectrum/sec. Mass data obtained from LC-MS was analyzed using Agilent MassHunter Qualitative Analysis software and Agilent MassHunter BioConfirm software version B.02.00.

2.2.5 Spectrophotometric coupled assay

The enzymatic activity of *Mt*SK was assayed by a double coupled assay involving the enzymes pyruvate kinase (EC 2.7.1.40) and lactate dehydrogenase (EC 1.1.1.27) following procedures described by Rosado et al [55]. In this assay, the release of ADP (adenosine diphosphate) by the shikimate kinase-catalyzed reaction leads to oxidation of NADH (nicotinamide adenine dinucleotide) to NAD^+, and the decrease in NADH concentration is monitored at 340 nm (ε = 6220 M^{-1} cm^{-1}). Assay mixtures (1 mL final volume) consisted of 100 mM Tris-HCl, pH = 7.6, 100 mM KCl, 5mM $MgCl_2$, 5 mM shikimate, 1.2 mM ATP, 1.5 mM PEP, 0.2 mM NADH, 3 U/mL pyruvate kinase and 2.5 U/mL lactate dehydrogenase. Reactions were started by the addition of *Mt*SK (20 nM), and the change of absorption was monitored for 3 minutes at 340 nm. In this reaction, the oxidation of NADH is stoichiometrically equivalent to the production of ADP and S3P by *Mt*SK because *Mt*SK is the rate limiting factor of the coupled reaction.

Steady-state kinetic parameters were determined from initial velocity measurements using the same procedure described above with varying concentrations of one substrate and keeping the other substrate concentration fixed at a saturating concentration as follows: varying ATP (0.05 mM – 1.2 mM) and 5 mM shikimate; varying shikimate (0.2 mM – 5 mM) and 1.2 mM ATP. Data were collected in triplicate, and values of the steady-state kinetics parameters were obtained by fitting the data to the Michaelis-Menten equation (1) using GraphPad Prism 5.02 software (Mountain View, CA).

$$v_0 = \frac{V_{max}[S]}{K_M + [S]} \qquad (1)$$

All spectra were obtained at room temperature on a Shimadzu UV-1601 spectrophotometer (Columbia, MD) with a cell path length of 1.0 cm.

2.3 Results and discussion

2.3.1 Recombinant *Mt*SK LC-MS analysis

The deconvoluted ESI-MS spectrum of *Mt*SK demonstrated the presence of two species with an average molecular mass of 19,648.63 Da and 19,517.42 Da (Figure 2.2), respectively, exhibiting a mass difference of 131.2 Da. This mass difference is consistent with the post-translational removal of N-terminal methionine, a modification performed by the enzyme methionine aminopeptidase (MAP). This modification is often observed during expression of recombinant proteins by *E. coli* in which the second amino acid is alanine, glycine, proline, serine, threonine or valine [57-58]. The average molecular mass for intact *Mt*SK (19,648.63) was in good agreement with the theoretical mass calculated from the amino acid sequence (19,648.59 Da). This result thereby demonstrates the identity and purity of the recombinant *Mt*SK used for this study.

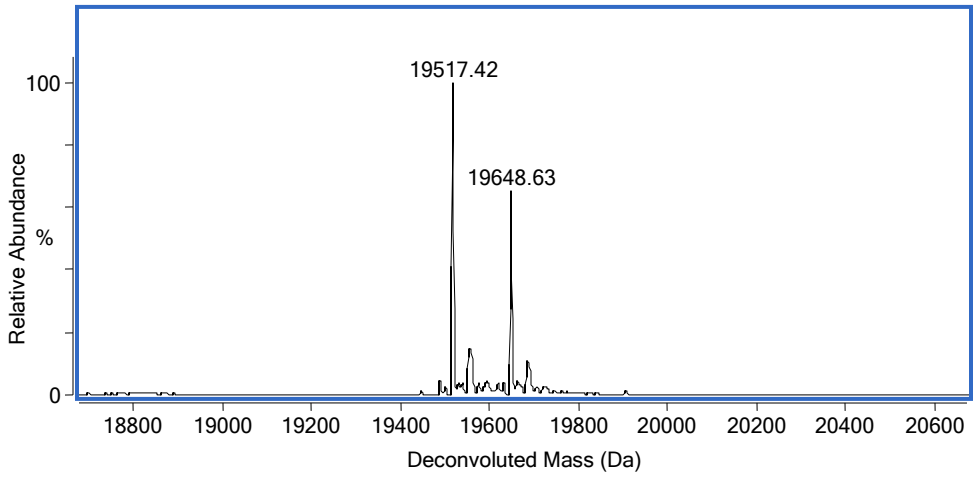

Figure 2.2. Deconvoluted ESI-MS spectrum showing both modified (19517.42) and unmodified (19648.63) recombinant *Mt*SK.

2.3.2 Kinetic characterization of *Mt*SK by spectrophotometric coupled assay

Determination of the optimum reaction conditions was carried out for the UV coupled assay. To yield valid steady-state kinetic parameters for *Mt*SK using this method, it was necessary to ensure that the rate of NADH consumption was strictly due to *Mt*SK functioning as the rate-limiting step. In order to determine the appropriate concentration of enzyme to be used in the coupled assay, different reactions using varying concentrations of shikimate kinase (0 – 80 nM) were performed while keeping the concentrations of the rest of the reagents constant. Figure 2.3 shows that at concentrations of *Mt*SK below 40 nM, a linear increase in activity was observed. Consumption of NADH was decreased at shikimate kinase concentrations upwards of 40 nM. Therefore, 20 nM of *Mt*SK was used for subsequent coupled assay experiments. All samples were run in triplicate, a molar extinction coefficient (ε) for NADH of 6220 M^{-1} cm^{-1} and a path length of 1 cm were used for the assay.

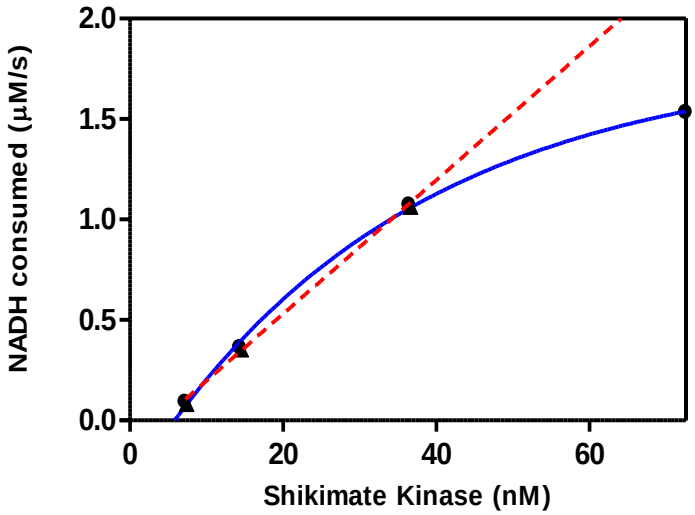

Figure 2.3. Effect of *Mt*SK concentration on NADH consumption to determine the optimum rate-limiting enzyme concentration.

Steady-state kinetics parameters for each substrate were determined by the coupled assay using the same range of concentrations for ATP and shikimate described above, 20 nM *Mt*SK and fixed concentrations of the other reagents (1.5 mM PEP, 0.2 mM NADH, 3 U/mL pyruvate kinase and 2.5 U/mL lactate dehydrogenase). The K_M and k_{cat} values calculated for ATP were 0.17 mM and 64 s^{-1}, respectively, and for shikimate these values were 0.51 mM and 63 s^{-1}, respectively (Fig. 2.4). Table 2.1 shows the kinetic constants calculated from the enzyme-coupled assay, as well as the ones reported in the literature.

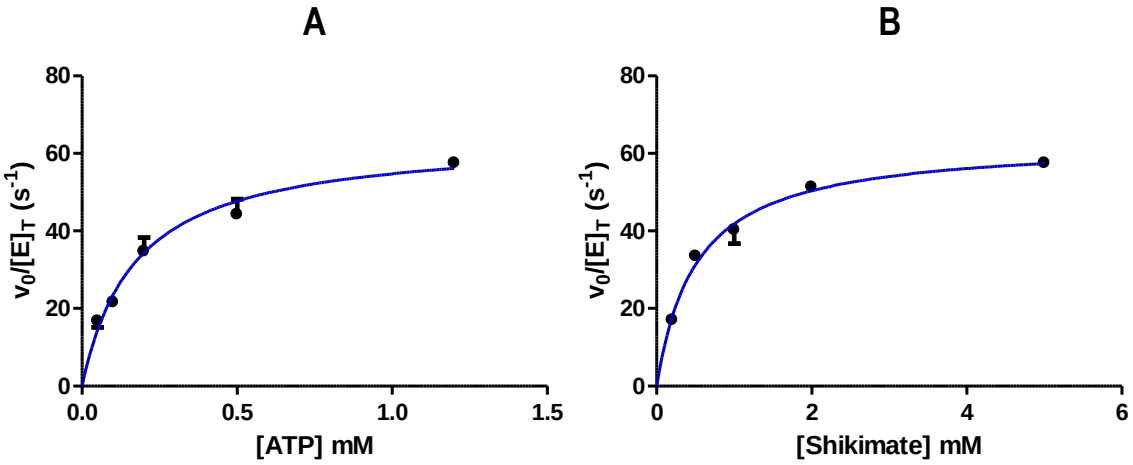

Figure 2.4. Initial velocity plots, showing Michaelis-Menten kinetics with respect to (A) ATP and (B) shikimate concentrations obtained by the coupled assay. Experiments were carried out in triplicate at five different concentrations of each substrate and at fixed concentrations of *Mt*SK (20 nM from insoluble purification prep.), PEP (1.5 mM), NADH (0.2 mM), PK (3 U/mL) and LDH (2.5 U/mL) at room temperature. Assays carried out for panel A contained 5 mM shikimate and assays carried out for panel B contained 1.2 mM ATP.

Table 2.1. Kinetic parameters of *Mt*SK calculated from the UV-coupled assay.

	UV-coupled assay[a]		Literature[b] UV-coupled assay		Literature[c] UV-coupled assay	
	ATP	**Shikimate**	**ATP**	**Shikimate**	**ATP**	**Shikimate**
K_M **(mM)**	0.17 ± 0.02	0.51 ± 0.04	0.11 ± 0.004	0.65 ± 0.03	0.08 ± 0.004	0.41 ± 0.02
k_{cat} **(s^{-1})**	64 ± 2	63 ± 1	60 ± 8	60 ± 8	44 ± 2	44 ± 2

[a]Values obtained in this study
[b]Values reported by Rosado et al.[55]
[c]Values reported by Gu et al.[31]

2.4 Conclusion

In this section, the pET20b-*Mt*SK plasmid was constructed by PCR, amplifying the protein coding region of shikimate kinase from the pProEX-*Mt*SK plasmid with the addition of an *Xho I* restriction sites restriction sites. The resulting construct was transformed into *E. coli* cells and the active enzyme was purified in soluble and insoluble states by immobilized-nickel ion affinity chromatography. The deconvoluted ESI-MS spectrum of *Mt*SK only showed signals corresponding to unmodified protein (19,648.63) and modified protein (19,517.42 Da) by the post-translational removal of N-terminal methionine residue (131.2 Da) verifying the identity of the purified protein. The functional activity of *Mt*SK was assessed by determination of the kinetic parameters using a spectrophotometric assay that couples the ATP hydrolysis catalyzed by *Mt*SK to the oxidation of NADH via the auxiliary enzymes pyruvate kinase and lactate dehydrogenase. Kinetic parameters of *Mt*SK (K_M and k_{cat}) determined by this method were in agreement with the values previously reported in the literature.

Chapter 3: Development of an ESI-LC-MS based assay for kinetic evaluation of *M. tuberculosis* shikimate kinase activity and inhibition.

3.1 Introduction

Due to the to the indistinct ultraviolet absorption of the substrates (ATP and shikimate) and products (ADP and S3P) present in the reaction catalyzed by *Mt*SK, the activity of this enzyme is usually measured by a spectrophotometric coupled assay involving the enzymes pyruvate kinase (PK) and lactate dehydrogenase (LDH) (Fig 3.1). This coupled assay is based on the conversion of ADP produced by *Mt*SK to ATP by pyruvate kinase (PK) in the presence of phosphoenol pyruvate (PEP). The pyruvate generated in the PK reaction is then reduced to lactate by lactate dehydrogenase (LDH) in the presence of NADH, which is oxidized to NAD^+ [59]. NADH has an absorption maximum at 340 nm, a wavelength that NAD^+ does not absorb. Consequently, the activity of *Mt*SK can be monitored by measuring the decrease in absorbance at 340 nm.

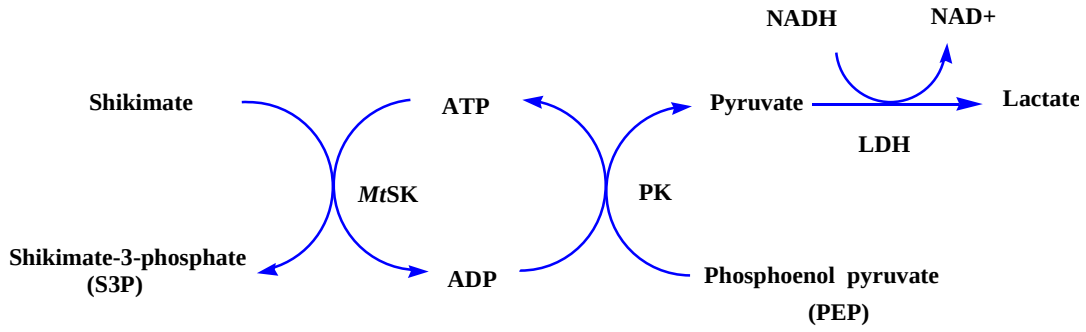

Figure 3.1. Pyruvate kinase (PK)/lactate dehydrogenase (LDH) coupled assay.

While this assay has been widely used for the determination of kinetic parameters of ATP-dependent kinases including SK from different species [55, 60-62], it presents major drawbacks and limitations. First, by monitoring the disappearance of NADH, this assay measures a decrease in signal rather than an increase, resulting in restrictions on the dynamic range of the assay if large amounts of NADH are used. Sensitivity is also compromised due to the relatively low extinction coefficient of NADH. Additionally, the presence of coupling enzymes and additional substrates adds more reaction steps, making the assay more difficult to optimize and more expensive to implement if one must purchase the coupling enzymes and co-substrates. Finally, and most importantly, this assay may have limitations for the screening and validation of compounds with inhibitory activity. Assay interferences can arise from the compounds themselves, as is the case for fluorescent compounds, leading to aberrant detection readouts. Often, false positives occur if the compounds being screened are potential inhibitors or substrates of the coupling enzymes, emphasizing the need for subsequent orthogonal and secondary assays for confirmation of hits [63].

Soft ionization methods, such as electrospray ionization (ESI) and matrix-assisted laser desorption/ionization (MALDI) mass spectrometry (MS) coupled to LC have been utilized as an alternative to spectrophotometric methods for the study of enzyme kinetics and inhibitor discovery [64-69]. MS methods can directly detect and quantify the formation of products and/or the consumption of substrates, eliminating the need for secondary enzymatic reactions unrelated to the target enzyme.

In this section, we describe a straightforward, sensitive and reproducible LC-MS assay for the kinetic characterization of *Mt*SK, including the screening and characterization of inhibitors. This assay is based on the detection of the reaction product shikimate-3-phosphate using ESI and

a quadrupole time-of-flight (Q-TOF) detector and it was developed using procedures previously described by Mulabagal et al., as a platform [70].

The method was validated for linearity, intra- and inter-day precision, limit of detection (LOD) and limit of quantitation (LOQ) using an S3P external standard, and it was successfully applied to the kinetic characterization of a previously reported inhibitor of shikimate kinase. A comparative analysis of this new LC-MS assay with a conventional coupled assay was also performed.

Kinetics parameters of *Mt*SK (K_M and k_{cat}), as well as the inhibition constants (K_i and ${}_{\alpha}K_i$) of the positive reference compound determined by the LC-MS assay were in good agreement with those determined using the coupled assay and with those reported in the literature. Furthermore, a noncompetitive mechanism of inhibition was delineated, verifying the accuracy and reliability of the LC-MS assay. Overall, the selectivity and enhanced sensitivity of LC-MS methods over conventional UV-vis spectroscopy methods demonstrates that LC-MS can be used for the screening of inhibitors and to accurately monitor steady-state kinetics of any enzymatic reaction where chromogenic substrates or products are not available, provided an appropriate external standard for calibration is found.

3.2 Materials and methods

3.2.1 Chemicals

Dimethyl sulfoxide (DMSO), shikimate-3-phosphate (S3P) used for the calibration curve, the substrates adenosine-5'-triphosphate (ATP) and shikimate were purchased from Sigma-Aldrich (St. Louis, MO). Reference standard for inhibition: (compound **1**: 3-methoxy-4-{[2-({2-

methoxy-4-[(4-oxo-2-thioxo-1,3-thiazolidin-5-ylidene) methyl] phenoxy} methyl) benzyl]oxy} benzaldehyde was purchased from ChemBridge (San Diego, CA). All organic solvents were HPLC or LC-MS grade and were purchased from Thermo Fisher (Hanover Park, IL). All buffers and media were prepared using water purified by a Milli-Q purification system (Millipore, Billerica, MA) or by a Barnstead EasyPure II system (18.2 MΩ/cm resistivity).

3.2.2 LC-MS activity assay

An end-point LC-MS assay based on the quantitative determination of the product S3P *m/z* = 253.0119 $[M - H]^-$ was employed. All assays were performed in a buffer consisting of 100 mM Tris-HCl pH = 7.6, 50 mM KCl and 5 mM $MgCl_2$ at 25 °C. Reactions were initiated by the addition of purified *Mt*SK (0.2 µM) to an Eppendorf tube containing assay buffer and the substrates at the following saturating conditions: ATP (1.2 mM) and shikimate (5 mM) to a final volume of 500 µL. After incubation for 30 seconds, reactions were quenched by the addition of 2 µL of 98% formic acid followed by vortexing.

For mass spectrometric analyses, 5 µL of quenched reaction mixtures were injected onto a reversed-phase column (Zorbax Eclipse Plus Phenyl-hexyl, 4.6 x 100 mm 3.5 µm, Agilent Technologies, Inc.). The mobile phase consisted of water with 0.1% (v/v) formic acid (A) and acetonitrile 100% (B) with a gradient elution as follows: 0 min, 2% B held for 4 min, to 30% B in the next 2 min. Each run was followed by a 1 min post-run with 2% B. The total run-time analysis was 7 min at a flow rate of 0.4 mL/min and a column temperature of 45 °C. All acquisitions were performed under negative ionization mode using a narrow *m/z* range (*m/z* 100-300). Mass spectrometric detection was carried out in an Agilent (Little Falls, DE) 6520 Accurate-Mass Q-TOF mass spectrometer equipped with an Agilent 1200 RRLC. The

nebulizing and drying gases were nitrogen supplied at 25 psig and 10 L/h, respectively, and the drying gas temperature was 350 °C. A capillary voltage of 3200 V was used for the ESI source, and the fragmentor voltage was set to 175 eV. For quantification of S3P, extracted ion chromatograms (EIC) of m/z 253.0119 $[M - H]^-$ were integrated using Agilent MassHunter Workstation Qualitative Analysis software (version B.02.00), and the peak area was used to evaluate enzyme activity.

Determination of steady-state kinetic parameters for each substrate was performed using the same conditions described above but varying the concentration of one substrate and keeping the other substrate concentration fixed as follows: varying ATP (0.05 mM – 1.2 mM) and 5 mM shikimate; varying shikimate (0.2 mM – 5 mM) and 1.2 mM ATP. Samples were prepared in replicates and analyzed two times. The data were averaged and fitted to the Michaelis-Menten equation (Eq. 1) using GraphPad Prism 5.02 software (Mountain View, CA).

$$v_0 = \frac{V_{max}[S]}{K_M + [S]} \qquad (1)$$

3.2.3 Calibration curve and method validation

The optimized LC-MS method was validated using parameters such as linearity, limit of detection (LOD), limit of quantification (LOQ) and precision. The linearity of the method was evaluated by analyzing a series of concentrations (0.0004 - 1 mM) of shikimate-3-phosphate (S3P) standard. Standard solutions were prepared by weighting the proper amount of S3P reference standard (corrected for purity) and dissolving it in a solution containing 100 mM Tris-HCl pH 7.6, 50 mM KCl, 5 mM $MgCl_2$, 1.2mM ATP, 5 mM shikimate and 0.2 μM *Mt*SK pre-quenched with 98% formic acid. From this stock solution, serial dilutions were prepared to

obtain the desired range of concentrations. Calibration curves were constructed by injecting each standard solution at each concentration level in triplicate. The peak areas were calculated from extracted ion chromatograms (EIC) of the most abundant ion (*m/z* 253.0119 $[M - H]^-$) and the data were plotted against the corresponding concentration using least squares linear regression. The parameters of the linear equations were used to obtain concentration values of the S3P formed in each reaction mixture. The LOD and LOQ were defined as the lowest concentration with a signal-to-noise (S/N) ratio of 3 and 10, respectively. The precision of the method was evaluated by determining the intra-day and inter-day relative standard deviations (RSD) of the measured concentrations of S3P in a 100% control experiment (in the absence of inhibitor) and a 50% control experiment (in the presence of reference compound **1** at its K_i concentration). Each sample was injected 10 times the same day and on four consecutive days under the same experimental conditions.

3.2.4 Kinetic characterization of known inhibitor of shikimate kinase

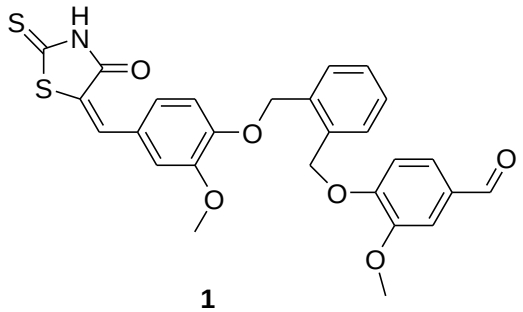

1

Figure 3.2. Structure of reference compound 1.

The inhibitory potency of compound **1**: 3-methoxy-4-{[2-({2-methoxy-4-[(4-oxo-2-thioxo-1,3-thiazolidin-5-ylidene)methyl]phenoxy}methyl)benzyl]oxy}benzaldehyde, a previously

reported inhibitor of SK [62], was evaluated using both the end-point LC-MS assay and the coupled assay described in chapter two.

For the LC-MS assay, compound **1** dissolved in DMSO was tested at four different concentrations ranging from 0 - 10 μM. All reactions were carried out in an assay buffer at room temperature as in section 3.2.2. For each concentration of reference compound, five ATP concentrations ranging from 0.05 to 1.2 mM were used while keeping the shikimate concentration constant at 5 mM (saturated). Conversely, five different concentrations of shikimate ranging from 0.2 to 5 mM were used while the concentration of ATP was kept constant at 1.2 mM (saturated). A total of 50 reaction mixtures (500 μL each) were prepared. Each reaction was initiated by the addition of 0.2 μM *Mt*SK, incubated for 30 seconds, and quenched by the addition of 2 μL of 98% formic acid and vortexing. All quenched samples were analyzed by LC-MS for quantification of S3P following procedures described above. Samples in the absence of reference compound were used as negative controls. The concentration of DMSO in each sample was kept lower than 2% (v/v), a concentration that was found not to affect the enzymatic activity of *Mt*SK.

For the coupled assay, compound **1** was tested in the same manner as described above. The *A*340 values at each compound concentration (0 - 10 μM) were background corrected and initial velocities were measured in the presence of various concentrations of compound as a function of substrate concentration. Each reaction was started by the addition of *Mt*SK (20 nM) and monitored for 3 minutes as described in materials and methods.

All data were analyzed using GraphPad Prism 5.02 software (Mountain View, CA). Steady-state inhibition constants for compound **1** were calculated by nonlinear fitting of the data to the

non-competitive inhibition equation (Eq. 2) where [I] is the inhibitor concentration in μM, K_i is the dissociation constant for the inhibitor–enzyme complex, and $_{\alpha}K_i$ is the dissociation constant for the inhibitor–enzyme–substrate complex. K_i values were determined by a minimum of two independent experiments.

$$v = \frac{V_{max}[S]}{[S]\left(1 + \frac{[I]}{\alpha K_i}\right) + K_M\left(1 + \frac{[I]}{K_i}\right)} \qquad (2)$$

3.3 Results and discussion

3.3.1 LC-MS assay development and validation

We have developed and validated an LC-MS enzymatic assay based on the quantitation of the reaction product shikimate-3-phosphate (*m/z* = 253.0119 $[M - H]^-$) formed during the *Mt*SK catalyzed reaction. For the chromatographic separation of shikimate-3-phosphate from the rest of the reaction components, several reversed-phase columns were tested. S3P is a very hydrophilic compound with a poor retention in conventional reversed-phase columns, and it co-elutes with the substrate shikimate and with other salts present in the reaction mixture. Among all the reversed-phased columns evaluated (ZORBAX Eclipse Plus Phenyl-Hexyl 4.6 mm x 100 mm, 3.5 μm; ZORBAX Eclipse XDB-C18 4.6 mm x 50 mm, 1.8 μm; Polaris NH2 2.0 mm x 100 mm, 3 μm and ZORBAX Eclipse Plus C18 2.1 mm x 100 mm, 1.8 μm), the ZORBAX Eclipse Plus Phenyl-Hexyl column (Agilent) provided a better desalting and separation. Additionally, an acidic water/acetonitrile mobile phase (pH 3.5) was employed to favor the neutral state of the ionizable groups present in S3P to improve the retention time. A representative total ion current (TIC) chromatogram of a typical *Mt*SK reaction mixture acquired in the negative ionization

mode is shown in Figure 3.3. Reproducible separation was achieved, with buffer salts, shikimate-3-phosphate and shikimate eluting at 2.2, 2.6 and 3.0 min, respectively, in a 6-min run using a gradient mode.

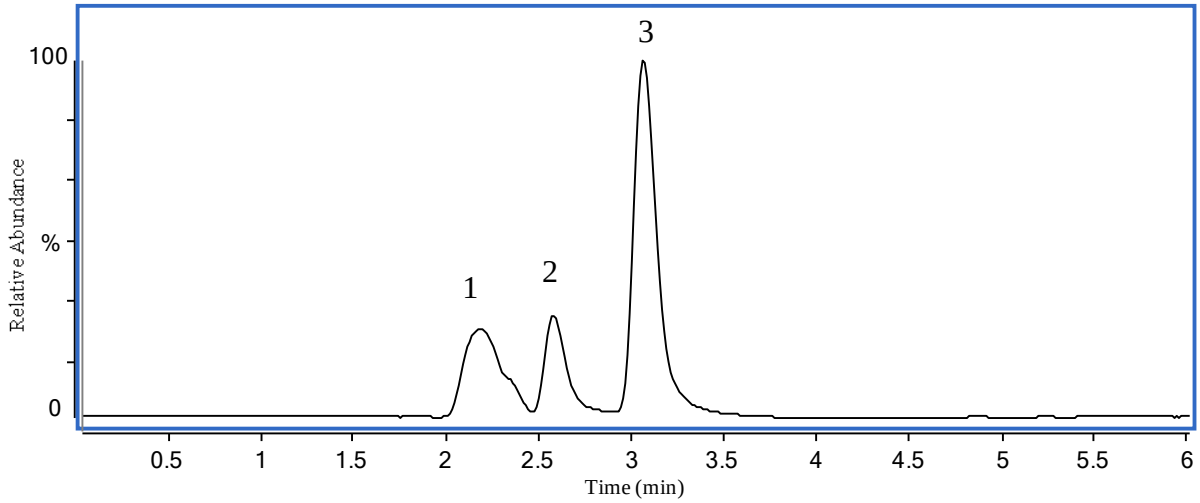

Figure 3.3. (A) Total ion current (TIC) chromatogram of *Mt*SK reaction mixture separated on a ZORBAX Eclipse Plus Phenyl-Hexyl column. The peaks are (1) buffer salts; (2) shikimate-3-phosphate; and (3) shikimate.

The linearity of the assay in terms of S3P concentration versus detector signal was evaluated using a series of concentrations of S3P reference standard in a pre-quenched *Mt*SK reaction mixture. The MS signal was linear ($y = [3 \times 10^7]x - 25714$; $R^2 = 0.999$) over a range of concentrations (0.0004 - 1 mM) sufficient to cover S3P formed in the wide variety of reactions performed. The limits of detection (LOD) and quantitation (LOQ) of S3P were 0.03 and 0.1 µg/mL, respectively.

The precision of the LC-MS assay was evaluated by determination of RSD of 100% (in the presence of DMSO) and 50% (in the presence of compound **1** at its K_i concentration) control samples. These samples were analyzed ten times in the same analytical run (intra-day) and on separate runs for four days (inter-day). Excellent intra-day and inter-day precision for 100% control sample (RSD % 2.7 and 3.2, respectively) and for 50% control sample (RSD % 3.8. and 4.4, respectively) was observed when the samples were kept at 4 °C, allowing for the analysis of large amounts of samples without significant loss of signal.

3.3.2 Kinetic characterization of *Mt*SK by LC-MS

Prior to measuring the kinetics parameters of *Mt*SK by the end-point LC-MS assay, determination of the optimum reaction conditions in terms of enzyme concentration and quenching time was performed. Determination of the appropriate amount of enzyme to be used in the assay was carried out by measuring the amount of S3P generated over a period of time for five different concentrations of *Mt*SK (0 – 1 µM), at saturating concentrations of shikimate and ATP. The concentration of enzyme at which the production of S3P was linear over time (0.2 µM) was selected for subsequent experiments. The appropriate reaction quenching time was determined by plotting the amount S3P formed versus time at a constant concentration of *Mt*SK (0.2 µM) (Fig. 3.4). The reaction was quenched at different time intervals from 0 - 4000 s. Production of S3P over the first 30 s was linear with time (Figure 3.4 inset) and corresponded to reaction times where less than 10% of the substrate had been consumed. Thus, a quench time of 30 s was considered suitable to avoid complications due to substrate depletion and inhibition by accumulated product [71]. Initial velocities were then calculated by dividing the concentration

of S3P by the reaction quenching time (V_0 = [S3P]/t_q). To report values in terms of active site catalytic cycles per unit time, V_0 was divided by enzyme concentration (i.e, $V_0/[E]_T$). Consequently, the asymptotic maximum $V_0/[E]_T$, approached at saturating concentrations of substrate was indicative of the enzyme's k_{cat}.

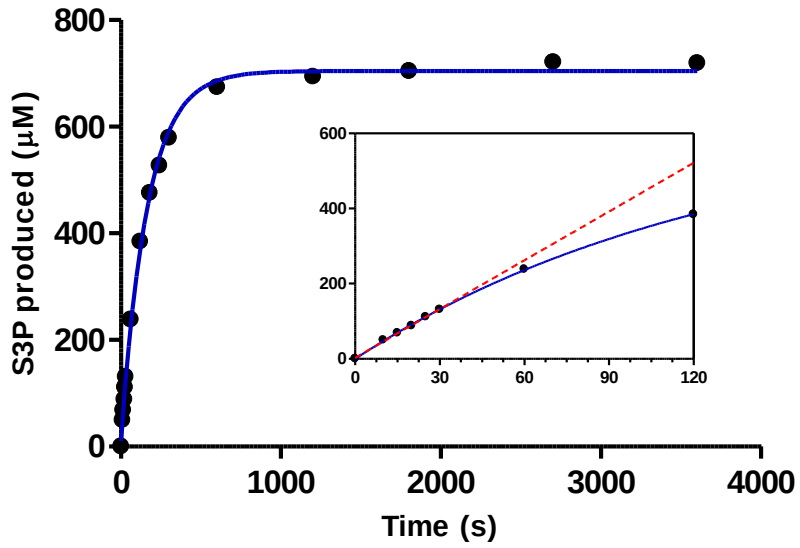

Figure 3.4. *Mt*SK reaction progress curve to determine optimum quenching time. [ATP] = 1.2 mM, [Shikimate] = 5 mM, [*Mt*SK] = 0.2 μM, pH = 7.6. The inset shows an expansion of the first 150 s of the curve. The dashed red line is from linear regression analysis of data collected over the first 30 s of the reaction.

3.3.3 Determination of K_M and k_{cat} for shikimate and ATP by LC-MS

For determination of the steady-state kinetic parameters for each substrate by LC-MS, one substrate was kept at a fixed saturated concentration while the other substrate concentration was varied in each reaction. Based on the K_M values (112 μM for ATP and 650 μM for

shikimate) previously reported in the literature for *Mt*SK [55], the concentration of the substrate to be varied in the experiments was ranged from 0.5 – 10 times the reported K_M. For the substrate to be fixed at saturating concentration, at least 10 – 15 times the reported K_M was included. Initial velocities were measured for each reaction and plotted against each substrate concentration using nonlinear regression to obtain the respective K_M and k_{cat} values. A hyperbolic response of *Mt*SK reaction rate was observed with increasing concentrations of ATP (Figure 3.5A) and shikimate (Figure 3.5B). A non-linear least squares fit of both data sets to a Michaelis-Menten rate equation produced an apparent K_M with respect to ATP of 0.20 mM and an apparent K_M with respect to shikimate of 0.53 mM. Both of these values were in good agreement with those reported in the literature, indicating the accuracy and precision of the LC-MS method. The k_{cat} values obtained from each plot were highly similar to one another (68 s^{-1} for ATP and 65 s^{-1} for shikimate) indicating that the maximum catalytic output of the enzyme was closely approached in both experiments. Likewise, the k_{cat} was nearly identical to the values observed by Rosado et al. and Gu et al. using spectrophotometric methods. Table 3.1 shows the kinetic constants calculated using the conventional enzyme-coupled assay and the LC-MS assay, as well as the ones reported in the literature.

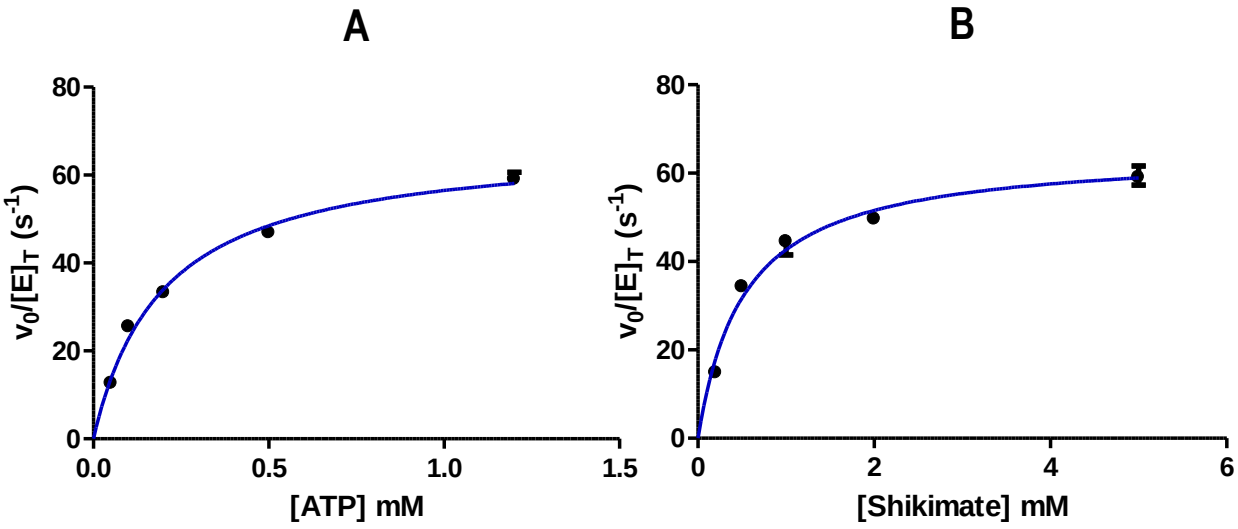

Figure 3.5. LC-MS-determined initial rates of S3P generation by *Mt*SK with increasing concentrations of ATP (A) and shikimate (B). Experiments were carried out in triplicate at five different concentrations of each substrate and at fixed *Mt*SK concentration of 0.2 µM at room temperature. Assays carried out for panel A contained 5 mM shikimate and assays carried out for panel B contained 1.2 mM ATP.

Table 3.1 Kinetic parameters of *Mt*SK calculated from both UV-coupled assay and the LC-MS assay.

	UV-coupled assay[a]		LC-MS assay[a]		Literature (UV-assay)[b]		Literature (UV-assay)[c]	
	ATP	Shikimate	ATP	Shikimate	ATP	Shikimate	ATP	Shikimate
K_M (mM)	0.17 ± 0.02	0.51 ± 0.04	0.20 ± 0.01	0.53 ± 0.05	0.11 ± 0.004	0.65 ± 0.03	0.08 ± 0.004	0.41 ± 0.02
k_{cat} (s^{-1})	64 ± 2	63 ± 1	68 ± 2	65 ± 2	60 ± 8	60 ± 8	44 ± 2	44 ± 2

[a]Values obtained in this study.
[b]Values reported by Rosado et al.[55]
[c]Values reported by Gu et al.[31]

3.3.4 Kinetic evaluation of known inhibitor

Shikimate kinase from *Mycobacterium tuberculosis* is considered a potential target for the development of novel anti-TB drugs [40]. To date, only a few inhibitors of this enzyme have

been identified, mostly through computational techniques [72-74] or through enzyme-coupled assays [75-76]. With coupled assays, there is a need for confirmatory methods to exclude false positives acting on the coupled-enzyme component of the assay, requiring multiple assay formats to help in the verification of hit compounds. Confirmation is usually done by counter-screening against the coupling enzymes, or by using a distinct detection method for analysis such as mass spectrometry [77]. As discussed in the next chapter, we have successfully screened a library of compounds against *Mt*SK using a direct and selective mass spectrometry-based method and provided IC_{50} values for the active compounds without the need for orthogonal testing [78].

For this report, a well characterized inhibitor of shikimate kinase from *Helicobacter pylori* (*Hp*SK) [62] was chosen to validate our assay and to determine if the kinetic data generated by LC-MS supported non-competitive inhibition as previously observed by compound **1**.

For the kinetic characterization of compound 1 using both the spectrophotometric and the LC-MS assay, each concentration of inhibitor (from 0 to 10 μM) was tested by varying the concentration of one substrate, while the concentration of the other substrate was kept constant as described in materials and methods. Plots of enzyme velocity generated as a function of substrate concentrations at varying concentrations of compound **1** displayed a hyperbolic decrease of the enzyme activity, while the apparent value of K_M was unaffected, consistent with non-competitive inhibition (Fig. 3.6) [77]. Fitting of the data to equation 2 was done to determine the inhibition constants K_i and $_{\alpha}K_i$ with respect to ATP and shikimate. Data were collected from two separate experiments, and the average dissociation constants obtained from the LC-MS assay and the coupled assay are shown in Table 3.2. The K_i and $_{\alpha}K_i$ values, as well as the mechanism of inhibition exhibited by compound **1** using both assays were consistent with

the inhibition study with *Hp*SK. These results indicate that the LC-MS assay can reveal not only kinetic parameters of bi-substrate enzymatic reactions, but it can also provide reliable information regarding inhibition potency and mode of action of active compounds.

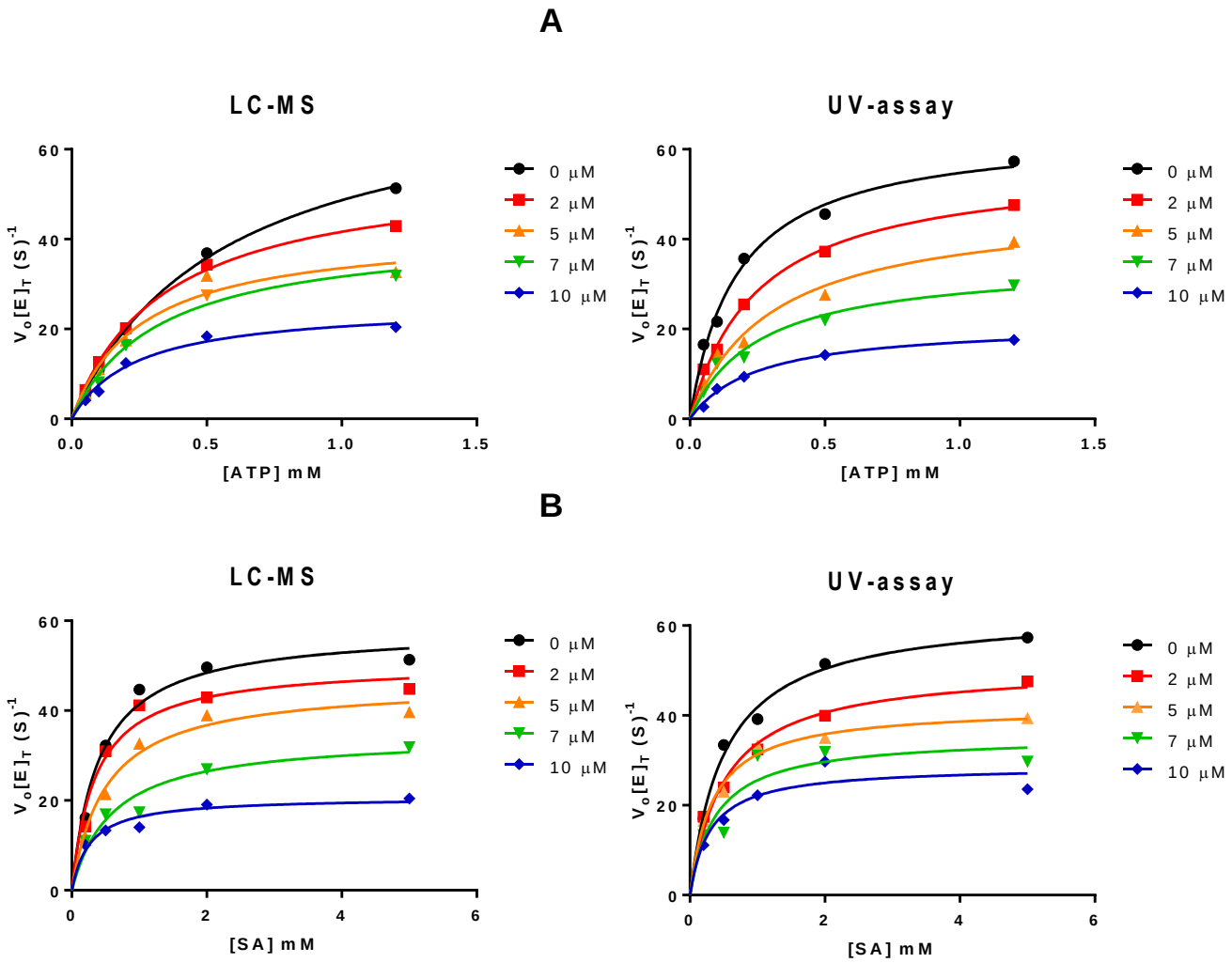

Figure 3.6. Kinetic *Mt*SK enzymatic studies with compound 1 show non-competitive mechanism of inhibition with respect to ATP and shikimate. The initial velocity of *Mt*SK obtained by the LC-MS assay (left) and the UV-assay (right) was plotted against various concentrations of (A) ATP and (B) shikimate in the presence of 0 µM (DMSO-black), 2 µM (red), 5 µM (orange), 7 µM (green) and 10 µM (blue) of compound 1. Michaelis-Menten kinetic experiments were performed with single points. Each data set represents 1 of 2 experiments with similar results.

Table 3.2. Inhibition constants of compound 1 against *Mt*SK determined by the LC-MS and the UV-coupled assay.

	LC-MS assay[a]	UV- assay[a]	Literature[b] UV-assay
K_i (μM)	10.90	9.87	9.48
αK_{iATP} (μM)	6.94	7.82	7.18
$\alpha K_{iShikimate}$ (μM)	10.09	8.07	10.67

[a]Values obtained in this study.
[b]Values reported by Han et al.[62]

3.4 Conclusion

In this section, we have developed a rapid and straightforward enzymatic assay for the kinetic characterization of *Mt*SK and for the evaluation of inhibitors using LC-MS. Performance of the method was evaluated by determination of the kinetic parameters of *Mt*SK (K_M and $k_{ca}t$) and inhibitory potency of a reference compound (K_i and αK_i). The results obtained by the LC-MS assay aligned with those obtained from the spectrophotometric coupled assays performed in our laboratory with our preparations of *Mt*SK as well as those reported in the literature, demonstrating the reliability of this assay. The greater specificity and sensitivity of the LC-MS assay over conventional coupled enzyme assays suggests that it can be applied for the kinetic characterization of enzymatic reactions for which spectrophotometric assays are not viable and/or as an orthogonal method for the validation of lead compounds identified by high throughput screening methods.

Chapter 4: Identification of shikimate kinase inhibitors among anti-*Mycobacterium tuberculosis* compounds by LC-MS.

4.1 Introduction

Increasing drug resistance has challenged the control and treatment of tuberculosis, sparking recent interest in finding new antitubercular agents with different chemical scaffolds and mechanisms of action. *Mycobacterium tuberculosis* shikimate kinase (*Mt*SK) represents an ideal target for therapeutic intervention given its absence in mammals.

Structural studies of protein-ligand interactions are useful to elucidate relationships between drugs and macromolecules in vivo [79]. Mass spectrometry (MS) based methods have great potential for studying these interactions and is increasingly being used to screen large combinatorial library mixtures for inhibitors of various macromolecular targets [80-83]. MS has numerous advantages over traditional optical and radioactive detection methods, for the discovery of biologically active small molecule enzyme inhibitors including a lack of analyte labeling, flexibility in qualitative and quantitative analysis, and the sensitivity and specificity of detection over a wide mass range, as well as the proficiency of high throughput screening, and the ability to determine K_D, the stoichiometry of binding, and the mode of binding [84-86]. As a result, MS is rapidly becoming a viable tool in drug discovery research.

To date only a small number of *Mt*SK inhibitors have been reported [72, 74, and 87]. The present study represents a follow-up target identification effort based on the high throughput phenotypic screens supported under the NIH TAACF program. Specifically, a small library of 404 phenotypic actives from the TAACF screens was further assayed against shikimate kinase

from *Mycobacterium tuberculosis*. Mining this select and diverse set of active samples from these whole cell phenotypic screens and pursuit of these "privileged" antibacterial scaffolds for specific target activity may preclude issues reported from years of pharmaceutical antibacterial HTS experience reporting poor results from purely target-based starting points [88]. The small library of TAACF phenotypic actives was first tested in an LC-MS-based functional *Mt*SK assay to determine inhibition rates and IC_{50} values. Follow-up docking studies with the crystal structure of *Mt*SK identified potential key interactions of the inhibitors within the catalytic binding site.

4.2 Materials and methods

4.2.1 Chemicals

The compound library tested in this study consisted of 404 compounds selected from a National Institute of Allergy and Infectious Diseases (NIAID) supported screen of 340,000 compounds for growth inhibition of *M. tuberculosis* H37Rv conducted by Southern Research Institute (SRI). This 404 compound library, covers a variety of heterocyclic compounds such as: pyrroles, furans, thiophenes, indoles and their benzo analogs, isoindolines, imidazoles, pyrazoles, triazoles, isoxazoles, thiazoles, oxadiazoles, thiadiazoles, pyridines, quinolines, pyridazines, pyrimidines, pyrazines, quinazolines, quinoxalines, pyrrolidines, piperazines and morpholines. Samples were supplied through the Tuberculosis Antimicrobial Acquisition and Coordinating Facility (TAACF) program. All compounds used on this study were supplied by the commercial vendors Chembridge and Life Chemicals with a minimum purity of 90% as analyzed by NMR to the NIAID supported screen program. Stock solutions were supplied by NIAID at 10 mg/mL in DMSO and stored at -80ºC prior to initial screening. Compounds that showed activity against

*Mt*SK (> 90 % inhibition) after initial screening were repurchased from Life Chemicals for retesting and determination of IC_{50} values. These compounds were supplied with a minimum purity of 90% as measured by HPLC.

Recombinant *Mt*SK used for this study was purchased from Biologics Process Development, Inc. (Poway, CA). Mass spectrometry was used to confirm the purity of the enzyme (> 95%) and the activity was 19 U/mg as measured by a coupled spectrophotometric enzymatic assay. The substrates adenosine-5'-triphosphate (ATP) and shikimic acid used in the functional assay, the positive control reference standard staurosporine and shikimate-3-phosphate for the calibration curve were purchased from Sigma-Aldrich (St. Louis, MO). All organic solvents were HPLC or LC-MS grade and were purchased from Thermo Fisher (Hanover Park, IL). Purified water was prepared using a Milli-Q purification system (Millipore, Billerica, MA).

4.2.2 LC-MS based *Mt*SK functional assay

An end point functional assay based on the formation of shikimate-3-phospate (S3P), the resulting product of the phosphorylation of shikimic acid catalyzed by *Mt*SK was employed. For this, test compounds at 50 μM and 15 nM of shikimate kinase were pre-incubated for 15 min in a microcentrifuge tube containing 455 μL of assay buffer (100 mM Tris-HCl pH = 7.5, 50 mM KCl and 5 mM $MgCl_2$) at 25°C. The reaction was initiated by the addition of an aqueous solution of shikimic acid and ATP (2 mM and 0.2 mM, final concentrations respectively) and quenched after 5 minutes by the addition of 2 μL of 100% formic acid. The total volume of the reaction mixture was 500 μL. A pyrazolone analog (benzenesulfonamide, 3, 5-dichloro-N-[6-(2,5-dihydro-3-methyl-5-oxo-1H-pyrazol-1-yl)-3-pyridinyl]-) previously described by Bandodkar et al. [75] as an *Mt*SK inhibitor, was used as a positive control for the functional

assay (Fig. 4.1). Negative control experiments were performed in a similar manner, adding DSMO instead of test compounds. The concentration of DMSO in the functional assay was kept lower than 2% (v/v), a concentration that was found not to influence the enzymatic activity of *Mt*SK. In order to ensure reproducibility, all functional assays were performed in duplicate and analyzed twice.

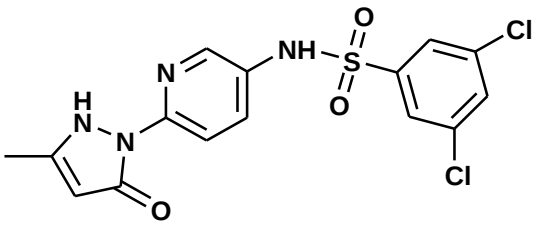

Figure 4.1. Structure of pyrazolone analogue (benzenesulfonamide, 3, 5-dichloro-N-[6-(2,5-dihydro-3-methyl-5-oxo-1H-pyrazol-1-yl)-3-pyridinyl]-) used as a positive control for *Mt*SK inhibition.

For the active compounds (> 90% inhibition), the concentration needed for 50% enzyme inhibition (IC_{50}) was determined by testing nine different concentrations of each compound ranging from 0.19 µM to 250 µM against 15 nM of *Mt*SK. The inhibition curves were plotted using GraphPad Prism 5.02 software (Mountain View, CA), and the IC_{50} value of each compound was calculated by fitting the data to a sigmoidal dose-response curve.

4.2.3 LC-MS analysis and quantification of shikimate-3-phosphate (S3P) for functional assay.

A 5 µL volume of the quenched reaction was injected onto a reversed-phase column (Zorbax Eclipse Plus Phenyl-hexyl, 4.6 x 100 mm 3.5 µm, Agilent Technologies, Inc.) The

mobile phase consisted of water with 0.1% formic acid (A) and acetonitrile 100% (B) with a gradient elution as follows: 0 min, 2% B held for 4 min, to 30% B in the next 2 min. Each run was followed by a 1 min post-run with 2% B. The total run-time analysis was 7 min at a flow rate of 0.4 mL/min and column temperature of 45°C. All acquisitions were performed under negative ionization mode under a narrow mass range (*m/z* 100-305). Mass spectrometric detection was carried out in an Agilent (Little Falls, DE) 6520 Accurate-Mass Q-TOF mass spectrometer equipped with an Agilent 1200 RRLC. The nebulizing and drying gases were nitrogen supplied at flow rates of 25 psig and 10 L/h, respectively, and the drying gas temperature was 350°C. A capillary voltage of 3200 V was used for the ESI source, and the fragmentor voltage was set to 175 eV. Quantification of S3P (*m/z* 253.0119 $[M - H]^-$) was accomplished using the Agilent MassHunter Workstation Qualitative Analysis software, version B.02.00. 2.4 in extractive ion monitoring mode.

Peak areas of S3P generated in each incubation sample were obtained and the inhibitory potency of each compound was determined by comparing the amount of S3P formed in the presence of test compounds to that formed in the negative control. To avoid carry over and ensure an accurate quantification of the reaction product, a series of S3P standard solutions were prepared in the same manner as incubation samples by adding known amounts of S3P. The calibration curve consisted of one blank sample and twelve calibration points in the concentration range of 0.4–1000 μg/mL. The analysis was performed in triplicate, and the calibration curve of S3P was constructed by plotting the resulting peak area against the different concentrations by using least-squares regression analysis.

4.2.4 Induced Fit docking of *Mt*SK inhibitor compounds.

The *M. tuberculosis* shikimate kinase crystal structure (PDB code 2DFT, conformer B) was utilized for docking all compounds (after structural refinement using Protein Preparation Wizard utility tools in the Schrodinger software). Co-crystallized ADP, Mg^{2+} and waters coordinating the metal were not deleted from the ATP binding site of the crystal structure since we chose to target the shikimate binding pocket for the purposes of docking the set presented in this study. Induced Fit docking (Schrodinger software) protocols were applied, combining Glide docking with Prime structural refinement tools to account for side chain flexibility in the ligand binding site. During docking side chains within 5 Å of docked ligand atoms were treated as flexible.

4.3 Results and discussion

4.3.1 *Mt*SK inhibitory activity

A library of 404 compounds active against *M. tuberculosis* (H37Rv) was screened for inhibitors of *Mt*SK using an LC-MS-based functional assay that consisted of quantification of shikimate-3-phosphate (S3P) formed during the reaction catalyzed by *Mt*SK. After incubation of the test compound with the enzyme and substrates, determination of S3P was carried out by LC-MS following a modified method from the one previously described by Mulabagal et al. [70]. Compounds that displayed a chromatographic reduction in the peak area of S3P when compared to that of the negative control (in the absence of test compound) were considered to be inhibitors of *Mt*SK. The extent of the *Mt*SK inhibition was calculated in percentages by using the equation **100(c0 - c)/c0**, where **c0** represents the S3P peak area observed in control experiments and **c** represents the peak observed in the presence of test compounds. The method was calibrated

using a series of standard solutions of S3P providing a broad linear detection range over three orders of magnitude ($R^2 \geq 0.99$).

A total of fourteen compounds displayed *Mt*SK inhibition exceeding 90% at 50 µM in the functional assay, representing a hit rate of 3.5%. For these compounds IC_{50} values were determined by measuring the S3P formed in the presence of nine concentrations of each inhibitor compared with control samples. To ensure the accuracy of the measurements, at least three concentrations above and three below the IC_{50} were tested [89]. Table 4.1 shows the determined IC_{50} for inhibition of *Mt*SK. Figure 4.2 shows an example for the IC_{50} determination of one of the active compounds. The IC_{50} for the pyrazolone analog used as a positive control for inhibition of *Mt*SK has been previously determined in our laboratory and reported as 0.18 µM (Table 4.1) by Mulagabal et al. [67].

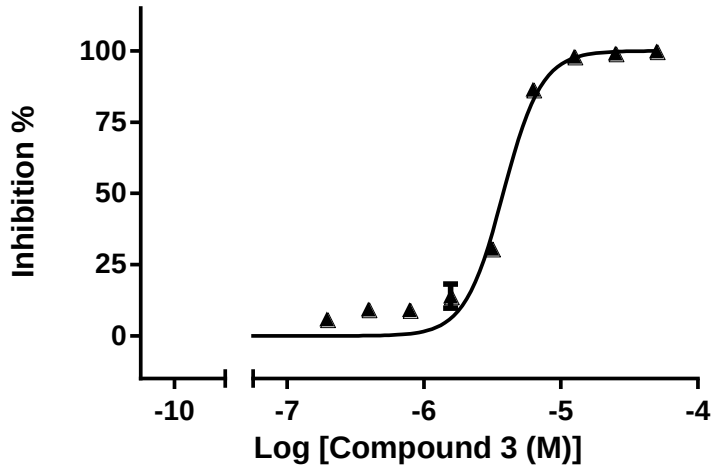

Figure 4.2. Dose-response curve for the inhibition of *Mt*SK by compound 3. The IC_{50} value of compound 3 was 3.79 ± 0.06 µM. Shown are the mean and deviation for triplicate analyses.

Table 4.1. IC_{50} values in µM of the active *Mt*SK inhibitors. IC_{50} for pyrazolone analogue (benzenesulfonamide, 3, 5-dichloro-N-[6-(2,5-dihydro-3-methyl-5-oxo-1H-pyrazol-1-yl)-3-pyridinyl]-) used as positive control for inhibition is also shown. The data shown are means +/- SEM of triplicate (n=3).

Compound no.	IC_{50} *Mt*SK (µM)
1	32.87 ± 0.04
2	13.81 ± 0.03
3	3.79 ± 0.02
4	10.35 ± 0.12
5	13.09 ± 0.06
6	36.04 ± 0.03
7	3.43 ± 0.04
8	28.36 ± 0.07
9	20.73 ± 0.03
10	15.14 ± 0.06
11	10.43 ± 0.04
12	29.93 ± 0.05
13	20.42 ± 0.06
14	1.94 ± 0.06
Positive control	0.18± 0.02

All fourteen compounds that inhibited *Mt*SK in vitro in this study have been previously shown to be active in vivo against *M. tuberculosis* H37Rv with IC_{90} < 5 µg/mL. Cytotoxicity for all analogs has been assessed using a Vero cell cytotoxicity counter-screen [90-92]. We define the ratio between the CC_{50} obtained in the cytotoxicity assay and H37Rv IC_{90} as a selectivity index (SI) ratio. Non-toxic compounds are associated with large SI values. All fourteen *Mt*SK inhibitors have SI values greater than 10 and are considered non-cytotoxic using this threshold. Cytotoxicity and selectivity index values are summarized in Tables 4.2-4.4 along with *Mt*SK IC_{50} and H37Rv dose-response activity. Out of the 14 *Mt*SK active compounds, ten hits share an

oxadiazole-amide core scaffold, which may be grouped into four distinctly decorated analog series, as listed in Tables 4.2 and 4.3 and four hits contain a 2-aminobenzothiazole substructure (Table 4.4).

Since the IC_{50} values towards purified shikimate kinase of almost all analogs were 5 to 10-fold higher than their respective whole-cell IC_{90} values, excepting compound 3, *Mt*SK may be only one of the possible targets of these compounds based on the weak correlation between the in vitro antibacterial data and the in vitro enzymatic data. Certainly, *Mt*SK represents a potential target for which analogs can be optimized, particularly with the use of lead optimization tools such as structure-based and computational methodologies as described in this article and elsewhere [93] to ensure selectivity of the these initial hits. In summary, we have identified one potential target for a small number of phenotypic actives that will allow more efficient optimization in a modern rational drug discovery program towards the development of new antitubercular drugs.

4.3.2 Oxadiazole-amides

The core scaffold 2-carboxamido-1,3,4-oxadiazole is present in ten of the fourteen hits. 2,5-Disubstituted-1,3,4-oxadiazole systems have been shown to have wide biological relevance as anticancer, anti-inflammatory, antifungal, antiviral, and antibacterial agents. They are particularly known to possess potent antibacterial and antimycobacterial activity [93-94].

All oxadiazole-amides in this series have H37Rv IC90 values below 5 µg/mL and SI values well over the threshold of ten (Tables 4.2 and 4.3). Two of these compounds also show MtSK IC_{50} values below 5µM. All compounds contain a phenyl at the 5-position of the oxadiazole ring with the exception of compound **9** possessing a furanyl substituent. The other

end the carboxamide is linked to a substituted phenyl in four compounds while others contain a furan or a thiophene at this position. Certain examples also have a short linker connecting the amide moiety and the distal phenyl group (Tables 4.2 – 4.3). For example, in the case of compound **3**, the phenyl is connected through an acrylic acid amide instead of a carboxamide. Compounds **3** and **7** have the most potent *Mt*SK IC_{50}s within the oxadiazole series, 3.79 and 3.43 μM, respectively (Table 4.1). Compound **6** contains a substituted phenyl ring at both ends flanking the oxadiazole-amide core structure where the phenyl substituents modulate the activity of related analogs.

Table 4.2. Activity of oxadiazole-amides analogs (1-5) against *Mt*SK along with their IC_{90} in μg/mL (versus *M. tuberculosis* H37Rv), *Mt*SK IC_{50} in μM, selectivity index (SI) and cytotoxicity against Vero cells (CC_{50}) in μg/mL.

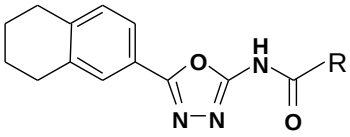

#	R	IC_{50} (μM) *Mt*SK	H37Rv IC_{90s} (μg/mL)	CC_{50} (μg/mL) Vero	SI (CC_{50}/IC_{90})
1	n-butyl	32.87	3.04	> 40	> 13.16
2	Ph-thio-Ethyl	13.81	1.93	26.52	13.74
3	Ph-CH=CH	3.79	1.68	> 40	> 23.95

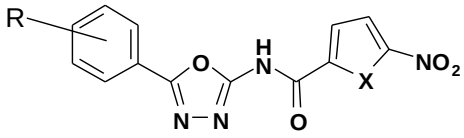

4	2,4-diMe, X=O	10.35	0.69	> 40[1]	> 57.97
5	2,5-diMe, X=S	13.09	3.09	> 40	> 12.94

[1] Compound showed no cytotoxicity up to the highest concentration used (40 μg/mL).

Table 4.3. Activity of oxadiazole-amides analogs (6-10) against *Mt*SK along with their IC_{90} values shown in µg/mL (versus *M. tuberculosis* H37Rv), *Mt*SK IC_{50} in µM, selectivity index (SI) and cytotoxicity against Vero cells (CC_{50}) in µg/mL.

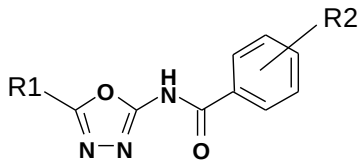

#	R1	R2	IC_{50} (µM) *Mt*SK	H37Rv IC_{90s} (µg/mL)	CC_{50} (µg/mL) Vero	SI (CC_{50}/IC_{90})
6	2,4-diMe-Ph	2-Cl	36.04	<0.20	5.30	> 26.50
7	2-Cl-Ph	3-O-Ph	3.43	0.86	> 40[1]	> 46.51

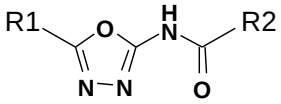

8	4-Br-Ph	t-bu	28.36	<0.20	10.62	> 53.10
9	2-furanyl	4-EtS-Ph	20.73	0.71	15.06	21.21
10	2,4-diMe-Ph	Ph-O-Ethyl	15.14	1.80	> 40	> 22.22

[1] Compound showed no cytotoxicity up to the highest concentration used (40 µg/mL).

4.3.3 2-Aminobenzothiazoles

While oxadiazole-amide scaffolds have been well documented as having potent antibacterial activity, the benzothiazole cores have not been well represented in antibacterial literature. They are more prevalent in kinase inhibitor literature, having been identified as inhibitors of kinases like SHP-2 and JNK kinases [95-97]. In our screen four compounds (**11** - **14**) displayed the 2-aminobenzothiazole core scaffold (Table 4.4). Their potent mycobacterial growth inhibition and *Mt*SK inhibition in our screen showed promise for further optimization as antimycobacterial agents. Compounds **11** and **13** are related structures, both containing a 3-imidazol-propyl moiety at R2 and a thiophene connected through a carboxamide or acrylic amide

at R1. Interestingly, substituting a pyrrolidine for R1/R2 is well tolerated without any significant loss of H37Rv growth inhibition. The most active compound in this series, **14** contains a 6-methylthio-benzothiazole at R1/R2. All four analogs have selectivity indexes greater than 10.

Table 4.4. Activity of 2-aminobenzothiazole analogs (11-14) against *Mt*SK along with their IC_{90} in µg/mL (versus *M. tuberculosis* H37Rv), *Mt*SK IC_{50} in µM, selectivity index (SI) and cytotoxicity against Vero cells (CC_{50}) in µg/mL.

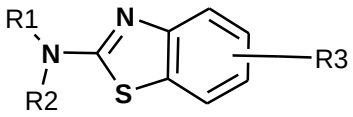

#	R1	R2	R3	IC_{50} (µM) *Mt*SK	H37Rv IC_{90s} (µg/mL)	CC_{50} (µg/mL) Vero	SI (CC_{50}/IC_{90})
11	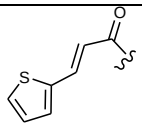	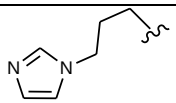	4-Ethyl	10.43	0.83	9.16	11.04
12	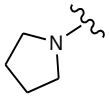		5,7-dimethyl	29.93	1.75	> 40	> 22.86
13	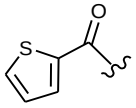	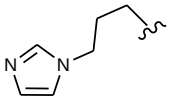	4,6-difluoro	20.42	2.38	> 40	> 16.81
14	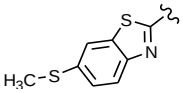	H	6-Acetylamino	1.94	<0.20	34.26	> 171.30

4.3.4 Induced Fit poses of oxadiazole-amide and 2-Aminobenzothiazole series inhibitors in the *Mt*SK shikimate binding site.

*Mt*SK is an α/β protein consisting of five central parallel β-strands flanked by α-helices. Based on structural flexibility considerations, Hartmann and co-workers [23] divided the structure into the following domains: an extended shikimate binding domain (ESB) that is capable of rigid body movements; the LID loop and the nucleotide binding domain (NB) are flexible regions, the latter consisting of the P-loop, AB loop and the helix α6.19. The remaining RC (reduced core) domain is the most rigid part of the structure. Figure 4.3 illustrates structural differences among *Mt*SK crystal structures representing distinct states of the *Mt*SK catalytic cycle which are mainly in the flexible LID and NB domains. Either shikimate or ATP may bind *Mt*SK first, inducing distinct conformational changes, as captured via a number of crystal structures, corresponding to distinct liganded states of *Mt*SK [23]. Binding of the first substrate will cause LID loop to close, a conformation stabilized by an extensive network of hydrogen bonding and electrostatic interactions involving bridging waters. Synergic effects facilitate the binding of the second substrate (shikimate or ATP) and associated conformational changes. In this study we utilized a nucleotide bound *Mt*SK crystal structure determined at 2.80 Å resolution (PDB ID 2DFT) with LID domain in closed conformation where ligands docked into the shikimate binding site may access the same amino acids which are important contributors to shikimate binding, such as D34, R58, G80, R136. Using ligand docking protocols detailed under 'Materials and Methods' we explored the shikimate binding site for docking the analog series listed in Tables 2.2 – 2.4. Scaffolds shared by compounds in these series possess a good fit in the shikimate binding pocket as exemplified by two representative compounds shown in Figure 4.4 from the two series. Compound **1** represents the oxadiazole-amide containing hit series

while compound **11** represents the 2-aminobenzothiazole series, forming favorable interactions as follows: a. Compound **1**: R58, a crucial shikimate contact residue forms a positive charge – π interaction with the aromatic ring of the tetrahydro-naphthaline of compound **1** while the rest of the ring structure forms non-polar interactions with L119 and P118. The oxadiazole ring is aligned for favorable polar interactions with the guanidinium group in R117 which also forms a salt bridge with phosphate groups of the co-crystallized ADP. The amide linker participates in the interaction network present in the crystal structure through hydrogen bonding with crystal waters while the terminal butyl favorably interacts with the V35 side chain. b. Compound **11**: The benzothiazole ring forms favorable aromatic-aromatic interactions with F57 which orients its 4-ethyl substituent into close proximity to the side chain of I45. The 4-ethyl group additionally participates in non-polar interactions with I37 also. I45 and V35 form steric interactions with the thiophene of **11**. Interestingly, the amide carbonyl contributes to the coordination of the Mg^{2+} in the docked pose (at 2.2 Å distance) while the 3-carbon linker forms non-polar interactions with P11. The terminal imidazole of **11** participates in favorable polar interactions with R136, a residue that is also crucial for the binding of shikimate.

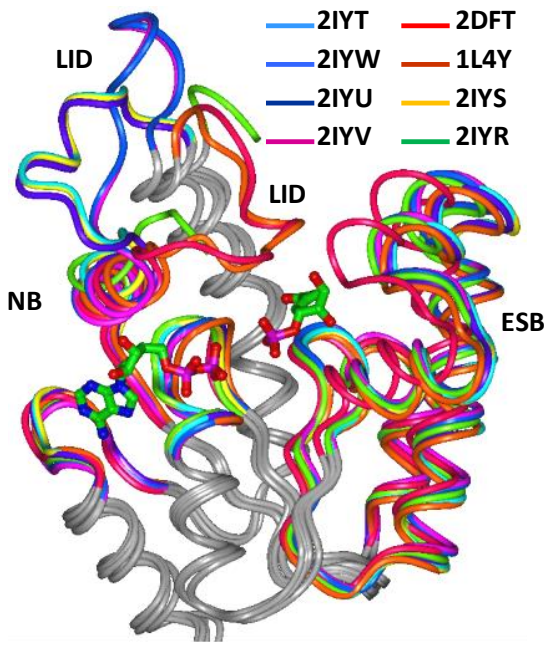

Figure 4.3. *Mt*SK structures superimposed based on RC domain (gray). Crystal structures are color coded by PDB ID.

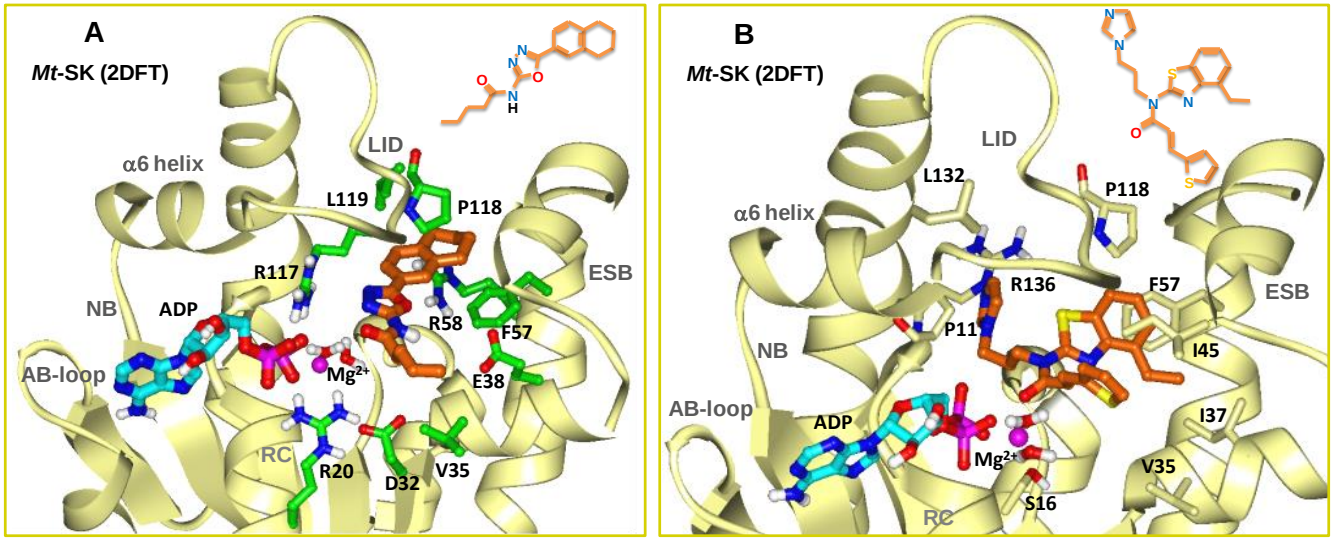

Figure 4.4. Induced Fit docked poses of compounds (A) 1 and (B) 11 in the *Mt*SK crystal structure (PDB id 2DFT). Co-crystallized ADP is shown with cyan colored carbons, docked ligands with orange colored carbons. Carbon atoms of *Mt*SK residues interacting with 1 are colored green while those interacting with 11 are light yellow. All other atoms are colored by atom type (oxygens red, nitrogens blue, phosphorus purple)

4.4 Conclusion

While the numerous actives from the NIH phenotypic H37Rv *Mtb* screens are an excellent resource, it has historically been extremely difficult to develop potent and selective compounds without specific target information. In this study, a library of 404 phenotypic antimycobacterial compounds supplied by the NIH TAACF program was screened by a functional LC-MS assay to identify inhibitors of *Mt*SK. Compounds with potent *Mt*SK inhibition that also display low IC_{90} values against *M. tuberculosis* have been identified representing analog series of oxadiazole-amide and aminobenzothiazole core scaffolds. Docking studies were used to further validate specific interactions of the core scaffolds with *Mt*SK. Our work suggests that one possible target of these phenotypic antimycobacterial compounds is the essential protein *Mt*SK. As such and with the information provided herein, the synthetically tractable active classes and the putative target *Mt*SK, there is an excellent starting point for the development of a rational medicinal chemistry program to develop new antitubercular agents with a novel mechanism of action.

Chapter 5: Characterization of manzamine alkaloids as inhibitors of shikimate kinase from *Mycobacterium tuberculosis* (*Mt*SK) by LC-MS

5.1 Introduction

For thousands of years, natural products from various sources have played an important role throughout the world in treating and preventing human diseases [98]. In the past few years, marine organisms have been intensively studied for their potential to provide new therapeutic agents against infectious diseases including tuberculosis [99]. Manzamine alkaloids, a novel structural class of compounds isolated from Indo-Pacific marine sponges, have been previously reported to possess extraordinary biological activities including cytotoxicity, anti-inflammatory, antiparasitic, insecticidal and antibacterial activities with their greatest potential being against malaria [100] and tuberculosis [101-103].

Manzamine alkaloids as potential anti-TB drugs

This family of compounds is known for their unique structural feature involving a complex polycyclic ring system coupled to a β-carboline moiety. Since the first report of manzamine A (**1**) by Higa and coworkers in 1986 [104], more than 80 manzamine and manzamine-related alkaloids have been isolated from more than 16 different species of marine sponges [105].

The prototype of this group, manzamine A (**1**) and its 8-hydroxy derivate (**2**) have shown promising anti-*Mycobacterium tuberculosis* (H37Rv) activity *in vitro* with MIC values of 1.5 and 0.9 μg/mL, respectively [106], an activity comparable to the first-line tuberculosis treatment drug rifampicin (MIC 0.5 μg/mL). Other manzamine alkaloids that this study focuses on that

have also inhibited *Mtb* growth *in vitro* are manzamine E (**4**), manzamine F (**5**) and 6-deoxymanzamine X (**6**), with MIC values of 3.8, 2.6 and 1.8 µg/mL, respectively [107].

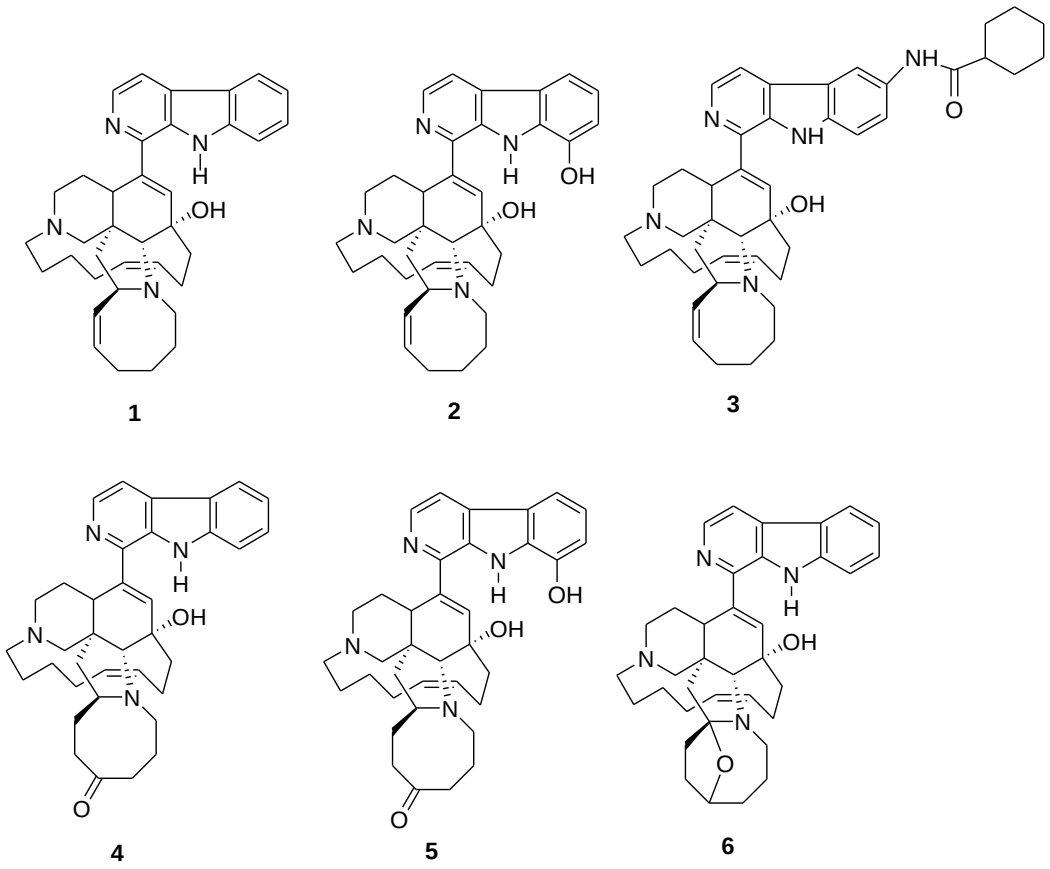

Figure 5.1 Structures of manzamine A (1), 8-hydroxymanzamine A (2), 6-cyclohexamidomanzamine A (3), manzamine E (4), manzamine F (5) and 6-deoxymanzamine X (6).

Despite the promising anti-TB activity of the manzamine alkaloids, a major drawback for their development into drugs is their cytotoxicity associated with higher doses, which could be due to DNA intercalation by the planar β-carboline moiety [108]. In an attempt to reduce the toxicity of this class of compounds, amidation of position 6 of the β-carboline moiety resulted in compound (**3**) 6-cyclohexamidomanzamine [107]. Although compound **3** exhibited slightly reduced activity against *Mycobacterium intracellulare* with an IC_{50} of 1.26 µM, as opposed to 0.640 µM exhibited by manzamine A (**1**), amidation at this position completely eliminated cytotoxicity in mammalian cells [107].

To date, the mechanism for the potent biological activities displayed by these alkaloids remains unclear. In this report, we have screened a library of 26 marine-derived alkaloids against *Mt*SK, and among them, six manzamine alkaloids (**1** - **6**) showed inhibitory activity, and their mechanisms of inhibition was further evaluated using an LC-MS based enzymatic assay and molecular docking. Our results suggest that manzamine alkaloids are viable lead compounds for the development of antimycobacterial drugs and that *Mt*SK could be a common target for the diversity of activities observed by these compounds, including, but not limited to their antitubercular activity.

5.2 Materials and methods

5.2.1 Chemicals

The library of 26 marine-derived compounds was provided by Prof. M. T. Hamann, University of Mississippi. All compounds evaluated on this study were supplied with a minimum purity of 90% as analyzed by HPLC or H-NMR. Dimethyl sulfoxide (DMSO), shikimate-3-phosphate (S3P) used for the calibration curve, the substrates adenosine-5'-

triphosphate (ATP) and shikimate were purchased from Sigma-Aldrich (St. Louis, MO). All organic solvents were HPLC or LC-MS grade and were purchased from Thermo Fisher (Hanover Park, IL). All buffers and media were prepared using water purified by a Milli-Q purification system (Millipore, Billerica, MA).

5.2.2 *Mt*SK LC-MS inhibition assay

The inhibitory effect of a small library of 26 marine-derived compounds was assessed by an end-point LC-MS enzymatic activity assay. This assay is based on the quantitative determination of the reaction product S3P m/z = 253.0119 $[M - H]^-$. All assays were performed in a buffer consisting of 100 mM Tris-HCl pH = 7.6, 50 mM KCl and 5 mM $MgCl_2$ at 25 °C in a final volume of 500 µL. Preliminary inhibition assessment of the library of compounds was carried out by measuring the activity of *Mt*SK in the presence of compounds dissolved in DMSO (50 µM) at saturated concentrations of the substrates ATP (1.2 mM) and shikimate (5 mM). Reactions were initiated by the addition of 0.2 µM of *Mt*SK, followed for 30 seconds and quenched by the addition of 2 µL of 98% formic acid and vortexing.

For mass spectrometric analyses, 5 µL of quenched reaction mixtures were injected onto a reversed-phase column (Zorbax Eclipse Plus Phenyl-hexyl, 4.6 x 100 mm 3.5 µm, Agilent Technologies, Inc.). The mobile phase consisted of water with 0.1% (v/v) formic acid (A) and acetonitrile 100% (B) with a gradient elution as follows: 0 min, 2% B held for 4 min, to 30% B in the next 2 min. Each run was followed by a 1 min post-run with 2% B. The total run-time analysis was 7 min at a flow rate of 0.4 mL/min and column temperature of 45 °C. All acquisitions were performed under negative ionization mode using a narrow *m/z* range (*m/z* 100-300). Mass spectrometric detection was carried out in an Agilent (Little Falls, DE) 6520

Accurate-Mass Q-TOF mass spectrometer equipped with an Agilent 1200 RRLC. The nebulizing and drying gases were nitrogen supplied at 25 psig and 10 L/h, respectively, and the drying gas temperature was 350 °C. A capillary voltage of 3200 V was used for the ESI source, and the fragmentor voltage was set to 175 eV. For quantification of S3P, extracted ion chromatograms (EIC) of *m/z* 253.0119 $[M - H]^-$ were integrated using Agilent MassHunter Workstation Qualitative Analysis software (version B.02.00), and the peak area was used to evaluate enzyme activity.

5.2.3 Kinetics of inhibition of manzamine alkaloids

5.2.3.1 Mixed-type inhibition kinetics

Compounds (**1**-**6**) that were able to inhibit the activity of *Mt*SK in the primary testing by 50% were further characterized by LC-MS. Initial rates of the *Mt*SK reaction were measured in the presence of ranging concentrations of compounds (0 - 250 μM) at 0 pre-incubation time. For each concentration of compounds, five ATP concentrations varying from 0.05 to 1.2 mM were evaluated while keeping the shikimate concentration constant at 5 mM (saturated). Conversely, five different concentrations of shikimate ranging from 0.2 to 5 mM were used, while the concentration of ATP was kept constant at 1.2 mM (saturated). Each reaction was initiated by the addition of *Mt*SK (0.2 μM), incubated for 30 seconds, and quenched by the addition of 2 μL of 98% formic acid and vortexing.

Steady-state inhibition constants for each compound were determined by plotting the data to a mixed-type inhibition model, and double-reciprocal (Lineweaver-Burk) plots were constructed for visual examination of the mechanism of inhibition using GraphPad Prism 5.02 software (Mountain View, CA).

5.2.3.2 Slow, tight-binding kinetics

Initial inhibition experiments demonstrated that the inhibition of the manzamine alkaloids on *Mt*SK proceeded through the slow formation of an enzyme-inhibitor complex, therefore, typical steady-state kinetics could not be used to accurately determine the inhibition constants for these compounds. Instead, *Mt*SK (0.2 μM) was pre-incubated with various fixed concentrations of inhibitors (0 – 250 μM) for 0 – 60 min. The reactions were initiated by the addition of shikimate (5 mM) and ATP (1.2 mM), followed for 30 seconds and quenched by the addition of 2 μL of 98% formic acid and vortexing. All reactions were performed using the same buffer and conditions as described above. Data generated were analyzed by the following equation for time dependent inhibition [77]:

$$v_t = v_i \exp(-k_{obs}t)$$

where v_t is the measured steady state velocity after pre-incubation time *t*, v_i is the steady state velocity at pre-incubation time = 0 and k_{obs} is the apparent first order rate constant for the interconversion between v_t and v_i. The values obtained for k_{obs} were re-plotted as a function of inhibitor concentration to determine the mechanism of slow-binding inhibition. For inhibitors that follow a one-step reversible slow mechanism as depicted in Scheme 1, the relationship between k_{obs} and inhibitor concentration is linear with a nonzero y-intercept, whereas for inhibitors that bind the enzyme rapidly and cause the enzyme to isomerize slowly in two-steps as depicted in Scheme 2, the relationship between k_{obs} and inhibitor concentration yields a rectangular hyperbola.

Scheme 1

$$E + I \underset{k_{off\ slow}}{\overset{k_{on\ slow}}{\rightleftharpoons}} EI \quad \text{Slow binding, one step}$$

Scheme 2

$$E + I \underset{k_{off\ fast}}{\overset{k_{on\ fast}}{\rightleftharpoons}} EI \underset{k_{off\ slow}}{\overset{k_{on\ slow}}{\rightleftharpoons}} EI^* \quad \text{Slow binding, two steps}$$

For tight binding kinetics, inhibitors at varying concentrations (0 - 250 μM) were pre-incubated with *Mt*SK for 60 min prior to starting the reactions with shikimate (5 mM) and ATP (1.2 mM). Reactions were followed for 30 seconds and quenched as described above. Initial velocities were measured and plotted against inhibitor concentration, and the values were fitted to Morrison's tight binding equation [77]:

$$\frac{v_i}{v_0} = 1 - \frac{([E]_T + [I]_T + K_i^{app} - \sqrt{([E_T] + [I_T] + K_i^{app})^2 - 4[E_T][I_T]}}{2[E_T]}$$

where v_i is the steady state velocity in the presence of inhibitor and v_0 is the unhibited reaction. $[E]_T$ is the total enzyme concentration, $[I]_T$ is the total concentration of inhibitor and K_i^{app} is the apparent inhibition constant, and it is related to the true inhibition constant K_i by the following equation:

$$K_i^{app} = K_i(1 + \frac{[S]}{K_M})$$

where [S] is the substrate concentration and K_M is the Michaelis-Menten constant for either shikimate or ATP.

5.2.4 Induced Fit docking

The *Mt*SK crystal structure (PDB code 2DFT) was refined applying Prime preparation and refinement tools of the Protein preparation wizard implemented in the Schrödinger software package. After the addition of hydrogens and detection of disulfide bonds, the structure was optimized applying default parameters of the Impref utility using the OPLS2001 force field. The maximum allowed root-mean-square deviation between the refined structure and the input crystal structure was 0.3. Ligand structures were prepared using the LigPrep utility at pH = 7.4. Induced Fit of the Schrödinger software applies the Glide docking method combined with Prime structural refinement tools to account for the flexibility of protein side chains within 5 Å of the ligand during docking. Three docking set-ups were used in the docking runs, defining the center of the docking grid based on the centroid position of ligands present in the *Mt*SK crystal structures as follows: a. shikimate, b. ADP and c. the center of mass of shikimate and ADP. The latter site definition allowed docking into the region that included both the shikimate and the ATP binding site. Induced Fit settings were at default values except the size of the box enclosing the targeted site, which was set to 30 Å. In the Induced Fit workflow, the initial Glide docking run used softened potentials (Van der Waals scaling of 0.50) followed by refinement of the structures, applying Prime side chain optimization of residues within 5 Å from docked ligand poses. The derived 'induced-fit' receptor structures were then utilized for the final step of Glide re-docking, with default parameters applied to structures within 30 kcal/mol of the lowest energy structure.

5.3 Results and discussion

5.3.1 Mixed-type inhibition kinetics of manzamine alkaloids

A preliminary assessment of the kinetic profiles of compounds (**1** – **6)** revealed that they induce a mixed-type inhibition with respect to both substrates shikimate and ATP. Each compound (0 - 250 μM) was tested against *Mt*SK (0.2 μM) by varying the concentration of one substrate, while the concentration of the other substrate was kept constant as described in materials and methods. Figure 5.2 shows the plots of enzyme velocity generated as a function of substrate concentrations at varying concentrations of compound **3**, where changes in both the apparent Vmax (decreased) and the K_M (increased) (Fig 5.2 A) are observed, while the Lineweaver–Burk plots (Fig 5.2 B) showed intersecting lines above the abscissa, consistent with mixed-type inhibition [77]. The same inhibition behavior was also observed for compounds **1**, **2**, **4**, **5** and **6**.

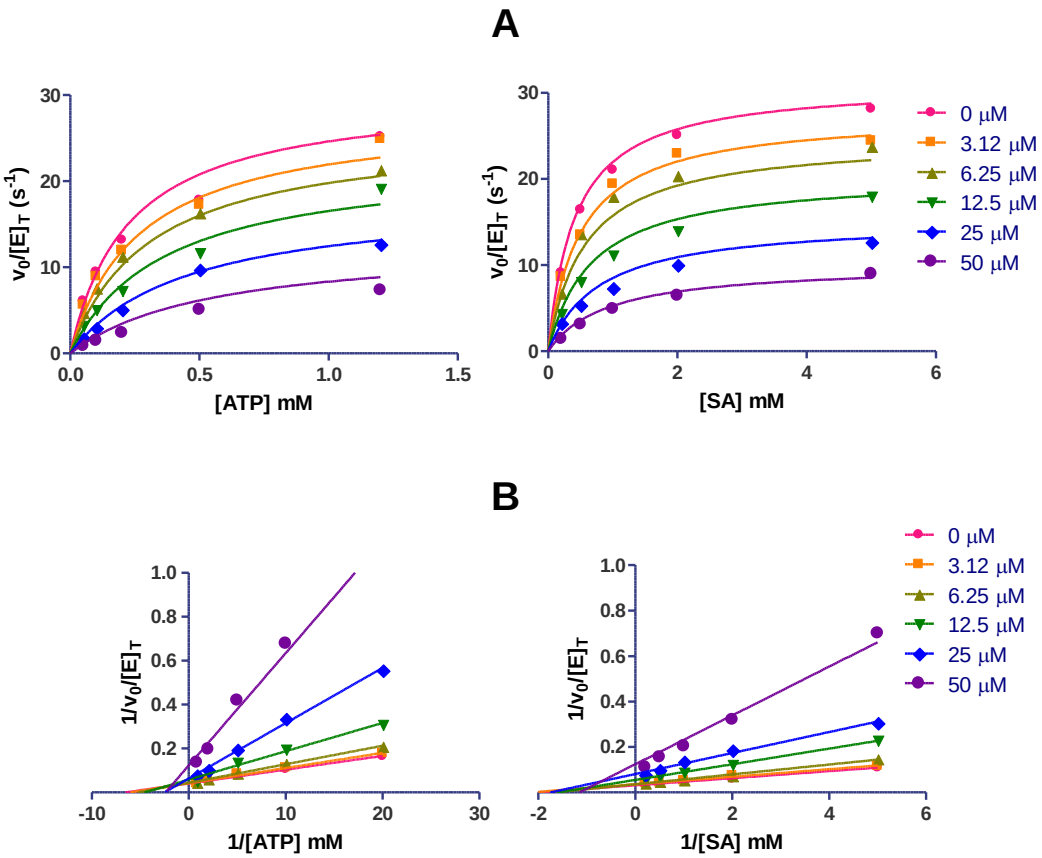

Figure 5.2 Kinetic analysis of the inhibition of *Mt*SK by 6-cyclohexamidomanzamine A. (A) Michaelis-Menten kinetic experiments at varying concentrations of compound with respect to ATP (left) and shikimate (right). (B) Lineweaver–Burk plots showing intersecting lines above the abscissa, consistent with mixed-type mechanism of inhibition.

Fitting of the data to a mixed-type inhibition model was done to determine the inhibition constant K_i of compounds (**1** – **6**) with respect to ATP and shikimate. From the preliminary results using rapid-equilibrium inhibition models, compound **3** showed the highest inhibition of *Mt*SK with respect to both substrates, followed by compounds **2** and **6**. Compounds **1**, **4** and **5**, showed less activity at zero pre-incubation time, displaying higher inhibition constants. Data were collected from two separate experiments, and the average inhibition constants obtained are shown in Table 5.1.

Table 5.1 Inhibition constants of manzamine alkaloids against *Mt*SK determined by the rapid-equilibrium mixed-type inhibition kinetic model.

Compound	Name	K_i ATP μM	K_i shikimate μM
1	Manzamine A	210.3	150.7
2	8-OH-manzamine A	75.84	31.2
3	6-cyclohexamidomanzamine A	10.6	8.7
4	Manzamine E	182.3	366.5
5	Manzamine F	121.5	142.1
6	6-deoxymanzamine X	96.32	77.64

5.3.2 Slow, tight-binding inhibition of *Mt*SK by manzamine alkaloids

Further kinetic analysis determined that compounds (**1** – **6)** are able to inhibit the activity of *Mt*SK in a time-dependent manner. This is illustrated in Figure 5.3A which shows the effect of pre-incubation time of compound **1** (left) and compound **6** (right) on the steady state velocity of *Mt*SK. In the presence of both compounds **1** and **3**, the velocity of *Mt*SK falls off exponentially with pre-incubation time, consistent with slow-binding inhibition, where the establishment of enzyme-inhibitor equilibrium is slower compared to that of conventional inhibitors. The effect of inhibitor concentration on the apparent first-order rate constant k_{obs} is shown in Figure 5.3B for compound **1** (left) and compound **3** (right). For compound **1**, the

relationship between k_{obs} varied linearly with inhibitor concentration, suggesting that it conforms to a one-step mechanism of slow-binding inhibition as depicted in Scheme 1, whereas for compound **3**, k_{obs} varied as a hyperbolic function of inhibitor concentration, suggesting a two-step mechanism as shown in Scheme 2. For compounds **2** and **4**, the relationship of k_{obs} with respect to inhibitor concentration was also linear, as it was for compound **1** (data not shown). Characterization of the slow-binding kinetics of compounds **5** and **6** is still underway.

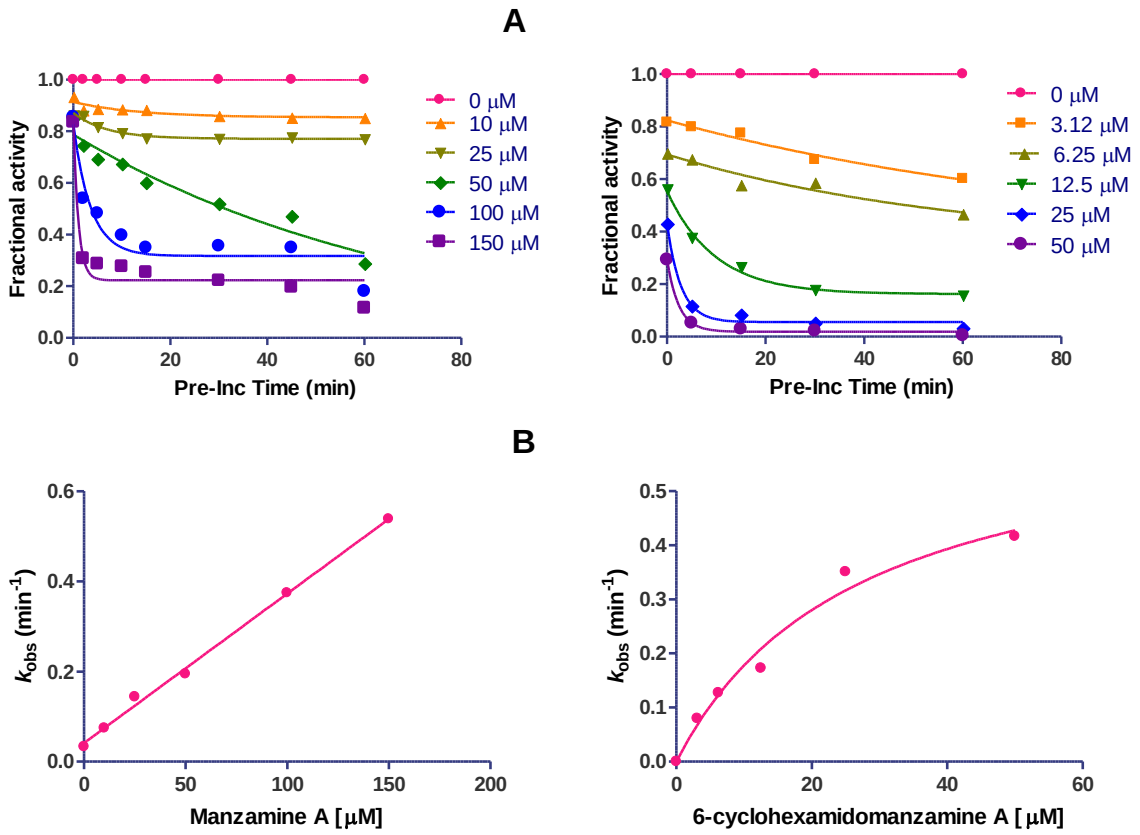

Figure 5.3 Kinetic analysis of the inhibition of compounds 1 and 3. (A) Effect of pre-incubation time on the activity of *Mt*SK by compound 1 (left) and compound 3 (right). Initial velocities were measured using 0.2 µM *Mt*SK, 5 mM shikimate and 1.2 mM ATP. (B) Plots of k_{obs} as a function of inhibitor concentration.

Inhibition constants for inhibitors conforming to the mechanism in Scheme 1 were estimated from the ratio of the y-intercept/slope of the linear fit of the data, and for inhibitors

conforming to the mechanism shown in Scheme 2, the concentration of inhibitor yielding a half-maximal value of k_{obs} is equal to K_i. Inhibition constants determined by slow-binding kinetic models along with the values yielded when fitting the data to Morrison's tight binding inhibition equation are summarized in Table 5.2.

Table 5.2 Inhibition constants of manzamine alkaloids against *Mt*SK determined by the slow and tight-binding inhibition models.

Comp.	Name	K_i (slow-binding) μM	K_i (tight-binding) μM
1	Manzamine A	10.9	4.2
2	8-OH-manzamine A	21.7	4.1
3	6-cyclohexamidomanzamine A	0.9	0.4
4	Manzamine E	11.4	4.2
5	Manzamine F	ND	ND
6	6-deoxymanzamine X	ND	1.3

ND = not determined

5.3.3 Modeling of manzamine analog into the *Mt*SK binding site

Several *M. tuberculosis* Shikimate kinase (*Mt*SK) crystal structures are available, representing distinct states of the *Mt*SK catalytic cycle. For the purposes of docking, we utilized the *Mt*SK crystal structure (PDB code 2DFT), co-crystallized with ADP, Mg and Cl. Induced Fit docking protocols implemented in the Schrödinger software package were applied, targeting the shikimate binding site, the ATP site and defining the targeted site to include both regions, as presented in more detail under materials and methods. The docked poses with the most favorable interactions in the manzamine analog series may be exemplified by the pose obtained for the most potent analog in this series, 6-cyclohexamidomanzamine. Figure 5.4 illustrates that

this compound may be accommodated in two alternative binding modes that significantly differ only in the positioning of the pyridoindol-c-hexamide moiety while the rest of the molecule shows close overlap comparing these two poses. The c-hexamide ending of this compound occupies overlapping space with shikimate in pose 1 and with ADP in pose 2. Pose 1 describes non-competitive binding with ATP and pose 2 ATP-competitive binding. This docking hypothesis that 6-cyclohexamidomanzamine may adopt two such bound poses is consistent with mixed-type inhibition, as supported by our investigation of inhibition mechanisms.

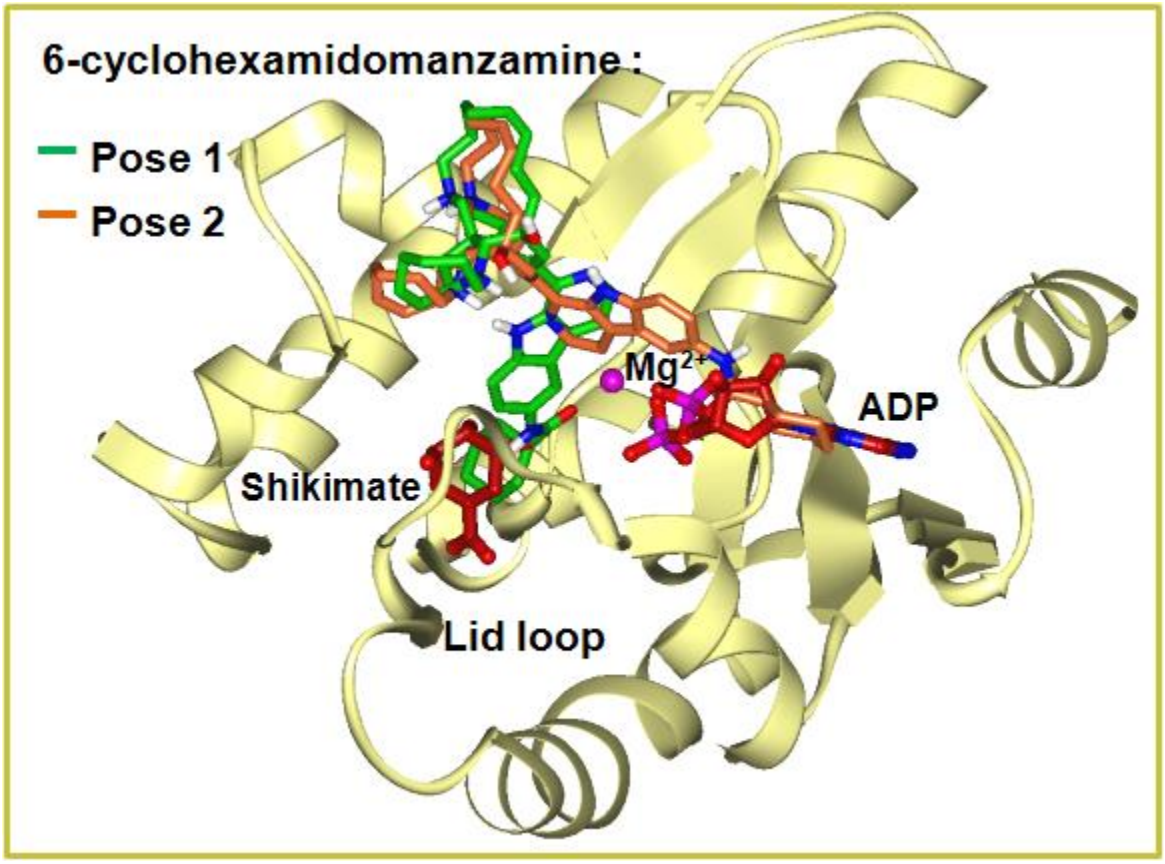

Figure 5.4. Docked poses of 6-cyclohexamidomanzamine A are shown in the *Mt*SK crystal structure. Positions of shikimate, ADP and Mg are also included for comparison. Carbon atoms in docked poses are colored as indicated; carbons in shikimate and ADP are colored dark brown. All other atoms are colored by atom type (oxygen red, nitrogen blue, hydrogen white, phosphorus magenta, Mg purple).

The Induced Fit docked pose 1 shown in Figure 5.5 predicts a number of favorable polar and hydrophobic interactions as follows. The side chain and backbone atoms of Thr115 participate in hydrogen bonding interactions with 6-cyclohexamidomanzamine, while Glu38 forms a salt bridge with a protonated amine of the ligand. The carbonyl oxygen of c-hexamide contributes to coordinating Mg^{2+}. Distances between atoms/atom groups participating in polar interactions are listed in Figure 5.5. The guanidinium group of Arg117 forms a positive charge – aromatic interaction with the pyridoindol ring system. Residues involved in non-polar or steric interactions are Pro11, Val35, Ile45, Phe49, Phe57, Val116 and Leu119, as shown in Figure 5.5.

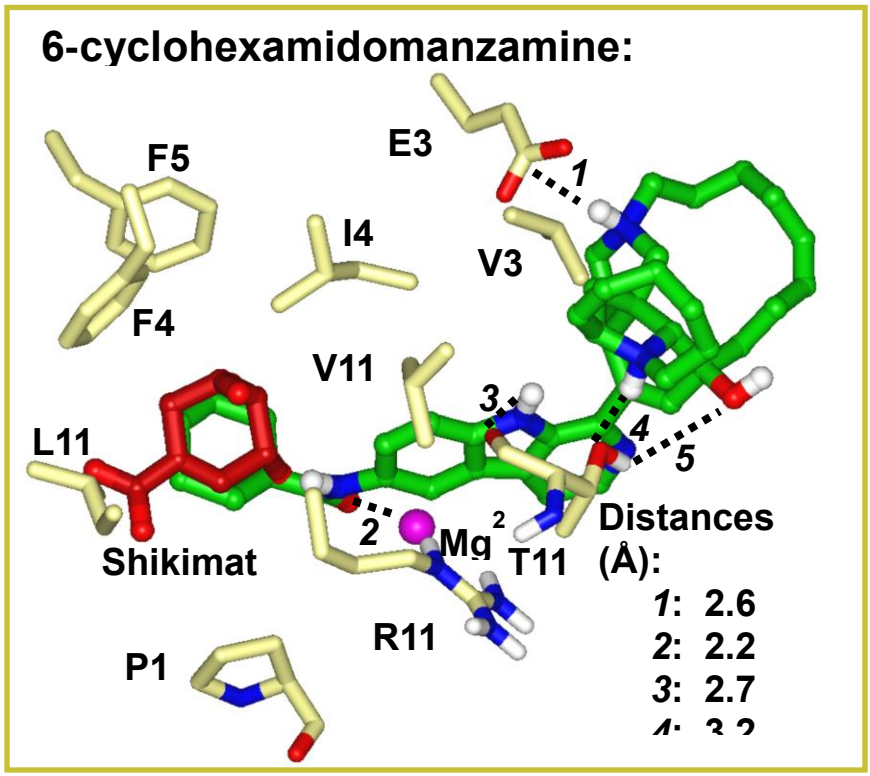

Figure 5.5. Docked pose 1 of 6-cylohexamidomanzamine A. The position of shikimate is included for comparison. Carbon atoms in the docked pose are colored green, in *Mt*SK residues light yellow. All other atoms are colored by atom type (as listed in Figure 5.2 legend). Hydrogen bonding and salt bridging interactions are indicated with dashed lines. Distances between participating atoms as shown are listed in units of Ångstrom. The distance shown for the salt bridging interaction (with E38) is between the center of mass of the carboxylate group and the hydrogen of the protonated amine.

A second docked pose of 6-cyclohexamidomanzamine, pose 2 is illustrated in Figure 5.6. In this pose Thr115 forms three hydrogen bonds with the ligand's amine group, hydroxyl and pyridine ring nitrogen. Glu38 salt bridges to a protonated amine, while Arg117 participates in hydrogen bonding with the amide group, as well as in favorable positive charge – aromatic interaction with the pyridoindol ring moiety. Amino acids forming non-polar or steric interactions are Thr17, Val35, Ile45, Val116, Pro155 and the aliphatic part of the Arg110 side chain.

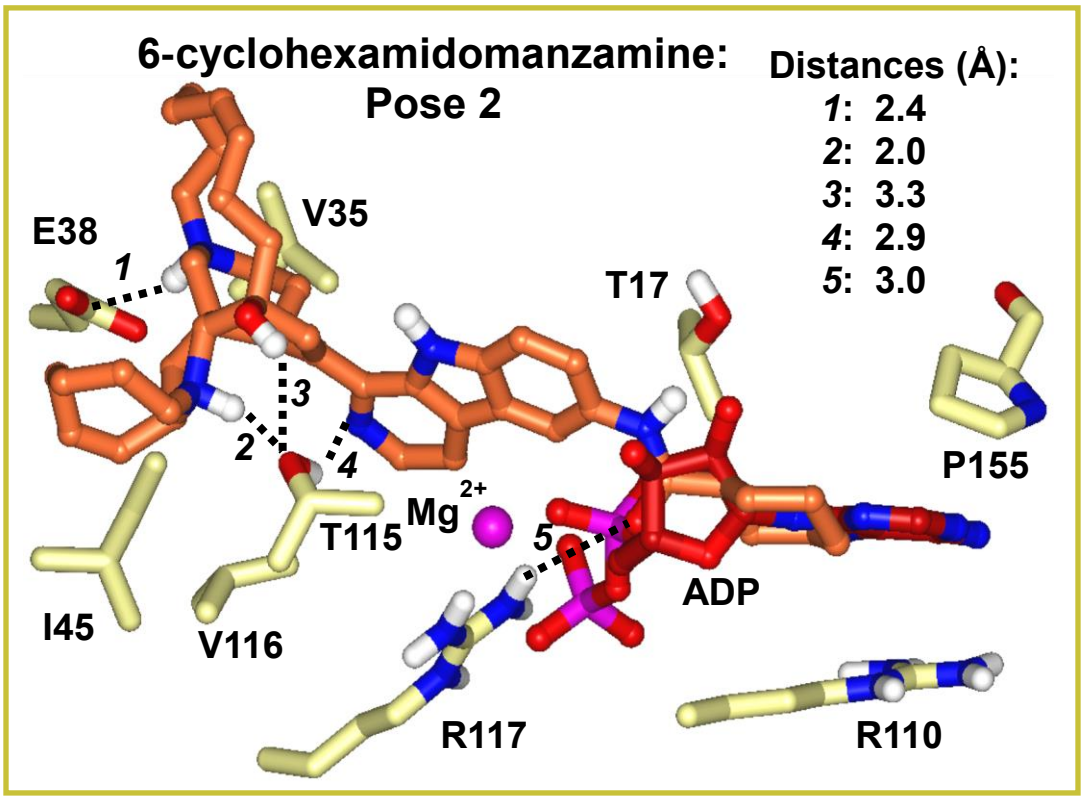

Figure 5.6. Docked pose 2 of 6-cyclohexamidomanzamine. The position of ADP is included for comparison. Carbon atoms in the docked pose are colored light brown, in *Mt*SK residues light yellow. All other atoms are colored by atom type (as listed in Figure 5.2 legend). Hydrogen bonding and salt bridging interactions are indicated with dashed lines. Distances between participating atoms as shown are listed in units of Ångstrom. The distance shown for the salt bridging interaction (with E38) is between the center of mass of the carboxylate group and the hydrogen of the protonated amine.

The structures of both poses of 6-cyclohexamidomanzamine show excellent complementarity between the bound ligand and the *Mt*SK binding site considering shape and polarity, and give insight into the structural basis of the binding manzamine analogs. The presented docking hypotheses may be utilized in future experimental designs to validate or refute the presence of predicted interactions between manzamine A analogs and *Mt*SK residues.

5.4 Conclusion

In this study, six manzamine alkaloids previously shown to be active in cell cultures of *M. tuberculosis* have been identified and characterized as inhibitors of *Mt*SK. Among them, the 6-cyclohexamide derivate of manzamine A, the prototype of this family of compounds, showed the most potent inhibition (K_i = 0.4 – 0.9 μM) of *Mt*SK. Several kinetic studies suggested that the manzamine alkaloids act as slow, tight-binding inhibitors conforming to a one-step (compounds **1**, **2** and **4**-**6**) or a two-steps mechanisms (compound **3**) of inhibition. Molecular docking studies revealed that the manzamine alkaloids may bind in two alternative binding modes that significantly differ only in the positioning of the β-carboline moiety, while the rest of the molecule shows close overlap. These findings, together with the experimental data, suggest that the manzamine alkaloids are able to induce a mixed-type inhibition of *Mt*SK with respect to both substrates shikimate and ATP. Taken all together, our results suggest that the manzamine alkaloids constitute a new scaffold from which drugs with novel mechanisms of actions could be designed for the treatment of tuberculosis.

Chapter 6: Detection of covalent modification and irreversible inhibition of *Mt*SK by ilimaquinone (IQ) using Liquid Chromatography Mass Spectrometry

6.1 Introduction

Terpenylquinones, a class of marine natural products, are considered privileged scaffolds for drug design due to their ubiquity in nature and their versatile bioactivities [109]. These compounds are characterized for having a sesquiterpene skeleton attached to a quinone moiety [110]. Among them, ilimaquinone (IQ) (Fig 6.1), first isolated in 1979 from the Red Sea sponge *Hippospongia metachromia* [111] have been reported to possess several biological activities including: antiviral, anti-inflammatory, antimicrobial, antimalarial and anti-HIV activities [112-115]. From all the studies performed with IQ over the years, the most remarkable activities reported are the ability to break down Golgi membranes into small vesicular structures, blocking cellular secretion in a reversible manner, also known as vesiculated Golgi membranes "VGMs", [116-117] and to cause an anti-proliferative effect in several types of cancer cell lines including prostate cancer (PC-3, DU145 and LNCaP), non-small cell lung cancer (A549), human osteosarcoma (MG63) and hepatocellular carcinoma (Hep3B) cells [110-111, 118-119].

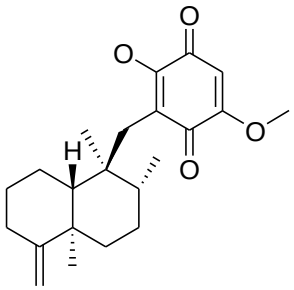

Figure 6.1 Structure of ilimaquinone (IQ)

Although ilimaquinone has been demonstrated to exert a myriad of biological activities through multiple pathways, such as activation of membrane-bound heterotrimeric G proteins [120], phospholipase D [121], and protein kinase D [122] to trigger Golgi vesiculation, time-dependent increase of G_1 phase arrest in the cell cycle resulting in anticancer activity [119], activation of hypoxia-inducible factor-1 (HIF-1) [123], and promotion of tumor necrosis factor-α (TNF-α) production [124], the specific interactions of IQ with its cellular targets are not clearly elucidated.

Radeke et al., demonstrated that ilimaquinone interacts with enzymes of the methyl cycle by using affinity chromatography methods, where they incubated tissue samples with ilimaquinone-attached resins, and proteins that were specifically retained by IQ were analyzed by SDS-PAGE [125]. Proteins identified by this method were further confirmed to be inhibited by ilimaquinone through activity assays with the isolated proteins.

Our particular interest in this compound arises from its ability to inhibit the activity of shikimate kinase from *Mycobacterium tuberculosis* irreversibly. In this study we demonstrated that ilimaquinone is capable of forming covalent adducts with *Mt*SK by analysis of intact protein by LC-MS, and we have also studied the inhibitory mechanism of IQ on *Mt*SK using an LC-MS based activity assay.

Despite the concerns of potential off-target reactivity, drugs that function through covalent mechanisms such as acetylsalicylic acid (Aspirin), esomeprazole (Nexium) and clopidogrel (Plavix), have been approved over the past 100 years for the treatment of different clinical indications and are highly profitable for the pharmaceutical industry [126]. In recent years, compounds that selectively react with a nucleophile that is poorly conserved across a target family (targeted covalent inhibitors TICs) have been considered for further chemical

optimization by drug discovery programs [126-127]. Covalent inhibitors possess several advantages over non-covalent inhibitors including increased biochemical efficiency of target disruption, longer duration of action that outlasts the pharmacokinetics of the compound, and the potential to prevent the emergence of acquired resistance conferred by mutations [128-129]. Mass spectrometry-based proteomics has been a valuable technique for the detection and identification of covalently modified proteins to aid in the discrimination between selective and non-selective binding of covalent inhibitors to off-target proteins in complex biological mixtures [130-131].

In this report we have demonstrated that the marine metabolite ilimaquinone is an irreversible inhibitor of *Mycobacterium tuberculosis* shikimate kinase (*Mt*SK). After *in vitro* incubation of recombinant *Mt*SK with ilimaquinone, an increase of ≈ 356 Da in the molecular mass of the native protein was observed by electrospray ionization mass spectrometry, indicating the formation of a covalent adduct. In an attempt to identify the sites and structures of the covalent adducts, proteolytic enzyme digestion was carried out with trypsin. Although our attempts to identify the amino acid residues modified by ilimaquinone led to inconclusive results, our findings provide new insight into the mechanism by which ilimaquinone could be interacting with its various reported targets. Furthermore, the covalent mechanism of action of the ilimaquinone scaffold may be pursued for the design of drugs to treat resistant strains of tuberculosis, provided target specificity is achieved.

6.2 Materials and methods

6.2.1 Chemicals

Ilimaquinone was provided by M. T. Hamann, University of Mississippi with a minimum purity of 90% as analyzed by HPLC or H-NMR. Dimethyl sulfoxide (DMSO), the substrates adenosine-5'-triphosphate (ATP) and shikimate were purchased from Sigma-Aldrich (St. Louis, MO). Pierce Trypsin Protease, MS Grade was purchased from Thermo Scientific (Rockford, IL). All organic solvents were HPLC or LC-MS grade and were purchased from Thermo Fisher (Hanover Park, IL). All buffers and media were prepared using water purified by a Milli-Q purification system (Millipore, Billerica, MA).

6.2.2 LC-MS based time-dependent inhibition assay

The effect of ilimaquinone on the activity of shikimate kinase from *Mycobacterium tuberculosis* (*Mt*SK) was evaluated by an *in vitro* time-dependent inhibition assay. In this assay, *Mt*SK (0.2 µM) was pre-incubated with ilimaquinone dissolved in DMSO at 0, 5, 10, 25, 50, 100 and 150 µM for 0-60 min prior to initiation of the reaction. All assays were performed in a buffer consisting of 100 mM Tris-HCl pH = 7.6, 50 mM KCl and 5 mM $MgCl_2$ at 25 °C in a final volume of 500 µL. Reactions were initiated by the addition of 5 mM shikimate and 1.2 mM ATP, followed for 30 seconds and quenched by the addition of 2 µL of 98% formic acid and vortexing. The amount of product (shikimate-3-phosphate, S3P) formed in each reaction was quantified using liquid-chromatography mass spectrometry.

For mass spectrometric analyses, 5 µL of quenched reaction mixtures were injected onto a reversed-phase column (Zorbax Eclipse Plus Phenyl-hexyl, 4.6 x 100 mm 3.5 µm, Agilent Technologies, Inc.). The mobile phase consisted of water with 0.1% (v/v) formic acid (A) and

acetonitrile 100% (B) with a gradient elution as follows: 0 min, 2% B held for 4 min, to 30% B in the next 2 min. Each run was followed by a 1 min post-run with 2% B. The total run-time analysis was 7 min at a flow rate of 0.4 mL/min and column temperature of 45 °C. All acquisitions were performed under negative ionization mode using a narrow *m/z* range (*m/z* 100-300). Mass spectrometric detection was carried out in an Agilent (Little Falls, DE) 6520 Accurate-Mass Q-TOF mass spectrometer equipped with an Agilent 1200 RRLC. The nebulizing and drying gases were nitrogen supplied at 25 psig and 10 L/h, respectively, and the drying gas temperature was 350 °C. A capillary voltage of 3200 V was used for the ESI source, and the fragmentor voltage was set to 175 eV. For quantification of S3P, extracted ion chromatograms (EIC) of *m/z* 253.0119 $[M - H]^-$ were integrated using Agilent MassHunter Workstation Qualitative Analysis software (version B.02.00), and the peak area was used to evaluate enzyme activity.

Data were collected in duplicate and initial velocities were calculated by dividing the concentration of S3P formed in each reaction by the reaction quenching time (V_0 = [S3P]/t_q). Determination of the inhibitory potency of ilimaquinone was done according to literature methods [77]. The percent of remaining *Mt*SK activity was determined by comparing the initial velocities in control experiments (in the presence of DMSO) to the initial velocities of the enzyme in the presence of various concentrations of ilimaquinone and plotted against the pre-incubation times. These data were fitted to the equation: $V_t = V_i \exp(-k_{obs}\, t)$ where V_t is the measured steady state velocity after pre-incubation time t, V_i is the steady state velocity when pre-incubation time is zero, and k_{obs} is the pseudo first-order constant of observed inactivation at a given inhibitor concentration. The k_{obs} values obtained were re-plotted as a function of ilimaquinone concentration using linear regression and the resulting slope corresponded to the

second-order rate constant (k_{inact}/K_I) which is indicative of the inhibitor effectiveness [77]. All data were fitted using GraphPad Prism (version 5.02).

6.2.3 Detection of covalent adducts by mass spectrometry

To follow the covalent modification of *Mt*SK by ilimaquinone, *Mt*SK (1 µM) was incubated with 100 µM ilimaquinone in a buffer consisting of 100 mM Tris-HCl pH = 7.6, 50 mM KCl and 5 mM $MgCl_2$ at 4 °C in a total volume of 300 µL. Analysis of modified *Mt*SK was performed on an Agilent (Little Falls, DE) 6520 Accurate-Mass Q-TOF mass spectrometer coupled to an Agilent 1200 RRLC system. ESI was conducted using a capillary voltage of 4000 V; the nebulizing and drying gases were nitrogen supplied at 25 psig and 10 L/h, respectively, and the drying gas temperature was 350 °C. The TOF fragmentor and skimmer were set to 180 V and 65 V, respectively.

A 10 µl aliquot of the mixture was removed at indicated times (0 – 48 h) and injected onto a Zorbax 300SB-C18 (2.1 x 100 mm; 3.5-Micron Agilent Technologies, Inc.) column with a flow rate of 0.4 mL/min. The mobile phase consisted of water with 0.1 % (v/v) formic acid (A) and acetonitrile with 0.1 % (v/v) formic acid (B) with a gradient elution as follows: 10 % B at 0 min, 50 % B at 4 min, 65 % at 7 min and 80% B at 10 min. Each run was followed by a 1 min post-run with 10% B. The total run-time analysis was 11 min and the column temperature was 27 °C. Spectra were acquired in the positive (ES+) ion mode, and full scan mass spectra (*m/z* 300–3200) were collected at a rate of 1 spectrum/sec. Mass data obtained from LC-MS was analyzed using Agilent MassHunter Qualitative Analysis software and Agilent MassHunter BioConfirm software version B.06.00.

6.2.4 Mapping of ilimaquinone adducts on *Mt*SK

Modified and unmodified *Mt*SK were digested with trypsin at a ratio of 1:20 (w/w) trypsin/substrate overnight at 37 °C in an assay buffer consisting of 100 mM Tris-HCl pH = 7.6, 50 mM KCl and 5 mM $MgCl_2$. Tryptic digests were analyzed by LC-MS and peptides were separated using the same column and conditions described above for intact protein analysis.

6.3 Results and discussion

6.3.1 Kinetics of ilimaquinone (IQ) inhibition on *Mt*SK

To study the irreversible inhibition of IQ on *Mt*SK, time-dependent inhibition studies were performed. After different pre-incubation times with IQ, the remaining activity of *Mt*SK was measured by addition of the substrates shikimate and ATP. As shown in Figure 6.2A, inhibition of *Mt*SK activity by IQ was dependent on the time of pre-incubation, an observation that is consistent with an irreversible mechanism of inhibition. Additionally, dialysis was performed to evaluate if the inhibition of IQ was reversible. After dialysis for 4, 8 and 24 h, the activity of *Mt*SK was not recovered (data not shown), corroborating the irreversible inhibition of ilimaquinone. Pseudo-first-order rate constants (k_{obs}) of inactivation for each concentration of ilimaquinone were determined from a plot of percent of remaining enzyme activity versus pre-incubation time (Fig. 6.2A). The second-order rate constants for inactivation of *Mt*SK by IQ were determined by re-plotting of the k_{obs} values as a function of inhibitor concentration as illustrated in Figure 6.2B.

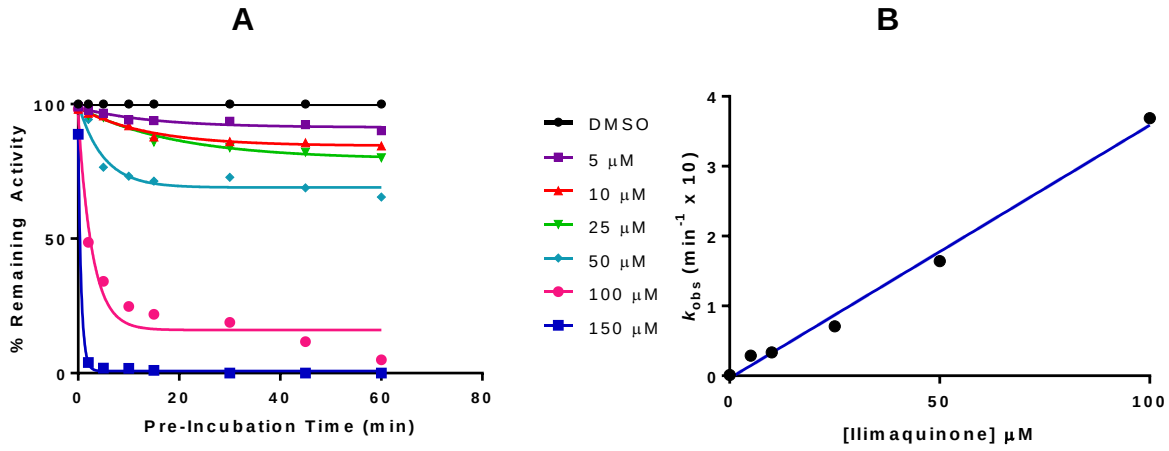

Figure 6.2. Time-dependent inhibition of *Mt*SK by ilimaquinone. (A) Plot of % activity remained versus pre-incubation time at different IQ concentrations. *Mt*SK (0.2 µM) was incubated with 0-150 µM of IQ and reactions were initiated after incubation times of 0, 2, 5, 10, 15, 30, 45 and 60 min by addition of 5 mM shikimate and 1.2 mM ATP. Activity is expressed as percent of control, each curve was used to determine k_{obs} values by fitting of the data to an exponential equation. (B) Plot of k_{obs} versus IQ concentrations, the slope of the curve corresponds to the second-order rate of inactivation k_{inact}/K_I. Results represent the average of two injections.

Plots of k_{obs} as a function of ilimaquinone concentration showed a linear non-saturating relationship (Fig 6.2B) passing through the origin, yielding an apparent inactivation rate constant (k_{inact}/K_I) of 0.03623 ± 0.001643 µM^{-1} min^{-1}. These results suggest a single-step inactivation involving a mechanism where there is no dissociation of inhibitor from the inactivated enzyme complex as depicted in the following Scheme [77]:

$$E + I \xrightarrow{k_{inact}[I]} E\text{-}I$$

6.3.2 Analysis of modified and unmodified intact *Mt*SK by LC-MS

Due to the ability of ilimaquinone to inhibit the activity of *Mt*SK irreversibly, the formation of covalent adducts was investigated by analysis of intact protein by mass spectrometry. To follow the modification of *Mt*SK, the enzyme was incubated with ilimaquinone at 4 °C (to avoid rapid protein degradation observed at room temperature) and aliquots were injected onto LC-MS at various time intervals as described in materials and methods. Data were collected over 48 hours and mass spectra were deconvoluted using Agilent MassHunter Qualitative Analysis software and Agilent MassHunter BioConfirm software version B.06.00.

The deconvoluted ESI-MS spectrum of control *Mt*SK demonstrated the presence of two species with an average molecular mass of 19,648.74 Da and 19,517.57 Da (Fig. 6.3), respectively, exhibiting a mass difference of 131.2 Da, consistent with the post-translational removal of N-terminal methionine. Incubation of *Mt*SK with IQ resulted in a shift of 326, 652 and 978 Da of the molecular mass of *Mt*SK (Fig. 6.4). These shifts corresponded to the mass of one, two and three molecules of ilimaquinone, respectively, with an average loss of 32.2 Da from a methoxy group plus hydrogen from the protein (H-OCH_3) or two atoms of oxygen (O_2). These findings support the results obtained by the time-dependent inhibition assays demonstrating that ilimaquinone is able to inhibit the activity of *Mt*SK irreversibly by the formation of covalent adducts.

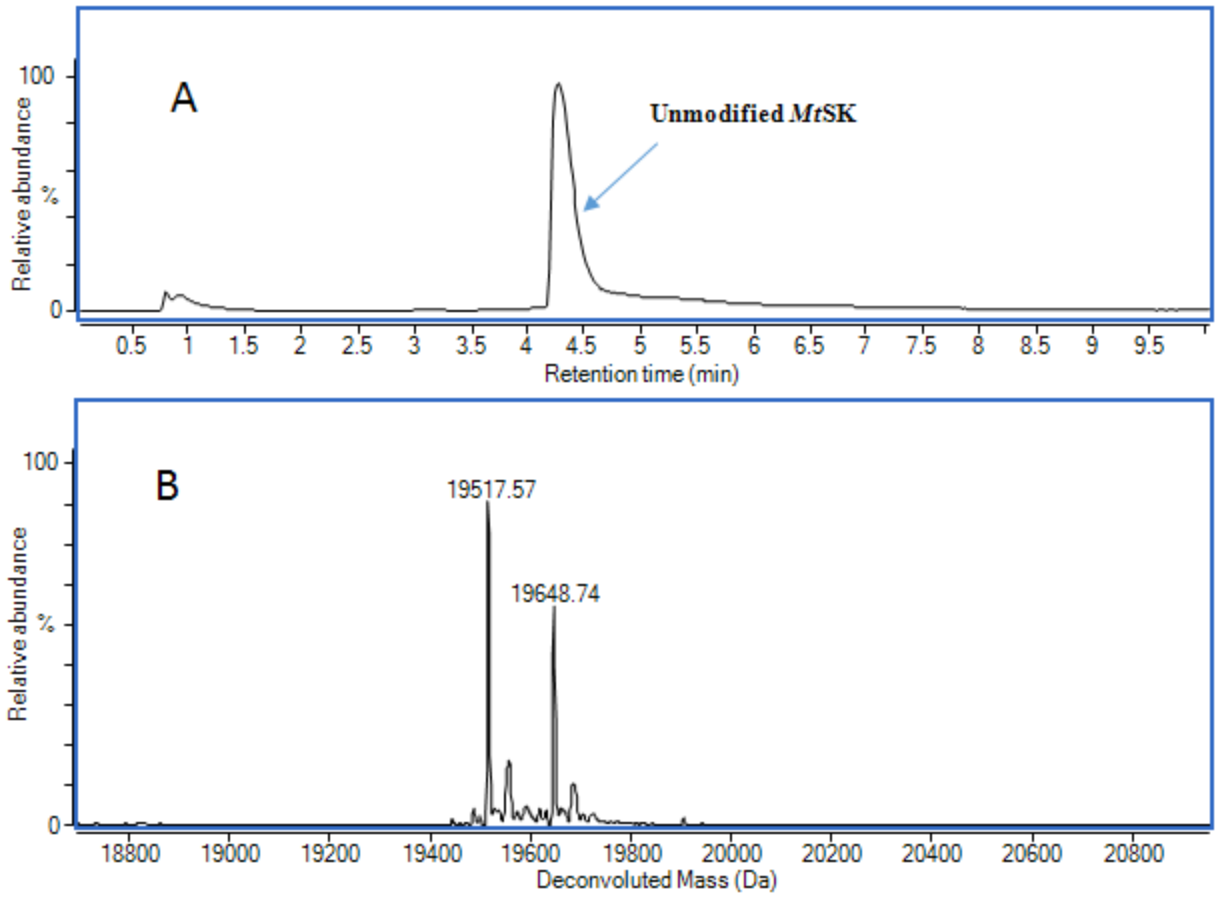

Figure 6.3. Intact protein LC-MS analysis of unmodified *Mt*SK. (A) Control *Mt*SK chromatogram showing a single peak for unmodified protein, RT = 4.27 min. (B) Deconvoluted mass spectrum of *Mt*SK showing the presence of two species corresponding to intact *Mt*SK (19648.74) and *Mt*SK with cleaved methionine (19517.57).

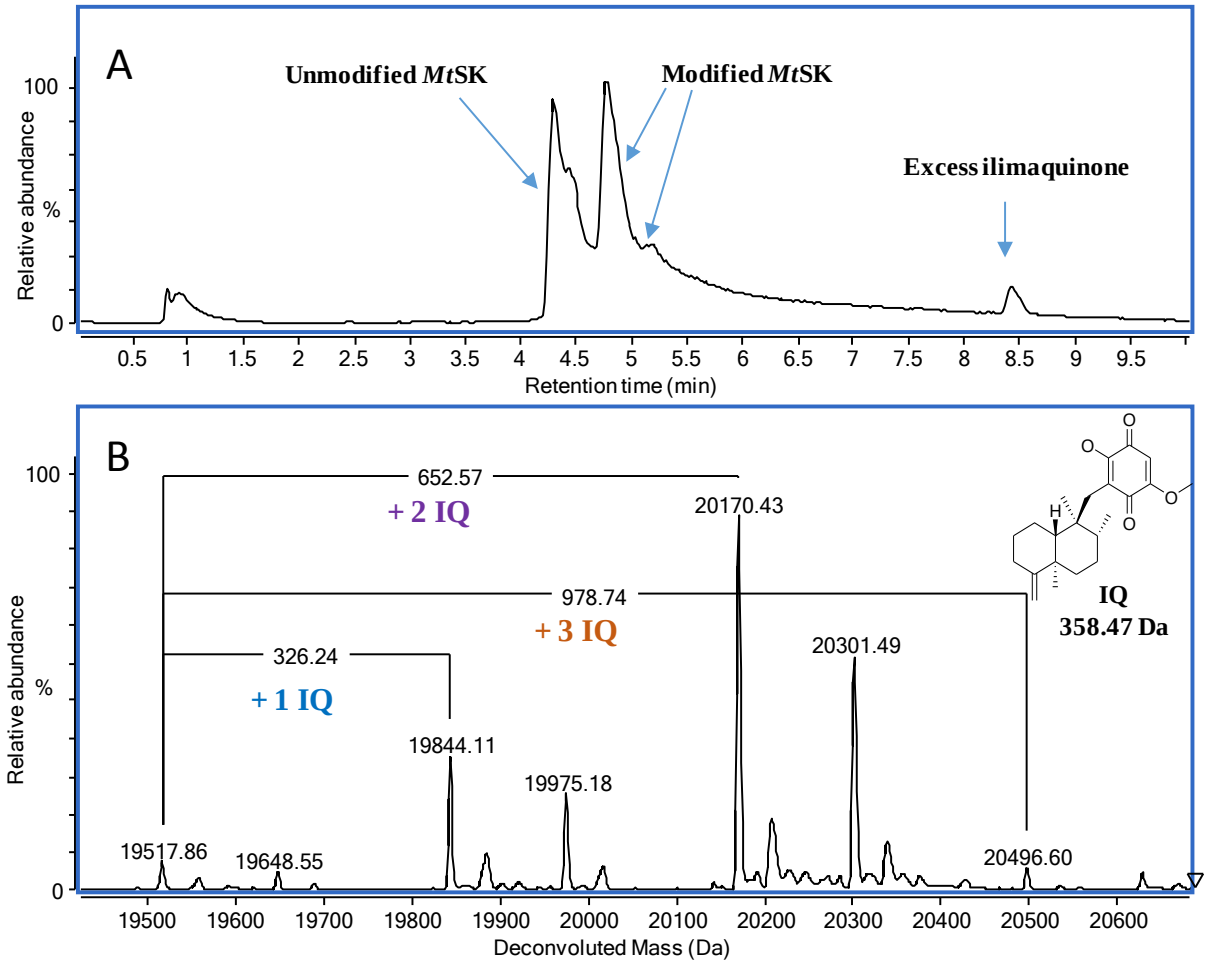

Figure 6.4. Intact protein LC-MS analysis of modified *Mt*SK. (A) Chromatogram of *Mt*SK incubated with 100 µM IQ for 48 hours at 4 °C showing peaks corresponding to unmodified *Mt*SK (RT = 4.27 min), modified *Mt*SK (RT = 4.77 and 5.18 min) and excess ilimaquinone (RT = 8.42). (B) Deconvoluted mass spectrum from 4.5 - 5.5 min showing the mass shits of 326.24, 652.57 and 978.74 Da corresponding to one, two and three adducts of ilimaquinone, respectively. Adducts were formed with both the intact and the methionine-cleaved species of *Mt*SK. Loss of 32.2 is consistent with the loss of a methoxy group plus hydrogen from the protein (H-OCH_3) or two atoms of oxygen (O_2).

6.3.3 Identification of ilimaquinone covalent adducts on tryptic digests of *Mt*SK

After incubation with ilimaquinone (100 µM) for 48 hours at 4 °C, *Mt*SK was digested with trypsin overnight at 37 °C and the resulting peptides were analyzed by LC-MS. As shown in Figure 6.5, peptides from control sample (Fig 6.5A) and from enzyme incubated with ilimaquinone (Fig 6.5B) were chromatographically resolved with a Zorbax 300SB-C18 (2.1 x 100 mm; 3.5) column using the conditions described above. To identify the potential peptides modified by ilimaquinone, a list of peptide masses was generated in the Agilent MassHunter BioConfirm software using the "Find Compound by Molecular Feature" option. Peptides with an added mass of 326.2, 652.57 or 978.74 Da and a low error (ppm) were selected as potential sites of modification.

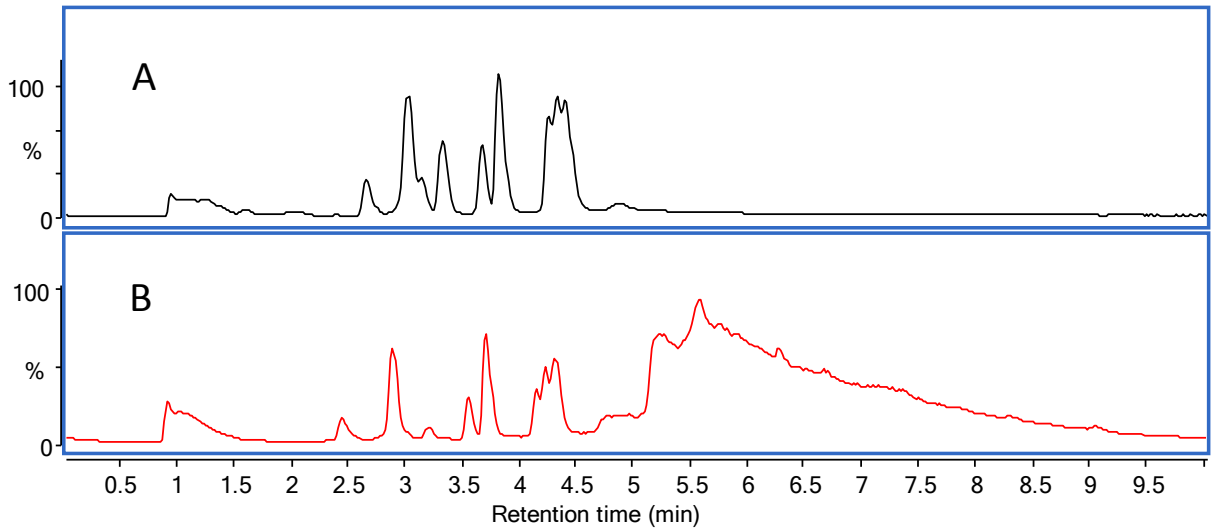

Figure 6.5. Total ion chromatogram (TIC) from the tryptic digest of (A) control *Mt*SK (1 µM) and (B) *Mt*SK (1 µM) incubated with ilimaquinone (100 µM) for 48 h at 4 °C using a Zorbax 300SB-C18 (2.1 x 100 mm; 3.5) column.

A mapping scheme of the proposed sites of modification is shown in Figure 6.6 and parameters of the identified peptides are described on Table 6.1. Further MS/MS experiments on the proposed peptides performed to obtain sequence information and to investigate the structure of the formed adducts yielded inconclusive results.

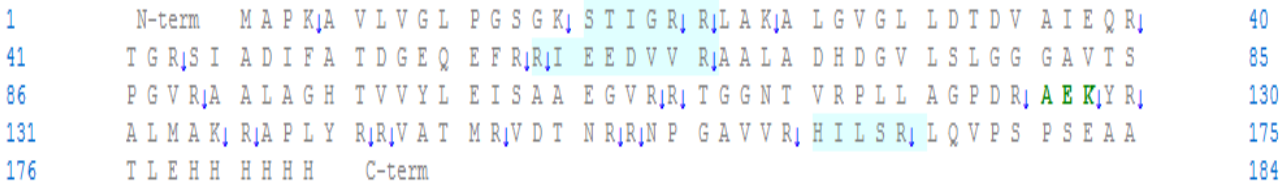

Figure 6.6 Mapping of sequence of *Mt*SK showing potential sites of modification by ilimaquinone. Proposed binding sites using the Agilent MassHunter BioConfirm software are highlighted in light blue. Amino acid sites of trypsin cleavage are denoted by blue arrows. Amino acids highlighted in green correspond to a sequence that was not covered by the software.

Table 6.1 Sequences of *Mt*SK showing predicted modifications by ilimaquinone (IQ) identified using the Agilent MassHunter BioConfirm software.

Sequence	Position	Theoretical mass	Observed mass	Error (ppm)	Predicted modification
STIGRR	A16-21	1014.5862	1014.5884	2.12	+1 IQ
RIEEDVVR	A59-66	1993.1832	1993.1759	-3.62	+3 IQ
HILSR	A161-165	1618.9666	1618.9716	3.05	+3 IQ

6.4 Conclusion

Several studies have reported that ilimaquinone, a metabolite of marine sponges, has a broad range of biological activities, such as anti-HIV, anti-microbial and anti-cancer activities. In the present study, we used LC-MS based approaches to demonstrate that ilimaquinone inhibits the activity of *Mt*SK irreversibly. Time-dependent inhibition studies showed that ilimaquinone inactivates *Mt*SK through a single-step consistent with an affinity-labeling mechanism. Additionally, the covalent mechanism of inactivation was confirmed by analysis of intact protein by LC-MS. Pre-incubation of the protein with ilimaquinone over 48 hours suggested that ilimaquinone can form up to three adducts on the structure of *Mt*SK. However MS/MS experiments were inconclusive and sites of inactivation were not clearly elucidated, the data generated in this study can provide insights into the mechanism of action of ilimaquinone on its various targets. Future experiments will aim to optimize the reaction conditions for the covalent adduct formation to further identify the binding sites and structure of the modified protein.

REFERENCES

1. V. Kumar, A. K. Abbas, N. Fausto, R. N. Richard. Robbins Basic Pathology (8th Ed). Saunders Elsevier. pp. 516–522, **2007**. ISBN 978-1-4160-2973-1.
2. S. W. Jr. Dooley, K. G. Castro, M. D. Hutton, R. J. Mullan, J. A. Polder, D. E. Jr. Snider. Guidelines for preventing the transmission of tuberculosis in health-care settings, with special focus on HIV-related issues. *MMWR Recomm Rep*. **1990**, 7, 1–29.
3. C. Nunes-Alves, M. G. Booty, S. M. Carpenter, P. Jayaraman, A. C. Rothchild, S. M. Behar. In search of a new paradigm for protective immunity to TB. *Nature Reviews Microbiology* **2014**, 12, 289–299.
4. N. M. Parrish, J. D. Dick, W. R. Bishai. Mechanisms of latency in *Mycobacterium tuberculosis*. *Trends Microbiol*. **1998**, 6, 107–112.
5. K. Patel, S. J. Singh, P. P. Singh. Models of Latent Tuberculosis: Their Salient Features, Limitations, and Development. *J Lab Physicians* **2011**, 3, 75–79.
6. Institute of Medicine (US) Forum on Microbial Threats. Microbial Evolution and Co-Adaptation: A Tribute to the Life and Scientific Legacies of Joshua Lederberg: Workshop Summary. Washington (DC): National Academies Press (US); **2009**. 5, Infectious Disease Emergence: Past, Present, and Future.Available from: http://www.ncbi.nlm.nih.gov/books/NBK45714/
7. WHO. Global tuberculosis control: WHO report **2012**. WHO, Geneva, Switzerland.
8. Centers for Disease Control and Prevention. Basic TB Facts (**2010**). Retrieved from http://www.cdc.gov/TB/TOPIC/basics/default.htm

9. M. L. Grayson, D. Heymann, D. Pittet Didier. The evolving threat of antimicrobial resistance- Options for action World health organization. WHO, Vol. 1 (**2012**).

10. National Intelligence Council. The Global Infectious Disease Threat and Its Implications for the United States. National Intelligence Estimate. http://www.dni.gov/nic/PDF_GIF_ otherprod/infectiousdisease/infectiousdiseases.pdf **2000.**

11. K. Thomas. F.D.A Approves New Tuberculosis Drug. *The New York Times*, December 31, **201**2. Retrieved from http://www.nytimes.com

12. A. Mattelli, A. C. Carvalho, K. E. Dooley, A. Kritski. TMC207: the first compound of a new class of potent anti-tuberculosis drugs. *Future Microbiol***. 2010**, 5, 849–858.

13. K. Duncan. Progress in TB drug development and what is still needed. *Tuberculosis* **200**3, 83, 201–207.

14. K. M. Herrmann. The shikimate pathway: early steps in the biosynthesis of aromatic compounds. *Plant Cell* **1995**, 7, 907–919.

15. H. G. Floss. Natural products derived from unusual variants of the shikimate pathway. *Nat. Prod. Rep.* **1997**, 14, 433–452.

16. R. Bentley. The shikimate pathway: a metabolic tree with many branches. *Crit. Rev. Biochem. Mol. Biol.* **1990**, 25, 307–384.

17. J. J. Voos, K. Rutter, B. G. Schroder, H. Su, Y. Zhu, C. B. 3rd Barry. The salicylate-derived mycobactin siderophores of *Mycobacterium tuberculosis* are essential for growth in macrophages. *Proc. Natl. Acad. Sci. USA* **2000**, 97, 1252–1257.

18. J. R. Coggins, C. Abell, L. B. Evans, M. Frederickson, D. A. Robinson, A. W. Roszak, A. P. Lapthorn. Experiences with the shikimate-pathway enzymes as targets for rational drug design. *Biochem. Soc. Trans*. **2003**, 31, 548–552.

19. E. Schönbrunn, S. Eschenburg, W. A. Shuttleworth, J. V Schloss, N. Amrhein, J. N. Evans W. Kabsch. *Proc. Natl. Acad. Sci*. **2001**, 98, 1376–1380.

20. F. Roberts, C. W. Roberts, J. J. Johnson, D. E. Kyle, T. Krell, J. R. Coggins, G. H. Coombs, W. K. Milhous, S. Tzipori, D. J Ferguson, D. Chakrabarti, R. McLeod. *Nature* **1998**, 393, 801–805.

21. G. M. Davies, K. J. Barret-Bee, D. A. Jude, M. Lehan, W. W. Nichols, P. E. Pinder, J. L. Thain, W. J. Watkins, R. G. Wilson. (6S)-6-fluoroshikimic acid, an antibacterial agent acting on the aromatic biosynthetic pathway. *Antimicrob. Agents Chemother*. **1994**, 38, 403–406.

22. T. Krell, J. R. Coggins, A. J. Lapthorn. The three-dimensional structure of shikimate kinase. *J. Mol. Biol*. **1998**, 278, 983–997.

23. M. D. Hartmann, G. P. Bourenkov, A. Oberschall, N. Strizhof, H. D. Bartunik HD. Mechanism of phosphoryl transfer catalyzed by shikimate kinase from *Mycobacterium tuberculosis*. *J. Mol. Biol*. **2006**, 364, 411–423.

24. C. L. Schmidt, H. J. Danneel, G. Schultz, B. B. Buchanan. Shikimate kinase from Spinach chloroplasts: Purification, characterization, and regulatory function in aromatic amino acid biosynthesis. *Plant Physiol*. **1990**, 93, 758–766.

25. B. Dhaliwal, C. E. Nichols, J. Ren, M. Lockyer, I. Charles, A. R. Hawkins, D. K. Stammers. Crystallographic studies of shikimate binding and induced conformational changes in *Mycobacterium tuberculosis* shikimate kinase. *FEBS Lett*. **200**4, 574, 49–54.

26. T. Parish, N. G. Stoker. The common aromatic amino acid biosynthesis pathway is essential in *Mycobacterium tuberculosis*. *Microbiology* **2002**, 148, 3069–3077.

27. W. Jr Filgueira de Azevedo, F. Canduri, J. Simões de Oliveira, L. A. Basso, M. S. Palma, J. H. Pereira, D. S. Santos. Molecular model of shikimate kinase from *Mycobacterium tuberculosis*. *Biochem. Biophys. Res. Commun.* **2002**, 295, 142–148.

28. H. Yan, M. D. Tsai. Nucleoside monophosphate kinases: structure, mechanism, and substrate specificity. *Advan. Enzymol. Relat. Areas Mol. Biol.* **1999**, 73, 103–134.

29. J. E. Walker, M. Saraste, M. J. Runswick, N. J. Gay. Distantly related sequences in the alpha- and beta-subunits of ATP synthase, myosin, kinases and other ATP-requiring enzymes and a common nucleotide binding fold. *EMBO J*, **1982**, 1, 945–951.

30. T. Krell, J. Maclean, D. J. Boam, A. Cooper, M. Resmini, K. Brocklehurst, S. M. Kelly, N. C. Price, A. J. Lapthorn, J. R. Coggins. Biochemical and X-ray crystallographic studies on shikimate kinase: the important structural role of the P-loop lysine. *Protein Sci*. **2001**, 10, 1137–1149.

31. Y. Gu, L. Reshetnikova, Y. Li, Y. Wu, H. Yan, S. Singh, X. Ji X. Crystal structure of shikimate kinase from *Mycobacterium tuberculosis* reveals the dynamic role of the LID domain in catalysis. *J. Mol. Biol*. **2002**, 319, 779–789.

32. C. Vonrhein, G. J. Schlauderer, G. E. Schulz. Movie of the structural changes during a catalytic cycle of nucleoside monophosphate kinases. *Structure* **1995**, 3, 483–490.

33. A. Matte, L. W. Tari, T. J. Delbaere. How do kinases transfer phosphoryl groups? *Structure* **1998**, 6, 413–419.

34. W. P. Jencks. Binding energy, specificity, and enzymic catalysis: the circe effect. *Adv. Enzymol. Relat. Areas Mol. Biol.* **1975**, 43, 219–410.

35. T. Krell, J. R. Coggins, A. J. Lapthorn. The three-dimensional structure of shikimate kinase. *J. Mol. Biol*. **1998**, 278, 983–997.

36. S. Surade, T. L. Blundell. Structural biology and drug discovery of difficult targets: the limits of ligandability. *Chem Biol*. **2012**, 19, 42–50.

37. B. Blanco, V. Prado, E. Lence, J. M. Otero, C. Garcia-Doval, M. J. van Raaij, A. L. Llamas-Saiz, H. Lamb, A. R. Hawkins, C. González-Bello. *Mycobacterium tuberculosis* Shikimate Kinase Inhibitors: Design and Simulation Studies of the Catalytic Turnover. *J. Am. Chem. Soc.* **2013**, 135, 12366–12376.

38. J. D. Coracini, W. F. Jr de Azevedo. Shikimate kinase, a protein target for drug design. *Curr. Med. Chem*. **2014**, 21, 592–604.

39. J. H. Pereira, J. S. de Oliveira, F. Canduri, M. V. Dias, M. S. Palma, L. A. Basso, D. S. Santos, W. F. Jr de Azevedo. Structure of shikimate kinase from *Mycobacterium tuberculosis* reveals the binding of shikimic acid. *Acta Crystallogr. D Biol. Crystallogr.* **2004**, 60, 2310–2319.

40. J. H. Pereira, I. B. Vasconcelos, J. S. Oliveira, R. A. Caceres, W. F. Jr de Azevedo, L. A. Basso, D. S. Santos. Shikimate kinase: a potential target for development of novel antitubercular agents. *Curr. Drug Targets* **2007**, 8, 459–468.

41. D. D. Leipe, E. V. Koonin, L. Aravind. Evolution and classification of P-loop kinases and related proteins. *J Mol Biol*. **2003**, 31, 333, 781–815.

42. R. G. Ducati, L. A. Basso, D. S. Santos. Mycobacterial shikimate pathway enzymes as targets for drug design. *Curr Drug Targets* **2007**, 8, 423–435.

43. A. G. Marshall, C. L. Hendrickson. High-resolution mass spectrometers. *Annu. Rev. Anal. Chem.* **2008**, 1, 579–599.

44. A. J. Goraczko. Correlation between the spectrum resolution and the peak location accuracy in the isotopomeric cluster. *Int. J. Mass Spectrom*. **2011**, 303, 51–54.

45. A. G. Brenton, A. R. Godfrey. Accurate mass measurement: Terminology and treatment of data. *J. Am. Soc. Mass Spectrom*. **2010**, 21, 1821–1835.

46. W. A. Korfmacher. Principles and applications of LC–MS in new drug discovery. Drug *Discov. Today* **200**5, 10, 1357–1367.

47. J. Michnowicz. Mass spectrometry in drug discovery and development. *Nature Reviews Drug Discovery* **200**2, 1, 651.

48. G. J. Deng, G. Sanyal. Applications of Mass Spectrometry in Early Stages of Target Based Drug Discovery. *J. Pharm. Biomed. Anal*. **2006**, 40, 528–538.

49. D. A. Annis, E. Nickbarg, X. Yang, M. R. Ziebell, C. E. Whitehurst. Affinity selection-mass spectrometry screening techniques for small molecule drug discovery. *Curr. Opin. Chem. Biol.* **2007**, 11, 518–526.

50. M. A. Raji, P. Frycak, M. Beall, M. Sakrout, J. M. Ahn, Y. Bao, D. W. Armstrong, K. A. Schug. Development of an ESI-MS Screening Method for Evaluating Binding Affinity between Integrin Fragments and RGD-Based Peptides. *Int. J. Mass Spectrom*. **2007**, 262, 232–240.

51. G. Deng, R. F. Gu, S. Marmor, S. L. Fisher, H. Jahic, G. Sanyal. Development of an LC-MS based enzyme activity assay for MurC: application to evaluation of inhibitors and kinetic analysis. *J. Pharm. Biomed. Anal*. **2004**, 35, 817–828.

52. J. A. Butera. Phenotypic screening as a strategic component of drug discovery programs targeting novel antiparasitic and antimycobacterial agents: an editorial. *Med. Chem*. **2013**, 56, 7715–7718.

53. G. L. Mandell, J. E. Bennett, R. Dolin. Mandell, Douglas, and Bennett's principles and practice of infectious diseases (7th Ed). Churchill Livingstone/Elsevier, Chapter 250, **2010**. Philadelphia, PA. ISBN 978-0-443-06839-3.

54. S. T. Cole, R. Brosch, J. Parkhill, T. Garnier, C. Churcher, D. Harris, S. V. Gordon, K. Eiglmeier, S. Gas, C. E. 3rd Barry, F. Tekaia, K. Badcock, D. Basham, D. Brown, T. Chillingworth, R. Connor, R. Davies, K. Devlin, T. Feltwell, S. Gentles, N. Hamlin, S. Holroyd, T. Hornsby, K. Jagels, A. Krogh, J. McLean, S. Moule, L. Murphy, K. Oliver, J. Osborne, M. A. Quail, M. A. Rajandream, J. Rogers, S. Rutter, K. Seeger, J. Skelton, R. Squares, S. Squares, J. E. Sulston, K. Taylor, S. Whitehead, B. G. Barrell. Deciphering the biology of *Mycobacterium tuberculosis* from the complete genome sequence. *Nature* **1998**, 393, 537–544.

55. L. A. Rosado, I. B. Vasconcelos, M. S. Palma, V. Frappier, R. J. Najmanovich, D. S. Santos, L. A. Basso. The Mode of Action of Recombinant *Mycobacterium tuberculosis* Shikimate Kinase: Kinetics and Thermodynamics Analyses. *PLoS ONE* **2013**, 8, e61918.

56. C. L. Varnado, K. M. Hertwig, R. Thomas, J. K. Roberts, D. C. Goodwin. Properties of a novel periplasmic catalase-peroxidase from *Escherichia coli* O157:H7. *Arch. Biochem. Biophys*. **2004**, 421, 166–174.

57. P. T. Wingfield. In Current Protocols in Protein Science (Coligan, J. E.; Dunn, B. M.; Ploegh, H. L.; Speicher, D. W.; eds.), John Wiley and Sons: New York, **1997**; pp 6.01–6.1.22.

58. S. Spector, J. M. Flynn, B. Tidor, T. A. Baker, R. T. Sauer. Expression of N-formylated proteins in *Escherichia coli*. *Protein Expr. Purif*. **2003**, 2, 317–322.

59. C. Blondin, L. Serina, L. Wiesmüller, A. M. Gilles, O. Bârzu. Improved spectrophotometric assay of nucleoside monophosphate kinase activity using the pyruvate kinase/lactate dehydrogenase coupling system. *Anal. Biochem*. **1994**, 220, 219–221.

60. Oliveira JS1, Pinto CA, Basso LA, Santos DS. Cloning and overexpression in soluble form of functional shikimate kinase and 5-enolpyruvylshikimate 3-phosphate synthase enzymes from *Mycobacterium tuberculosis*. *Protein Expr. Purif*. **2001**, 22, 430–435.

61. E. Cerasoli, S. M. Kelly, J. R. Coggins, D. J. Boam, D. T. Clarke, N. C. Price. The refolding of type II shikimate kinase from *Erwinia chrysanthemi* after denaturation in urea. *European Journal of Biochemistry* **2002**, 2124–2132.

62. C. Han, J. Zhang, L. Chen, C. Kaixian, X. Shen, H. Jiang. Discovery of *Helicobacter pylori* shikimate kinase inhibitors: bioassay and molecular modeling. *Bioorg. Med. Chem*. **2007**, 15, 656–662.

63. J. Inglese, R. L. Johnson, A. Simeonov, M. Xia, W. Zheng, C. P. Austin, D. S. Auld. High-throughput screening assays for the identification of chemical probes. *Nat. Chem. Biol*. **2007**, 3, 466–479.

64. K. Chikh, F. Flourie, K. Arab, J. P. Steghens. Kinetic measurement by LC/MS of gamma-glutamylcysteine ligase activity. *J. Chromatogr. B Analyt. Technol. Biomed. Life Sci*. **2005**, 827, 32–38.

65. C. T. Houston, W. P. Taylor, T. S. Widlanski, J. P. Reilly. Investigation of Enzyme Kinetics Using Quench-Flow Techniques with MALDI-TOF Mass Spectrometry. *Anal. Chem.* **2000**, 72, 3311–3319.

66. D. L. Zechel, L. Konermann, S. G. Withers, D. J. Douglas. Pre-steady state kinetic analysis of an enzymatic reaction monitored by time-resolved electrospray ionization mass spectrometry. *Biochemistry* **1998**, 37, 7664–7669.

67. B. Bothner, R. Chavez, J. Wei, C. Strupp, Q. Phung, A. Schneemann, G. Siuzdak. Monitoring enzyme catalysis with mass spectrometry. *J. Biol. Chem*. **2000**, 275, 13455–13459.

68. N. Pi, J. I. Armstrong, C. R. Bertozzi, J. A. Leary. Kinetic analysis of NodST sulfotransferase using an electrospray ionization mass spectrometry assay. *Biochemistry* **2002**, 41, 13283–13288.

69. A. Liesener A, U. Karst. Monitoring enzymatic conversions by mass spectrometry: a critical review. *Anal. Bioanal. Chem*. **2005**, 382, 1451–1464.

70. V. Mulabagal, A. I. Calderón. Development of an ultrafiltration-liquid chromatography/mass spectrometry (UF-LC/MS) based ligand-binding assay and an LC/MS based functional assay for *Mycobacterium tuberculosis* shikimate kinase. *Anal. Chem*. **2010**, 82, 3616–3621.

71. H. B. Brooks, S. Geeganage, S. D. Kahl, C, Montrose, S. Sittampalam, M. C. Smith, J. R. Weidner. In Basics of enzymatic assays for HTS. G. S. Sittampalam, J. Weidner, D. Auld, M. Glicksman, M. Arkin, A. Napper, J. Inglese, editors. Bethesda, MD: Eli Lilly & Company and the National Center for Advancing Translational Sciences; **2004**. pp. 5–7.

72. C. P. Vianna, W. F. Jr de Azevedo. Identification of new potential *Mycobacterium tuberculosis* shikimate kinase inhibitors through molecular docking simulations. *J. Mol. Model*. **2012**, 18, 755–764.

73. K. C. Hsu, W. C. Cheng, Y. F. Chen, H. J. Wang, L. T. Li, W. C. Wang, J. M. Yang. Core Site-Moiety Maps Reveal Inhibitors and Binding Mechanisms of Orthologous Proteins by Screening Compound Libraries. *PLoS ONE* **2012**,7, e32142.

74. A. Segura-Cabrera, M. A. Rodriguez-Perez. Structure-based prediction of *Mycobacterium tuberculosis* shikimate kinase inhibitors by high-throughput virtual screening. *Bioorg. Med. Chem. Lett.* **2008**,18,3152–3157.

75. B. S. Bandodkar, S. Schmitt. Pyrazolone derivates, processes for preparing them, pharmaceutical compositions containing them, and their use as inhibitors of the *Mt*SK (*Mycobacterium tuberculosis* shikimate kinase) enzyme. Patent: WO/2007/020426 A1.

76. B. Blanco, V. Prado, E. Lence, J. M. Otero, C. Garcia-Doval, M. J. van Raaij, A. L. Llamas-Saiz, H. Lamb, A. R. Hawkins, C. González-Bello. *Mycobacterium tuberculosis* Shikimate Kinase Inhibitors: Design and Simulation Studies of the Catalytic Turnover. *J. Am. Chem. Soc.* **2013**, 135, 12366–12376.

77. R. A. Copeland. Evaluation of enzyme inhibitors in drug discovery. A guide for medicinal chemists and pharmacologists. *Methods Biochem. Anal*. **2005**, 46, 1–265.

78. J. Simithy, N. Reeve, J. V. Hobrath, R. C. Reynolds, A. I. Calderón. Identification of shikimate kinase inhibitors among anti-*Mycobacterium tuberculosis* compounds by LC-MS. *Tuberculosis* **2014**, 94, 152–158.

79. W. F. de Azevedo. Protein targets for development of drugs against *Mycobacterium tuberculosis*. *Curr. Med. Chem*. **2011**, 8, 1255–1277.

80. D. Nikolic, S. Habibi-Goudarzi, D. G. Corley, S. Gafner, J. M. Pezzuto, R. B. van Breeman. Evaluation of cyclooxygenase-2 inhibitors using pulsed ultrafiltration mass spectrometry. *Anal. Chem*. **2000**, 72, 3853–3859.

81. D. Liu, J. Guo, Y. Luo, D. J. Broderick, M. I. Schimerlik, J. M. Pezzuto, R. B. van Breemen. Screening for ligands of human retinoid X receptor-α using ultrafiltration mass spectrometry. *Anal. Chem*. **2007**, 79, 9398–93402.

82. Y. Choi, R. B. van Breemen. Development of a screening assay for ligands to the estrogen receptor based on magnetic microparticles and LC-MS. *Comb. Chem. High Throughput Screen*. **2008**, 11, 1–6.

83. A. R. De Boer, H. Lingeman, W. M. A Niessen, H. Irth H. Mass spectrometry-based biochemical assays for enzyme inhibitor screening. *Trends Anal. Chem*. **2007**, 26, 867–883.

84. K. D. Greis. Mass spectrometry for enzyme assays and inhibitor screening: an emerging application in pharmaceutical research. *Mass Spectrom. Rev*. **2006**, 26, 324–339.

85. M. M. Siegel. Early discovery drug screening using mass spectrometry. *Curr. Top. Med. Chem.* **2002**, 2, 13–33.

86. M. C. Jecklin, D. Touboul, R. Jain, E. N. Toole, J. Tallarico, P. Drueckes, P. Ramage, R. Zenobi. Affinity classification of kinase inhibitors by mass spectrometric methods and validation using standard IC_{50} measurements. *Anal. Chem*. **2009**, 81, 408–419.

87. M. Kumar, S. Verma, S. Sharma, A. Srinivasan, T. P. Singh, P. Kaur. Structure-based in silico design of a high-affinity dipeptide inhibitor for novel protein drug target Shikimate kinase of *Mycobacterium tuberculosis*. *Chem. Biol. Drug Des*. **2010**, 76, 277–284.

88. D. J. Payne, M. N. Gwynn, D. J. Holmes, D. L. Pompliano. Drugs for bad bugs: confronting the challenges of antibacterial discovery. *Nat. Rev. Drug Discov*. **2007**, 6, 29–40.

89. Assay Guidance Manual Version 5.0, 2008, Eli Lilly and Company and NIH Chemical Genomics Center. Available online at: http://www.ncgc.nih.gov/guidance/manual_toc. html

90. S. Ananthan, E. R. Faaleolea, R. C. Goldman, J. V. Hobrath, C. D. Kwong, B. E. Laughon, J. A. Maddry, A. Mehta, L. Rasmussen, R. C. Reynolds, J. A. 3rd Secrist, N. Shindo, D. N. Showe, M. I. Sosa, W. J. Suling, E. L. White. High-throughput screening for inhibitors of *Mycobacterium tuberculosis*. *Tuberculosis* **2009**, 89, 334–353.

91. J. A. Maddry, S. Ananthan, R. C. Goldman, J. V. Hobrath, C. D. Kwong, C. Maddox, L. Rasmussen, R. C. Reynolds, J. A. 3rd Secrist, M. I. Sosa, E. L. White, W. Zhang. Antituberculosis activity of the molecular libraries screening center network library. *Tuberculosis* **2009**, 89, 354–363.

92. R. C. Reynolds, S. Ananthan, E. Faaleolea, J. V. Hobrath, C. D. Kwong, C. Maddox, L. Rasmussen, M. I. Sosa, E. Thammasuvimol, E. L. White, W. Zhang, J. A. 3rd Secrist. High throughput screening of a library based on kinase inhibitor scaffolds against *Mycobacterium tuberculosis* H37Rv. *Tuberculosis* **2012**, 92, 72–83.

93. R. R. Somani, P. Y. Shirodkar. Synthesis, antibacterial, and antitubercular evaluation of some 1,3,4-oxadiazole analogues. *Asian J. Chem.* **2008**, 20, 6189–6194.

94. S. R. Pattan, P. A. Rabara, J. S. Pattan, A. A. Bukitagar, V. S. Wakale, D. S. Musmade. Synthesis and evaluation of some novel substituted 1,3,4-oxadiazole and pyrazole derivatives for antitubercular activity. *Indian J. Chem. B* **2009**, 48B, 1453–1456.

95. A. Geronikaki, P. Eleftheriou, P. Vicini, I. Alam, A. Dixit, A. K. Saxena. 2-Thiazolylimino/heteroarylimino-5-arylidene-4-thiazolidinones as new agents with SHP-2 inhibitory action. *J. Med. Chem*. **2008**, 51, 5221–5228.

96. K. D. Surya, L-H. Chen, J. L. Stebbins, T. Machleidt, M. Riel-Mehan, R. Dahl, V. Chen, H. Yuan, E. Barile, A. Emdadi, R. Murphy, M. Pellecchiaa. Discovery of 2-(5-nitrothiazol-2-

ylthio)benzol[d]thiazoles as novel c-Jun N-terminal kinase inhibitors. *Bioorg. Med. Chem*. **2009**, 17, 2712–2717.

97. T. P. Holler, A. G. Evdokimov, L. Narasimhan. Structural biology approaches to antibacterial drug discovery. *Exp. Opin. Drug Dis*. **2007**, 2, 1085–1101.
98. H-F. Ji, X-J. Li, H-Y. Zhang. Natural products and drug discovery. Can thousands of years of ancient medical knowledge lead us to new and powerful drug combinations in the fight against cancer and dementia? *EMBO rep*. **2009**, 10, 194–200.
99. K. A. El Sayed, P. Bartyzel, X. Shen, T. L. Perry, J. K. Zjawiony, M. T. Hamann. Marine Natural Products as Antituberculosis Agents. *Tetrahedron* **2000**, 56, 949–953.
100. K. K. H. Ang, M. J. Holmes, T. Higa, M. T. Hamann, U. A. K. Kara. *In Vivo* Antimalarial Activity of the Beta-Carboline Alkaloid Manzamine A. *Antimicrob. Agents Chemother*. **200**0, 44, 1645–1649.
101. M. Yousaf, K. A. El Sayed, K. V. Rao, C. W. Lim, J. F. Hu, M. Kelly, F. Franzblau, O. Peraud, R. T. Hill, M. T. Hamann. 12,34 Oxamanzamine, novel biocatalytic and natural products from manzamine Indo-Pacific producing sponges. *Tetrahedron* **2002**, 59, 7397–7402.
102. K. V. Rao, B. D. Santarsiero, A. D. Mesecar, R. F. Schinazi, B. L. Tekwani, M. T. Hamann. New manzamine alkaloids with activity against infectious and tropical parasitic diseases from Indonesian sponges. *J. Nat. Prod*. **2003**, 66, 823–827.
103. K. V. Rao, N. Kasanah, S. Wahyuono, B. L. Tekwani, R. F. Schinazi, M. T. Hamann. Three new manzamine alkaloids from common Indonesian sponges and their activity against infectious and tropical parasitic diseases. *J. Nat. Prod*. **2004**, 67, 1314–1318.

104. R. Sakai, T. Higa, C. W. Jefford, G. Bernardinelli. Manzamine A, a novel antitumor alkaloid from a sponge. J. *Am. Chem. Soc*. **1986**, 108, 6404–6405.

105. R. A. Edrada, P. Proksch, V. Wray, L. Witte, W. E. Müller, R. W. Van Soest. Four new bioactive manzamine-type alkaloids from the Philippine marine sponge Xestospongia ashmorica. J. *Nat. Prod*. **1996**, 59, 1056–1060.

106. J. Peng, S. Kudrimoti, S. Prasanna, S. Odde, R. J. Doerksen, H. K. Pennaka, Y. M. Choo, K. V. Rao, B. L. Tekwani, V. Madgula, S. I. Khan, B. Wang, A. M. Mayer, M. R. Jacob, L. c. Tu, J. Gertsch, M. T. Hamann. Structure--Activity Relationship and Mechanism of Action Studies of Manzamine Analogues for the Control of Neuroinflammation and Cerebral Infections. *J. Med. Chem*. **2010**, 53, 61–76.

107. A. E. Wahba, J. Peng, S. Kudrimoti, B. L. Tekwani, M. T. Hamann. Structure-activity relationship studies of manzamine A: amidation of positions 6 and 8 of the beta-carboline moiety. *Bioorg. Med. Chem*. **2009**, 17, :7775–7782.

108. A. L. Waters, R. T. Hill, A. R. Place, M. T. Hamann. The expanding role of marine microbes in pharmaceutical development. *Curr. Opin. Biotechnol*. **2010**, 21, 780–786.

109. M. E. Welsch, S. A. Snyder, B. R. Stockwell. Privileged scaffolds for library design and drug discovery. *Curr. Opin. Chem. Biol*. **2010**, 14, 347–361.

110. L. Espinoza Catalán, E. Baeza Maturana, K. Catalán Marín, M. Osorio Olivares, H. Carrasco Altamirano, M. Cuellar Fritis, J. Villena García. Synthesis and Antitumor Activity of Diterpenylhydroquinone Derivatives of Natural Ent-Labdanes. *Molecules* **2010**, 15, 6502–6511.

111. S. Park, E. Yun, I. H. Hwang, S. Yoon, D. E. Kim, J. S. Kim, M. Na, G. Y. Song, S. Oh. Ilimaquinone and ethylsmenoquinone, marine sponge metabolites, suppress the proliferation

of multiple myeloma cells by down-regulating the level of β-catenin. *Mar. Drugs* **201**4, 12, 3231–3244.

112. B. G. Kim, T. G. Chun, H. Y. Lee, M. L. Snapper. A new structural class of S-adenosylhomocysteine hydrolase inhibitors. *Bioorg. Med. Chem*. **2009**, 17, 6707–6714.

113. L. A. Tziveleka, C. Vagias, V. Roussis. Natural products with anti-HIV activity from marine organisms. *Curr. Top Med. Chem*. **2003**, 3, 1512–1535.

114. A. M. Popov, S. I. Stekhova, N. K. Utkina, N. M. Rebachuk. Antimicrobial and cytotoxic activity of sesquiterpenequinones and brominated diphenyl esters isolated from marine sponges. *Pharm. Chem. J.* **1999**, 33, 71–73.

115. K. A. El Sayed, D. C. Dunbar, D. K. Goins, C. R. Cordova, T. L. Perry, K. J. Wesson, S. C. Sanders, S. A. Janus, M. T. Hamann. The marine environment A resource for prototype antimalarial agents. *Journal Of Natural Toxins* **1996**, 5, 261–285.

116. B. Veit, J. K. Yucel, V. Malhotra. Microtubule independent vesiculation of Golgi membranes and the reassembly of vesicles into Golgi stacks. *J. Cell Biol*. **1993**, 122, 1197–1206.

117. P. A. Takizawa, J. K. Yucel, B. Veit, D. J. Faulkner, T. Deerinck, G. Soto, M. Ellisman, Malhotra V. Complete vesiculation of Golgi membranes and inhibition of protein transport by a novel sea sponge metabolite, ilimaquinone. *Cell* **1993**, 73, 1079–1090.

118. P.A. Feldman, J. Kim, D.W. Laird. Loss of Gap Junction Plaques and Inhibition of Intercellular Communication in Ilimaquinone-treated BICR-M1Rk and NRK Cells. *J Membr. Biol*. **1997**, 155, 275–287.

119. P. H. Lu, S. C. Chueh, F. L. Kung, S. L. Pan, Y. C. Shen, J. H. Guh. Ilimaquinone, a marine sponge metabolite, displays anticancer activity via GADD153-mediated pathway. *Eur. J. Pharmacol*. **2007**, 556, 45–54.

120. C. Jamora, P. A. Takizawa, R. F. Zaarour, C. Denesvre, D. J. Faulkner, V. Malhotra. Regulation of Golgi structure through heterotrimeric G proteins. *Cell* **1997**, 91, 617–626.

121. H. Sonoda, T. Okada, S. Jahangeer, S. I. Nakamura. Requirement of Phospholipase D for Ilimaquinone-induced Golgi Membrane Fragmentation. *J. Biol. Chem*. **2007**, 282, 34085–34092.

122. C. Jamora, N. Yamanouye, J. Van Lint, J. Laudenslager, J. R. Vandenheede, D. J. Faulkner, V. Malhotra. Gβγ-Mediated Regulation of Golgi Organization Is through the Direct Activation of Protein Kinase D. *Cell* **1999**, 98, 59–68.

123. L. Du, Y-D Zhou, D. G. Nagle. Inducers of Hypoxic Response: Marine Sesquiterpene Quinones Activate HIF-1. *J. Nat. Prod*. **2013**, 76, 1175–1181.

124. T. Oda, W. Wang, K. Ukai, T. Nakazawa, M. Mochizuki. A sesquiterpene quinone, 5-Epi-smenospongine, promotes TNF-α production in LPS-stimulated RAW 264.7 Cells. *Mar. Drugs* **2007**, 5, 151–156.

125. H. S. Radeke, C. A. Digits, R. L. Casaubon, M. L. Snapper. Interactions of (-)-ilimaquinone with methylation enzymes: implications for vesicular-mediated secretion. *Chem. Biol*. **1999**, 6, 639–647.

126. J. Singh, R. C. Petter, T. A. Baillie, A. Whitty. The resurgence of covalent drugs. *Nat. Rev. Drug. Discov.* **2011**, 10, 307–317.

127. M. H. Potashman, M. E. Duggan. Covalent Modifiers: An Orthogonal Approach to Drug *Design. Med. Chem*. **2009**, 52, 1231–1246.

128. D. S. Johnson, E. Weerapana, B. F. Cravatt. Strategies for discovering and derisking covalent, irreversible enzyme inhibitors. *Future Med. Chem*. **201**0, 2, 949–964.

129. L. Garuti, M. Roberti, G. Bottegoni G. Irreversible protein kinase inhibitors. *Curr. Med. Chem.* **2011**, 18, 2981–2994.

130. W. Lohmann, H. Hayen, U. Karst. Covalent protein modification by reactive drug metabolites using online electrochemistry/liquid chromatography/mass spectrometry. *Anal. Chem.* **2008**, 80, 9714–9719.

131. S. S. Khandekar, B. Feng, T. Yi, S. Chen, N. Laping, N. Bramson. A liquid chromatography/mass spectrometry-based method for the selection of ATP competitive kinase inhibitors. J. *Biomol. Screen*. **2005**, 10, 447–455.